Spatially-Distributed Modeling of Hydrology and Nitrogen Export from Watersheds

Porranee Thanapakpawin

A dissertation
submitted in partial fulfillment of the
requirements for the degree of

Doctor of Philosophy

University of Washington

2007

Program Authorized to Offer Degree:

Department of Chemical Engineering

University of Washington
Graduate School

This is to certify that I have examined this copy of a doctoral dissertation by

Porranee Thanapakpawin

and have found that it is complete and satisfactory in all respects,
and that any and all revisions required by the final
examining committee have been made.

Chair of the Supervisory Committee:

____
Graham Allan

Reading Committee:

____
Graham Allan

____
Barbara Krieger-Brockett

____
Jeffrey Richey

Date: _______________

In presenting this dissertation in partial fulfillment of the requirements for the doctoral degree at the University of Washington, I agree that the Library shall make its copies freely available for inspection. I further agree that extensive copying of this dissertation is allowable only for scholarly purposes, consistent with "fair use" as prescribed in the U.S. Copyright Law. Requests for copying or reproduction of this dissertation may be referred to Proquest Information and Learning, 300 North Seeb Road, Ann Arbor, MI 48106-1346, 1-800-521-0600, to whom the author has granted "the right to reproduce and sell (a) copies of the manuscript in microform and/or (b) printed copies of the manuscript made from the microform."

Signature________________________________

Date____________________________________

University of Washington

Abstract

Spatially-Distributed Modeling of Hydrology and Nitrogen Export from Watersheds

Porranee Thanapakpawin

Chair of the Supervisory Committee:
Professor Graham Allan
Department of Chemical Engineering

Water and land management is a topic of great importance, and the impact of these management decisions play a direct role in the environmental and economic sustainability of the lands in which our lives and livelihoods depend. A comprehensive set of tools, used to accurately predict the impact of land use is needed in order to make well informed decisions, to plan our land use strategies.

DHSVM, the Distributed Hydrology Soil Vegetation Model, is used to accurately simulate the hydrologic process of watersheds. The DHSVM Solute Export Model (D-SEM), an adaptation of DHSVM created in support of this dissertation, integrates biogeochemical modeling research into DHSVM and leverages heterogeneous landscape data, such as topography, vegetation cover, and soil type, to predict hydrologic flow and nutrient export from a watershed level.

D-SEM provides the intelligence needed to perform landuse scenario analysis. The model's primary interest is in hydrologic modeling and dissolved nitrogen species, predicting how landuse changes may affect concentrations and loads of chemicals into streams and determine the relative nitrogen contributions from human, vegetation, and atmospheric sources.

In the first part of the dissertation, DHSVM is used to assess the impact of land use changes on the hydrologic regime of the Mae Chaem River in northwest Thailand. Three

forest-to-crop expansion scenarios and one crop-to-forest reversal scenario were developed with emphasis on influences of elevation bands and irrigation diversion.

D-SEM is then applied as a test-of-concept to two dissimilar Hood Canal sub-basins, the Big Beef Creek basin which is high in anthropogenic activities and North Fork Skokomish River basin which is pristine. Hood Canal suffers from low dissolved oxygen levels caused by the fjord's characteristics and algal blooms fed by nitrogen rich waters. The application of D-SEM on these two basins will not only aid in the understanding of the Hood Canal dissolved oxygen problem, but will also help show that D-SEM is portable, and application of D-SEM will be possible to a variety of basins with no adjustments necessary. This is important because it will allow D-SEM to be applied to basins with low levels of field sampling, and also basins with hypothetical land-use changes, with a higher degree of confidence in the results generated.

Table of Contents

List of Figures

List of Tables

Table Number Page

Acknowledgements

I would like to thank my committee (Graham Allan, Jeffrey Richey, Barbara Krieger-Brockett, Michael Brett, and Dennis Lettenmaier) for their superb guidance and support. Thanks to Graham Allan for always listening to my problems and sharing his wisdoms and for encouraging me to think and reach out for the best. Thanks to Jeffrey Richey for being flexible in the different ideas I had throughout the years for the scope of this dissertation and for coaching and giving me a wonderful experience to explore my interest in this interdisciplinary study. It was Barbara Kriger-Brockett who taught me the fundamental methodology for conducting research and shares her expertise in the kinetics and reactions field. Michael Brett and Dennis Lettenmaier always eagerly share their expertise in the limnology and hydrology arena.

Special thanks to Robert Edmonds for sharing his expertise in the terrestrial nutrient cycling and for his valuable discussion on the conceptual representation of my model. Darlene Zabowski also helps me understand the soil science and nutrient cycling. Miles Logsdon significantly contributes to my knowledge in GIS and the spatial modeling.

The work on incorporating and implementation of the solute export model within the DHSVM could not happen without tremendous collaboration with Matthew Wiley. Several input data used in Chapter 4 were prepared by him. I also thank Matt, and the other DHSVM experts including Laura Bowling, Colleen Doten, Edwin Maurer, Pascal Storck, Kyle Comanor, and Michael Miller for training and troubleshoot the DHSVM operations. Special thanks to Garret Liles for giving me an exploration of field sampling and his enthusiasm for work is a big inspiration for me. Thank you Peter Steinberg and Suzanne Osborne for the Hood Canal field data and the valuable discussions. I thank Bruce Campbell for creating the fantastic visualization of outputs for the Mae Chaem project.

I thank Harry Ehlers, my mentor for graduate studies, for his guidance during the difficult times and for giving me an opportunity for networking with professionals in the consulting field. I am thankful to the past and present members of the River Systems Group, including Sarah Rodda, Kellie Fay, Sonya Remington, Simone Alin, Erin Ellis, Lauren McGeoch, Deirdre Lockwood, Gordon Holtgrieve, Emilio Mayorga, Anthony Aufdenkampe for their help, friendship, and valuable discussions. Mariza Costa-Cabral and Yinjie Tang share their thoughts and ideas which also contribute to my success.

Finally I thank my family and my family in-law for their love and tremendous support, especially Ann who is an excellent companion and keeps me entertained in the US. I greatly appreciate my husband, Jason Robert Swearingen, who truly devotes himself helping me in every way, including technical support. His love truly makes this dissertation possible.

Dedication

To my parents who taught me to always move forward and never give up

Chapter 1: Introduction

1.1: Motivation

Water and land management is a topic of great importance, and the impact of these management decisions play a direct role in the environmental and economic sustainability of the lands in which our lives and livelihoods depend. A comprehensive set of tools, used to accurately predict the impact of land use is needed in order to make well informed decisions, to plan our land use strategies.

This research focuses on the connection between watershed characteristics, basin hydrology, and solute nutrient export. This connection is important because urbanization and human activities (such as logging) cause landuse and landcover changes, which alters watershed features such as groundcover vegetation and soil properties. This results in an altered basin hydrology; changes in stream flow regime and stream nutrient loads. The consequence of these changes is an altered aquatic biological response. (Figure 1.1). Excessive loading of inorganic plant nutrients causes cultural eutrophication in lakes and slow-moving streams (Welch & Lindell, 2000). These terrestrial inputs of dissolved organic matter and dead photosynthetic organisms decrease dissolved oxygen levels via aerobic decomposition.

Figure 1.1. Circle of connection between watershed and downstream ecology

Informed decision making in the fields of Landscape and Water Resource Management relies on an increased understanding of basin hydrology, as well as the dynamics of solute export. It is crucial to understand the biogeochemistry of terrestrial ecosystems and their connection to riverine export, and to have a robust toolset to help evaluate the tradeoffs between different landuse scenarios.

1.2: Research objectives and scope

The first objective is to develop an integrated hydrological/biogeochemical model to simulate water and chemical fluxes across the landscape into rivers or streams. The purpose of which is to provide the intelligence needed to perform landuse scenario analysis. The scope of solute species in this study includes dissolved organic carbon (DOC), dissolved organic nitrogen (DON), and dissolved inorganic nitrogen including ammonium (NH_4), nitrite (NO_2) and nitrate (NO_3). The second objective is to apply this model to a sub-basin where N sources and contributions to water quality are in question. This will allow the evaluation of relative N-input magnitudes, and estimate stream N export as a real-world test application.

The name DHSVM Solute Export Model (D-SEM) is given to the hydrological/biogeochemical model presented in this dissertation. D-SEM is portable, and can be applied to basins with low levels of field sampling, and can also be used to simulate hypothetical basin land-use changes. D-SEM is currently a test-of-concept, and additional iterations, adjustments to the model, are needed before it can be applied to production. That said, D-SEM will allow land managers the ability to analyze not only current biogeochemical characteristics from otherwise unmeasured sources, but also predict how land changes will affect the environment.

1.3: Chapter summary

In Chapter 2, DHSVM is used to assess the impact of land use changes on the hydrologic regime of the Mae Chaem River in northwest Thailand. Three forest-to-crop expansion scenarios and one crop-to-forest reversal scenario were developed with emphasis on influences of elevation bands and irrigation diversion. This allows the assessment of land use from a water conservation perspective (irrigation schemes, etc), and additionally proves the hydrologic accuracy of DHSVM, which is then used in the creation of D-SEM.

Chapter 3 explains the development of the watershed–scale biogeochemical model D-SEM. D-SEM provides the intelligence needed to perform landuse scenario analysis. The model's primary interest is in hydrologic modeling and dissolved nitrogen species, predicting how landuse changes may affect concentrations and loads of chemicals into streams and determine the relative nitrogen contributions from human, vegetation, and atmospheric sources. The chapter begins with literature review of stream N studies and existing models to predict stream N export. The modeling framework, terrestrial and stream biogeochemical representation and input requirements are explained. Next, steps in D-SEM implementation and troubleshooting are elaborated on. Finally, mathematical representations of individual processes are given in Appendix 1.

Finally, Chapter 4 focuses on the test application of D-SEM to estimate monthly solute loads of nitrates from North-fork Skokomish and Big Beef Creek basins in Hood Canal, a fjord off Puget Sound in Washington State. Hood Canal has a water quality problem consisting of low dissolved oxygen due to both natural and anthropogenic factors. This modeling work is beneficial in addressing the consequence of landuse activities on water quality. This test of D-SEM on these basins will allow for the models analysis by comparing the stream nutrient concentration with field observation data. This is important because once D-SEM is sufficiently refined, it can be applied to basins with low levels of field sampling, and also basins with hypothetical land-use changes, with a high degree of confidence in the results generated. This in turn will aid in finding the solution to the Hood Canal dissolved oxygen problem by increasing the confidence in how terrestrial inputs contribute to the problem.

Chapter 2: The effects of landuse change on the hydrologic regime of the Mae Chaem River basin in Northern Thailand

The scope of this chapter is to report the results and analysis of hydrologic modeling on a highland watershed in Thailand. This is performed by using a physically-based distributed hydrology model and scenario analysis of landuse change. The scientific merit of this modeling exercise is beneficial to the planning of water allocation and flood forecasting for a small catchment undergoing rapid commercialization. Furthermore, the insight of model mechanics provides basic understanding of the rationales in the design and development of the biogeochemical model to estimate solute export in the next chapter.

2.1: Introduction

Landscape and water resource management are major challenges for the socio-economic development of upland watersheds in Southeast Asia due to their association with downstream environmental impacts and water supply. During recent decades, concerns about the impacts of changing patterns of landuse associated with deforestation and agricultural transformation on water resources have created social and political tensions from local to national levels. Major concerns focus on consequences of landuse change for water supply and demand, for local and downstream hydrological hazards, and for biodiversity conservation. Ziegler *et al*. (2004) refer to studies by Sharma in 1992 and by Tuan in 1993, which conclude that shifting agriculture and deforestation in highlands of Vietnam result in watershed degradation such as soil and nutrient loss. In northern Thailand, the prevalent views are that logging, shifting cultivation by mountain ethnic minorities (the practice of farming land until it is unfertile, then moving to a new plot), and commercial agriculture in highland watersheds cause severe dry-season water supply shortages. Water demand is the other side of the equation, as it also places constraints on water availability. Dynamics of water use relate to landuse change, especially through expansion of lowland cultivation, irrigated upland fields, urban areas, and industrialization. Walker (2003) points out that public debate is mostly centered on consequences of highland activities on water supply, but there is little focus on increasing levels of stream water diversion by lowland dry-season irrigated agriculture. Controversy over the eight-dam hydropower cascade system on the Lancang River of the upper Mekong basin in China is an example at a wider, transboundary scale where potential effects on downstream river flows and sediment transport are an international issue for the five countries sharing the lower Mekong River.

In response, public policy decision-making processes are now seeking both economic and conservation goals. More informed decisions for watershed planning and water allocation must rely on the better understanding of highland basin hydrology and the relationship between landuse practices, flow generation processes, and associated water distribution and use. Furthermore, the ability to evaluate basin hydrology beyond just stream flow is crucial for determining spatially-explicit relationship between landscape structure, configuration of landuse change, and the hydrology across the landscape. Distributions of soil moisture across a basin impact agriculture, and provide the antecedent conditions for response to floods or droughts. Process-based distributed models of basin hydrology have the potential to assess these management objectives by quantifying and forecasting the dynamics of water availability with the landuse and climate change. But such models require considerable data, and are perceived to be not feasible for application in many cases. For example, Schreider *et al*. (2002) and Croke *et al*. (2004) applied IHACRES, a metric-conceptual rainfall-runoff model for hydrologic simulation in gauged and ungauged sub-basins in this region. But flow prediction at the Mae Chaem basin outlet was not done, due to sparse basin input data, and Croke *et al*. stated that this limitation makes use of a physically-based model inapplicable.

In this chapter the Distributed Hydrology-Soil Vegetation Model (DHSVM) (Wigmosta *et al*., 1994), a spatially-explicit landscape/hydrology model to evaluate the seasonal patterns and the hydrologic components of the Mae Chaem River is utilized. As DHSVM is a fully-distributed model that recognizes the spatial heterogeneity of the watershed, the spatial variation of hydrologic attributes inside the basin can be evaluated, and calculations based on the availability of data and level of complexity can be adjusted. My focus is to assess effects of landuse conversion between forest and croplands on the basin hydrology and on water availability in terms of annual and seasonal water yields. Specifically, the influence of elevation bands of agricultural fields (highlands versus lowlands) and irrigation diversion can be assessed. Scenario analysis eliminates interpretation problems associated with direct comparison of stream flow in paired watershed analyses where basins have different underlying geological settings (Bruijnzeel, 2004). In the process of conducting these analyses, the applicability of this class of physical model for use as a water resource tool, in basins where data are relatively sparse, will be assessed. This can be compared and contrasted to the work performed by Croke *et al*. (2004), as mentioned in the preceding paragraph.

2.2: Mae Chaem basin: the study area

The Mae Chaem (Chaem River) watershed is located in the Chiang Mai province of northern Thailand (Figure 2.1). It is a major upper tributary sub-basin of the Ping River, which in turn, is the largest tributary of central Thailand's Chao Phraya River. The Mae Chaem sub-basin is bounded by coordinates 18^{o} 06' - 19^{o} 10' N and 98^{o} 04' - 98^{o} 34' E, and includes a total area of 3,853 km^2 above the Royal Irrigation Department (RID) river gauge station P.14. The climate of this mountainous basin is defined by large variations in seasonal and annual rainfall that are influenced by Pacific-born typhoons, superimposed on the south-west monsoon (Walker, 2002). The orographic effect induces an altitudinal increase of spatial rainfall distribution (Dairaku *et al*., 2000; Kuraji *et al*., 2001). The average annual temperature ranges from 20 to 34 ^{o}C and the rainy season is from May to October.

Sharp relief and forest vegetation (and relatively sparse data) characterize the Mae Chaem. The basin has a wide range of elevation, from 282 m.a.s.l. at its lowest point to

2,565 m.a.s.l. at its highest peak, Doi Inthanon (Mount Inthanon). Altitude variation induces different climatic zones with distinctive types of natural landcover. Dominant vegetation includes dry dipterocarp and mixed deciduous forests below 1,000 m.a.s.l., tropical mixed pine forest from 900 – 1,500 m.a.s.l. alternating with hill evergreen forest that extends up to 2,000 m.a.s.l., and tropical montane cloud forest above 2,000 m.a.s.l. (Dairaku *et al*., 2000; Kuraji *et al*., 2001). Steep hillsides with slopes exceeding 25% are a common landscape element, resulting in rates of soil erosion that prevent advanced soil development. Thus, soils are relatively shallow and have limited water-holding capacity (Hansen, 2001). Dominant soil textures are sandy clay loam and clay loam.

The population of Mae Chaem is ethnically diverse and distributed among numerous small villages. The majority Karen and the Lua ethnic groups live primarily in mid-elevation zones between 600 to 1,000 m.a.s.l., with some communities extending into higher elevations. Ethnic northern Thai (khon muang) villages are mostly clustered in lowland areas below 600 m.a.s.l., whereas Hmong and Lisu ethnic groups live mostly in highland villages located above 1,000 m.a.s.l.

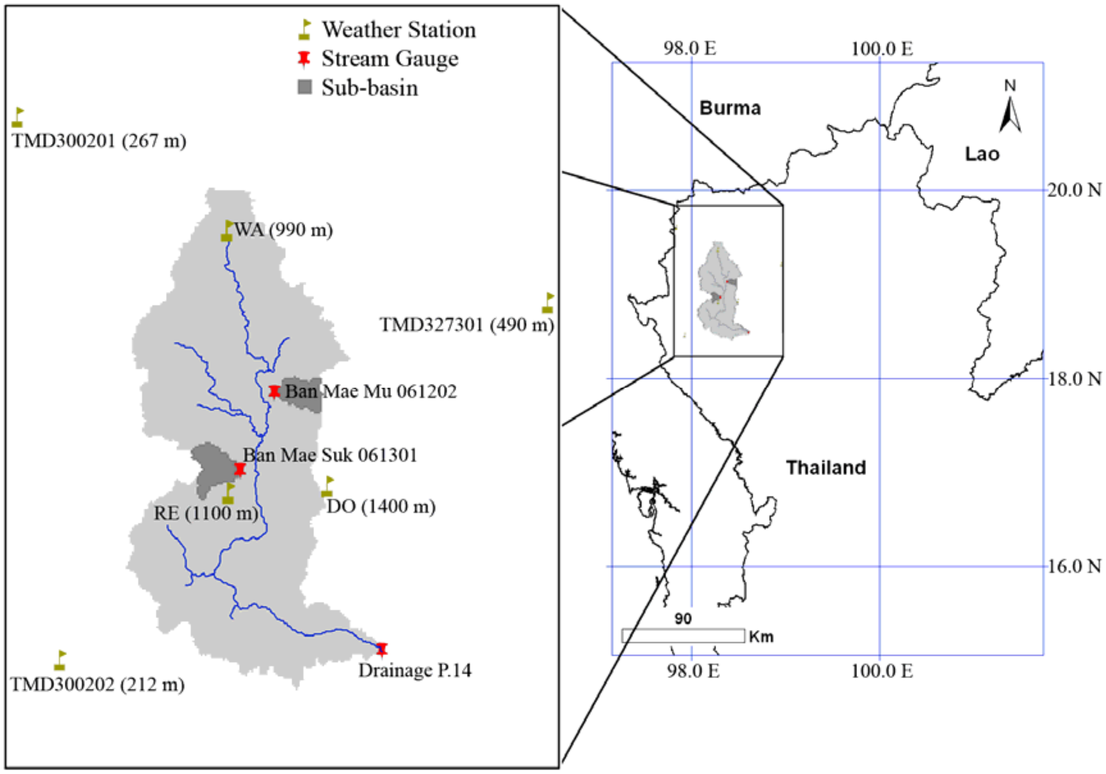

Figure 2.1. Location of Mae Chaem River watershed, stream gauges, and meteorological stations within and adjacent to the watershed.

Landuse patterns in Mae Chaem have undergone substantial change during the past several decades. As recently as the 1960s, the agriculture mosaic was comprised of highland (above 1,000 m.a.s.l.) pioneer shifting cultivation that often included opium, mid-elevation (600-1,000 m.a.s.l.) rotational forest fallow shifting cultivation with a decade long fallow period, and paddy and home garden-centered cultivation in the lowlands (Thomas *et al*., 2002; Walker, 2003). In the 1980s, development projects and programs in Mae Chaem began building infrastructure and promoting commercial agriculture, under programs to reduce rural poverty and promote alternatives to opium cultivation and shifting agriculture. Results have included significant increases in production of highland cash crops such as cabbage and carrots, expansion of industrial field crops such as soybeans and maize up watershed slopes above lowland paddies into mid-elevation zones, expansion of irrigated paddy fields wherever terrain allows, and planting of fruit orchards in some areas of all altitude zones (Praneetvatakul *et al*., 2001; Pinthong *et al*., 2000; Thomas *et al*., 2002; Walker, 2003).

2.3: Development of geospatial landscape/hydrology model

DHSVM is utilized for stream flow forecasting and for addressing hydrologic effects of land management or of climate change, for small to moderate drainage areas (typically less than about 10,000 km^2), over which digital topographic data allows explicit representation of surface and subsurface flows. It simulates soil moisture, snow cover, runoff, and evapotranspiration on a sub-daily time scale. It accounts for topographic and vegetation effects on a pixel-by-pixel basis, with a typical resolution of 30 to 150 m. Snow accumulation and snow melt, where needed, are calculated by a two-layer energy-balance model. Evapotranspiration follows the Penman-Monteith equation. The multi-layer soil column in each pixel is a series of soil moisture reservoirs, and saturated subsurface flow exists in the deepest soil layer. Runoff generation is represented by saturation excess and infiltration excess mechanisms. Stream segment storage volume is computed using linear-reservoir routing.

The model has been applied to basins in the USA (Bowling *et al*., 2000; Bowling and Lettenmaier, 2001; Storck, 2000; VanShaar *et al*., 2002) and in British Columbia (Schnorbus and Alila, 2004), and Southeast Asia (Cuo *et al*., 2006).

2.3.1: Development of the geospatial model of the Mae Chaem basin

2.3.1.1: Topography and flow network

Topography for the Mae Chaem basin was acquired as a 30-meter digital elevation model (DEM) constructed by the World Agroforestry Centre (ICRAF), Chiang Mai. This 30-meter DEM was then aggregated to 150-meter resolution (Figure 2.2) using the average of all 30-meter elevation data which were nested within the boundary of each 150-meter cell. Flow direction, flow accumulation, and stream network were derived from the 150-meter DEM. Soil depth was generated by DHSVM, based on the DEM, and was adjusted during model calibration.

2.3.1.2: Soil map and attributes

Soil data in Mae Chaem are very sparse and restricted to the lowlands (Land Development Department (LDD), Ministry of Agriculture and Cooperatives, Thailand). The majority of the area is mountainous and is classified only as 'slope complex' in the soil survey. Therefore, a soil map containing physical and chemical properties was constructed using SoilProgram software (Carter and Scholes, 1999), which derives 5-minute resolution (about 10 km) soil data from the WISE pedon-database (Batjes, 1995) developed by the International Soil Reference and Information Centre (ISRIC) and the FAO-UNESCO Digital Soil Map of the World (FAO, 1995). The soil map was re-sampled to 150-meter resolution, with the number of soil types equal to the number of unique values of physical and chemical soil properties. Soil texture was assigned based on the percent sand and clay. Porosity and field capacity were estimated from the soil texture triangle hydraulic properties calculator (Saxton *et al*., 1986). Infiltration rates and an estimated range of soil depths were quantified using a local descriptive soil survey (Putivoranart, 1973).

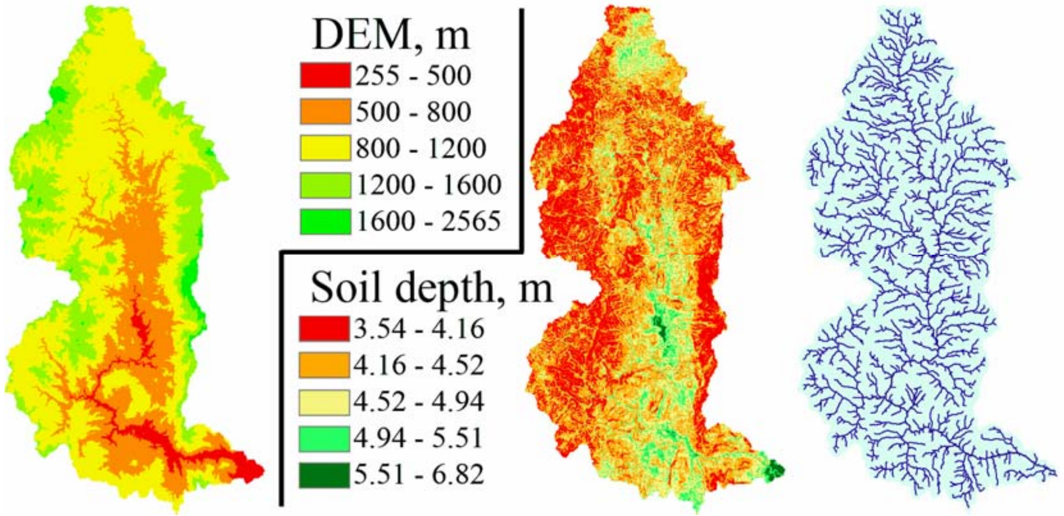

Figure 2.2. DEM, soil depth, and stream network grids (left to right) represented by the 150-meter resolution.

2.3.1.3: Vegetation and landuse: 1989, 2000, future

Two landcover datasets form the basis for the landcover change scenarios in the hydrology model. The original classification schemes of these data vary significantly, so scheme modifications were made to achieve similarity between landcover data.

The first dataset in the landcover time series is a historical 1989 dataset, acquired from the LDD. These data, subsequently referred to as Veg 1989, originated as polygons, which were converted to a 150-meter raster grid representation using a nearest-neighbor assignment algorithm. Data were then generalized into 11 classes (Figure 2.3) from its original 39. The second dataset represents landcover for the year 2000, referred to as current landcover or Veg 2000. This dataset, also from LDD, was prepared for the model using the same procedure as utilized for the 1989 data. However, since the original 47 class names in this dataset differed from those in the 1989 data, class names were reconciled by performing a combinatorial analysis between the 1989 reclassified dataset and the 2000 original data. In this way a correlation between the 11 classes in 1989 and the 47 original classes in 2000 was established. This type of spatial overlay analysis returns not only the frequency of all unique combinations of landcover types, but also a map product of the spatial commonalities. A plot was made to identify the frequency of occurrence between a 2000 value (1 to 47) and a 1989 value (1 to 11). Based on this plot, the 2000 vegetation values were re-assigned a value consistent with the frequency distribution of shared space with the 1989 dataset.

Veg 2000 is employed as the reference landuse case, and four future scenarios (Figure 2.3) were created based on the transition from Veg 1989 to Veg 2000, with a focus on forest-to-crop conversion. The first scenario represents reversal of all croplands back to evergreen needleleaf forests in zones above 1,000 m.a.s.l., and to deciduous broadleaf forests below 1,000 m.a.s.l. Selected forest types were generally in accord with actual dominant vegetation in the respective elevation zones. The second scenario forecasts the doubling of cropland area in Veg 2000 by growing a buffer of new crop cells around all existing crop patches. This ultimately increased the cropland share of total basin area from 10.4% in 2000 to 19.9%. Finally, the third and fourth scenarios depict a doubling of cropland that is limited to either highland zones of the basin (above 1,000 m.a.s.l.), or to lowland and midland basin zones (below 1,000 m.a.s.l.). Growth of croplands limited to highland and to lowland-midland basin zones increased cropland shares of total basin area to 18.0% and 19.1%, respectively. In both cases, crops were expanded around existing patches in the selected elevation range, while crop cell areas outside the selection remained the same as in 2000.

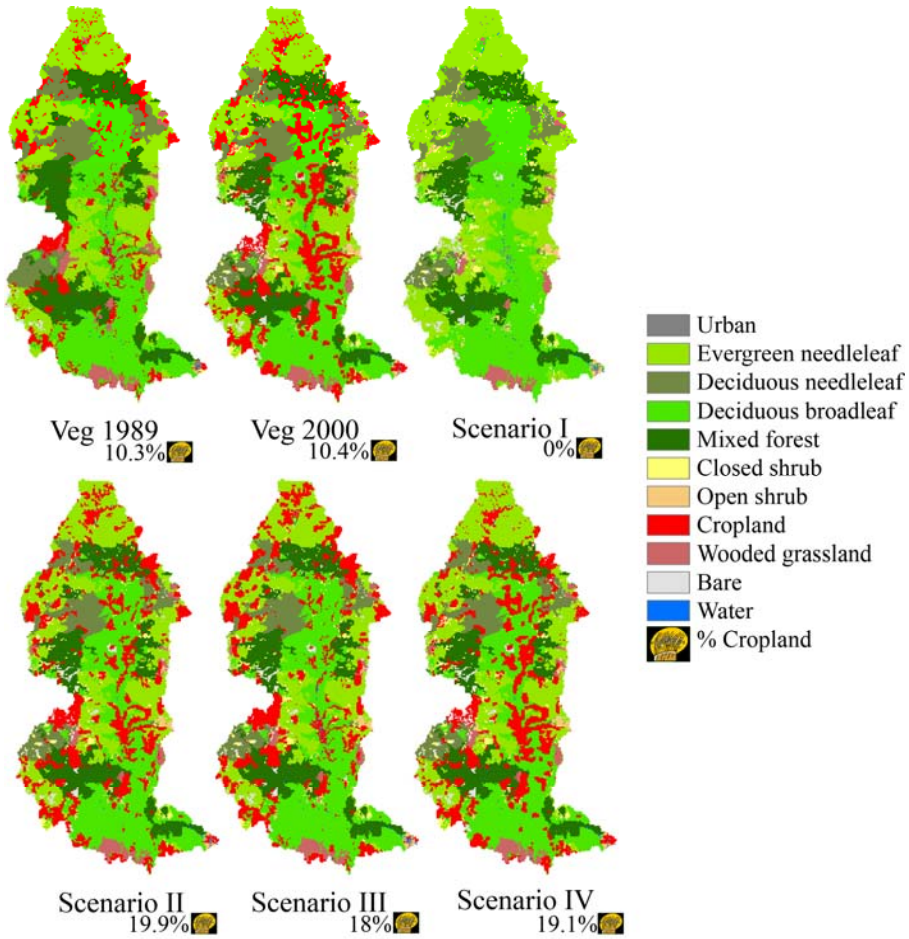

Figure 2.3. Mae Chaem landcover scenarios from top left to bottom right: (Veg 1989) re-processed 1989, (Veg 2000) re-processed 2000, (Scenario I) conversion from crops to forest, (Scenario II) double crop areas, (Scenario III) more upland crops, and (Scenario IV) more lowland-midland crops.

2.3.2: Climate forcing and hydrology

The meteorological variables required by the DHSVM are precipitation, temperature, relative humidity, shortwave, and longwave radiation. To best represent climatic variation within the catchments, daily rainfall, and maximum and minimum air temperature records for the period of 1993-2000, which were obtained from five meteorological stations and one agro-meteorological station, were used (Figure 2.1). Doi Inthanon (DO) and Wat Chan (WA) stations are operated by the Royal Project Foundation, and their recorded values were obtained from both ICRAF and the Royal

Project Foundation. The Research Station (RE) belongs to the Global Energy and Water Cycle Experiment (GEWEX) Asian Monsoon Experiment-Tropics (GAME-T), led by the University of Tokyo in Japan. Mae Jo Agromet (TMD327301), Mae Hong Son (TMD300201), and Mae Sariang (TMD300202) stations are managed by the Thai Meteorological Department (TMD). Data for these stations were acquired directly from the respective agencies. TMD300201 has 2 gaps in temperature data from September 24 - October 14 1995 and February 19 – March 23 1997 and were filled by linear interpolation of data from the nearest station. DO has a gap in rainfall data in 1998 and the daily rainfall from another GAME-T meteorological station located on Doi Inthanon at 2565 m was used instead. Wind speed was set to the model default value of 2 m/s for all stations except RE and TMD327301, where actual daily wind speed records are available, whose mean speeds were slightly lower. After disaggregated 3-hourly data was generated, the 3-hour precipitation values in 1998 – 2000 were then replaced by observed records for all TMD stations.

The Mae Chaem hydrologic regime consists of high flow from May to October, contributing to 70% of the total flow. The base-flow is from November to April, and from 1989-2000 there is an average annual water yield of 270 mm (the water year is considered to begin in November of the year previous to the year cited). Due to the strong orographic effect on precipitation (Figure 2.4), the surface runoff ratio could be between 12 – 25%, depending on selection of reference rainfall stations and the interpolation scheme. Walker (2002) provides thorough discussions on the long-term rainfall-discharge relationship in Mae Chaem.

The gauge at Kaeng Ob Luang (RID gauge P.14) represents the basin output, and is the primary record used here. 1993-1999 discharge records were acquired from GAME-T, and the estimated daily discharge in 2000 was computed from the stage height observation obtained from the RID Hydrology and Water Management Center for the Upper Northern Region. For local calibration and validation purposes, the 1993 - 2000 daily average stream flow measurements at the Ban Mae Mu gauge 061202 on the 70.6

km^2 Mae Mu River subcatchment and at the Ban Mae Suk gauge 061301 on the 86.5 km^2 Mae Suk River subcatchment (Figure 2.1) were obtained from ICRAF.

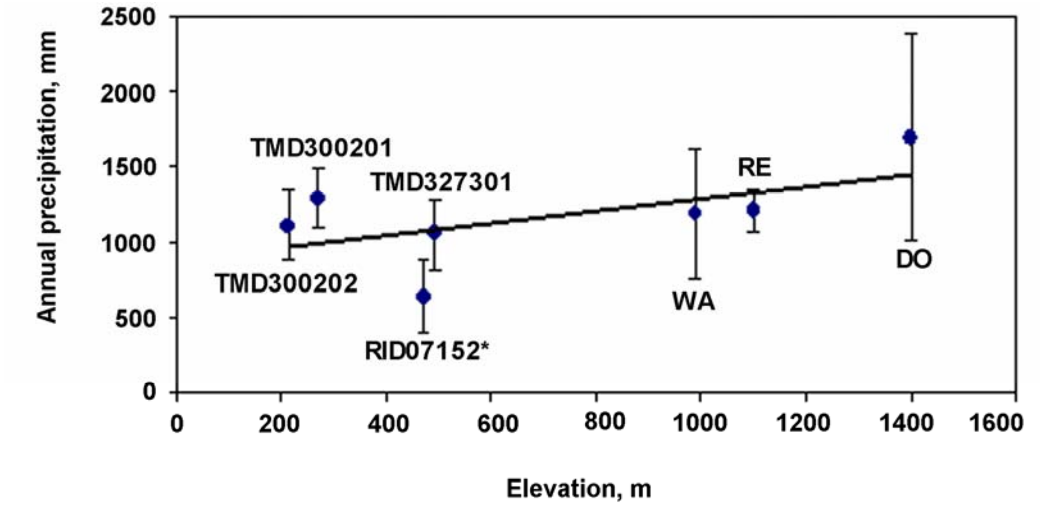

Figure 2.4. Orographic effects on average annual rainfall (1989-2000). * Rainfall from this station is used only for demonstration of orographic effect, but not in actual simulation

2.4: Model setup and operations

2.4.1: Simulation conditions and parameter estimation

The spatial domain was partitioned into 150-meter grid cells and the simulation was performed on a 3-hour time step using the current landcover (Veg 2000) as the base case for calibration and validation. Disaggregated 3-hourly temperature, radiation and relative humidity were generated from daily records using a diurnal interpolation scheme from the Variable Infiltration Capacity (VIC) model (Liang *et al*., 1994; Maurer *et al*., 2002). In this scheme, total daily rainfall was evenly distributed through sub-daily intervals. Climate data across the basin was computed from data of the 6 meteorological stations using a nearest-station interpolation. The soil profile was divided into 3 root zones, 0-30 cm, 30-60 cm, and 60-100 cm. Lateral subsurface flow was calculated using a topographic gradient. In the routing scheme, roads were not included, and stream classification was based on Strahler stream order and segment slope, derived from the DEM. A precipitation lapse rate of 0.0005 m/m was estimated from the rate of increase in average annual rainfall, as it corresponds with station elevation (Figure 2.4), using data from 1989-2000. For the temperature lapse rate, first, daily temperature was calculated using the mean of daily maximum and minimum temperatures at each station. The temperature lapse rate of -0.0053 ^{o}C/m was then approximated from the gradient of average daily temperature (1993-2000) with the elevation. Both precipitation and temperature lapse rates were assumed constant for the entire catchment. A rain LAI multiplier (leaf area index multiplier to determine interception capacity for rain) of 0.0005, a reference height of 40 m, and an aerodynamic roughness of bare ground of 0.02 m were set as constants. The initial spatial distribution of soil depth was created using ArcInfo (ESRI, Inc.) macro language script as part of DHSVM pre-processing, based on the specified range of soil depths and the DEM. The soil depth was then adjusted during calibration. The initial vegetation parameters came from Global Land Data Assimilation Systems (GLDAS) by NASA and were tuned to northern Thailand based on forest description by Gardner *et al*. (2000) and by parameters in the transpiration estimation of Tanaka *et al*. (2003). After the simulation, the approximate amount of irrigation diversion was subtracted from simulated stream flows before comparing to observed values.

To study the effects of landuse change, the same set of climate data and parameters were used for all vegetation scenarios, both with and without irrigation. When irrigation was considered, daily irrigation consumption was calculated, divided by the irrigation efficiency coefficient, and then subtracted from computed daily discharge to account for water diversion to irrigated area. Crops were divided into 3 categories based on their water demand: wet-season rice, dry-season rice, and cash crops (Table 2.1). Irrigated areas were approximated from the number of pixels of each crop type in the original 1989 and 2000 landcover data sets. Percentages of total irrigated areas in the basin in 1989 and 2000 were used to project a range of potential irrigated areas in the future scenarios. The following assumptions were made in calculating irrigation diversion: First, only 1/8 of the area designated as swidden cultivation in the original classification scheme was used for irrigated cropping. Second, for general field-crop classes, half of the area was wet-season rice and the other half was cash-crop; the composition of incremental cropland in future scenarios was divided in the same manner. Irrigation efficiency coefficients were based on the estimation by the Royal Irrigation Department and the values were 0.6 and 0.85 for wet and dry seasons respectively. The diverted water in the amount equal to crop water demand was then added to simulated evapotranspiration to maintain the water balance. Table 2.2 summarizes all simulation conditions.

Table 2.1. Monthly irrigation water demand (in mm) of northern agricultural crops (Schreider *et al.*, 2002).

Crop type	Month											
	Jan	Feb	Mar	Apr	May	Jun	Jul	Aug	Sep	Oct	Nov	Dec
Wet season rice	0	0	0	0	250	300	350	150	50	50	0	0
Dry season rice	250	200	200	0	0	0	0	0	0	0	300	500
Cash crops	150	150	100	0	0	0	0	0	0	0	300	100

Table 2.2. Simulation scenarios to look at effects of landuse type and irrigation.

Secondary factor	Primary factor : Landuse a change					
	Veg 1989	Veg 2000	Scenario I	Scenario II	Scenario III	Scenario IV
Irrigated areas						
0%	X	X	X	X	X	X
23%b	X			X	X	
35%c		X		X		X

a Veg 1989: re-processed 1989; Veg 2000: re-processed 2000; Scenario I: conversion from crops to forest; Scenario II: double crop areas; Scenario III: more upland crops; Scenario IV: more lowland crops
b Approximate maximum percentage of croplands being irrigated based on Veg 1989
c Approximate maximum percentage of croplands being irrigated based on Veg 2000

2.4.2: Calibration and testing procedures

Model calibration was done by optimizing the model simulation of daily discharges at the basin outlet (P.14), Ban Mae Mu and Ban Mae Suk. The main focus was on the result at the basin outlet. Three methods of quantitative assessment for the goodness of model fit are the relative efficiency E_{rel} (Krause *et al*., 2005) (1), the root mean square errors (RMSEs) of daily discharges (2) and bias.

$$E_{rel} \quad = \quad 1-\frac{\sum_{i=1}^{N}\left(\frac{Q_i - Q_i'}{Q_i}\right)^2}{\sum_{i=1}^{N}\left(\frac{Q_i - \overline{Q}}{\overline{Q}}\right)^2} \qquad (1)$$

$$RMSE \quad = \quad \sqrt{\frac{1}{N}\sum_{i=1}^{N}(Q_i' - Q_i)^2} \qquad (2)$$

Where Q_i is observed discharge at time step *i*, Q_i' is the simulated discharge at time step *i* after subtracting irrigation diversion, $\overline{Q}$ is the mean observed discharge, and N is the total number of time steps.

E_{rel} , a modified form of the model efficiency E (Nash and Sutcliffe, 1970), measures the goodness of model fit by comparing both the volume and shape of the discharge profile. The difference between simulated and observed values was quantified based on relative deviations instead of absolute values. The rationale for using E_{rel} is because E calculates the differences between the two time series as squared values. Consequently, an over- or under-estimation of higher values in the time series has greater influence than that of lower values (Krause *et al*., 2005). E_{rel} enhances the lower absolute differences during the low flow period since they are substantial when considered relatively. Thus, E_{rel} is more sensitive to systematic over- or under-prediction in the dry season. Since E_{rel} focuses on the reproduction of hydrograph dynamics, RMSE is also reported for quantifying the volume errors, and bias is the percent error in total stream discharge.

The climate data from March 1993 – February 1994 was used for model start-up. The calibration period was from March 1994 – March 1996 and the validation was from April 1996 - October 2000.

The key parameters for model calibration were first identified and then the optimization was done based on trial and error; one parameter was adjusted at a time. Whitaker *et al*. (2003) and Cuo *et al*. (2006) took a similar calibration approach in their DHSVM applications. The objective is to obtain E_{rel} closest to unity and to minimize RMSE and bias. Negative E_{rel} indicates that the mean value of observed data is a better predictor than the model.

The model was sensitive to total soil depth, soil lateral hydraulic conductivity, and exponent decrease in lateral hydraulic conductivity with depth, and these are chosen as calibration parameters. Among three parameters, soil depth is the parameter with the least information on and is important in influencing the basin moisture storage size; therefore, it is the first calibration parameter. Soil lateral hydraulic conductivity influences the rate of subsurface flow, the water table depth, and the relative importance of subsurface runoff to the overland flow (Whitaker *et al*., 2003). The adjustment of soil lateral hydraulic conductivity was constrained to be within an order of magnitude of the initial known value obtained from an application called SoilProgram. After calibration, the value of soil hydraulic conductivity was comparable to literature value and to those used in Cuo *et al*. (2006) on a small sub-basin nearby. For the exponent decrease, the choice is confined to the range used in Cuo *et al*. (2006).

In addition to calibrating the discharge, the estimated annual evapotranspiration was also compared with literature values to make sure the parameter set yielded reasonable results. Final calibration parameters are listed in Table 2.3 and 2.4.

2.4.3: Calibration results and assessment

During the calibration period, the stream flow at main basin outlet P.14 was reproduced reasonably well, though the performance at the two much smaller sub-basins (Mae Mu and Mae Suk) was not as consistent (Table 2.5).

For P.14 the model captured the onset of the storm season, and the peak flows well (Figure 2.5-a). The overall efficiency of 0.79 indicated reasonable model performance, even though the model systematically under predicted the dry-season flow by a little over 20% (Figure 2.7-a). The mean observed flow for the whole calibration period, 43.4 m^3/s, was underestimated by 9% with a RMSE of 75% (Table 2.5).

During the validation period, the model efficiency was 0.74, close to the results of the calibration period. The model captured the right timing and magnitude for peaks (Figure 2.6-a). The prediction of annual flow matched very well with the observed values (Figure 2.7-a) with a 2% overall bias in stream flow and RMSE of 23.6 m^3/s. This, like the calibration results, was 75% of the measured mean (31.3 m^3/s). The validation period also consistently underestimated dry-season flow by nearly 20%.

For the Mae Mu and Mae Suk sub-basins, the timing and magnitude of the modeled stream flow peaks had a higher variance than the actual observations (Figure 2.5-b, 2.5-c, 2.6-b, 2.6-c), contributing to a relatively poor performing model. The efficiencies during the calibration period were relatively low, but slightly better than in the validation period, which had negative values for overall model efficiency (Table 2.5). Through out the simulation for the Mae Mu, the modeled dry-season flow consistently under-predicted measured flow by 28% (Figure 2.7-b, Table 2.5). The modeled wet-season flow overestimated measured flow by varying amounts, with worst performance in the wet seasons of 1999 and 2000, with 92% and 65% bias respectively.

During the calibration period for the Mae Suk, the annual and seasonal flows were underestimated (Table 2.5), the overall bias was -50% and RMSE was in the same magnitude as the measured mean (1.5 m^3/s).

During the validation period, the overall bias of 5% was relatively small. However both annual and seasonal flows did not seem to correlate with the observation (Fig. 7-c). The wet-season flow in 2000 was highly overestimated with a 73% bias, and the simulation yielded several peak flows during the beginning of the wet season while the actual peak flows occurred late in September and October.

While it is possible to fine tune the results of the two sub-basins by adjusting soil depth or soil hydraulic properties, there is not enough information to justify the adjustment. With the sparse input data, the guiding rationale is that it is more important to capture the discharge dynamics of the whole basin rather than at the smaller catchments.

Table 2.3. DHSVM vegetation parameters.

Parameter	Overstory (Class 2-5, 9)a	Understory (Class 1-9)
Fractional trunk space height	0.4-0.5	N/A
Height, m	20-30	0.2-5
Aerodynamic attenuation coefficient	0.3-2	N/A
Radiation attenuation coefficient	0.1-0.2	N/A
Maximum stomatal resistance, s/m	4000-5000	600-4000
Minimum stomatal resistance, s/m	200-400	120-175
Vapor pressure deficit threshold, Pa	4000-5000	4000-5000
LAI	1-8.2 (broadleaf) 3.5-8.8 (needleleaf)	1-5.5
Albedo	0.2	0.2
Root fraction in layer 1,2, and 3	0.2, 0.4, 0.4	0.4, 0.6, 0.0

a Class 1: Urban; 2: Evergreen needleleaf; 3: Deciduous needleleaf; 4: Deciduous broadleaf; 5: Mixed forest; 6: Closed shrub; 7: Open shrub; 8: Cropland; 9: Wooded grassland; 10: Bare; 11: Water

Table 2.4. Final DHSVM soil parameters.

Parameter	Soil layer	Soil class	
		1	2
Texture		Sandy clay loam	Sandy clay loam
Lateral soil hydraulic conductivity, m/s		3.12 x 10-5	5.1 x 10-5
Exponent decrease rate of lateral saturated Hydraulic conductivity		0.5	0.5
Porosity, m^3/m^3	1 2 3	0.5 0.5 0.5	0.50 0.51 0.51
Vertical saturated hydraulic conductivity, x 10-5 m/s	1 2 3	36.0 15.6 15.6	4.52 2.55 2.55
Pore size distribution index	1 2 3	0.12 0.12 0.12	0.12 0.12 0.12
Air bubbling pressure, m	1 2 3	0.29 0.29 0.29	0.29 0.29 0.29
Field capacity, m^3/m^3	1 2 3	0.26 0.30 0.30	0.27 0.30 0.30
Wilting point, m^3/m^3	1 2 3	0.15 0.18 0.18	0.15 0.18 0.18
Maximum infiltration rate, m/s		1.0 x 10-5	1.0 x 10-5

Table 2.5. Model calibration performance for the main basin outlet: P 14, Mae Mu subcatchment, and Mae Suk subcatchment.

	Gauge location								
Year	Basin outlet (P. 14)			Ban Mae Mu			Ban Mae Suk		
	E_{rel}	Bias %	RMSE m^3/s	E_{rel}	Bias %	RMSE m^3/s	E_{rel}	Bias %	RMSE m^3/s
Calibration - overall	0.79	-9	32.7	0.15	7	1.2	0.43	-50	1.5
Wet season 1994	0.69	4	41.8	-0.86	32	1.4	0.14	-58	2.1
Dry season 1995	-0.07	-25	7.4	0.42	-29	0.2	-0.24	-56	0.5
Wet season 1995	0.63	-14	49.1	-0.56	27	1.8	-0.94	-48	2.0
Dry season 1996	0.16	-21	15.4	-1.83	-33	0.6	-2.52	-11	0.7
Validation - overall	0.74	2	23.6	-0.92	24	1.1	-2.22	-5	1.3
Wet season 1996	0.49	10	37.5	-1.95	42	1.5	-0.28	-21	1.4
Dry season 1997	0.33	-8	10.4	-0.16	-20	0.4	-6.15	-8	0.6
Wet season 1997	0.60	-9	20.0	-2.82	29	1.1	0.71	-47	2.1
Dry season 1998	0.63	-28	7.6	0.39	-37	0.2	0.72	-32	0.3
Wet season 1998	0.68	21	20.1	-0.02	-8	0.7	-19.44	17	1.1
Dry season 1999	0.14	-10	4.5	-0.87	-24	0.2	-2.48	26	0.2
Wet season 1999	0.42	7	29.5	-15.98	92	2.2	-1.87	-5	1.5
Dry season 2000	0.82	-22	19.6	0.64	-29	0.7	-0.23	-4	0.4
Wet season 2000	0.37	16	36.8	-7.76	65	1.5	-22.49	73	2.0

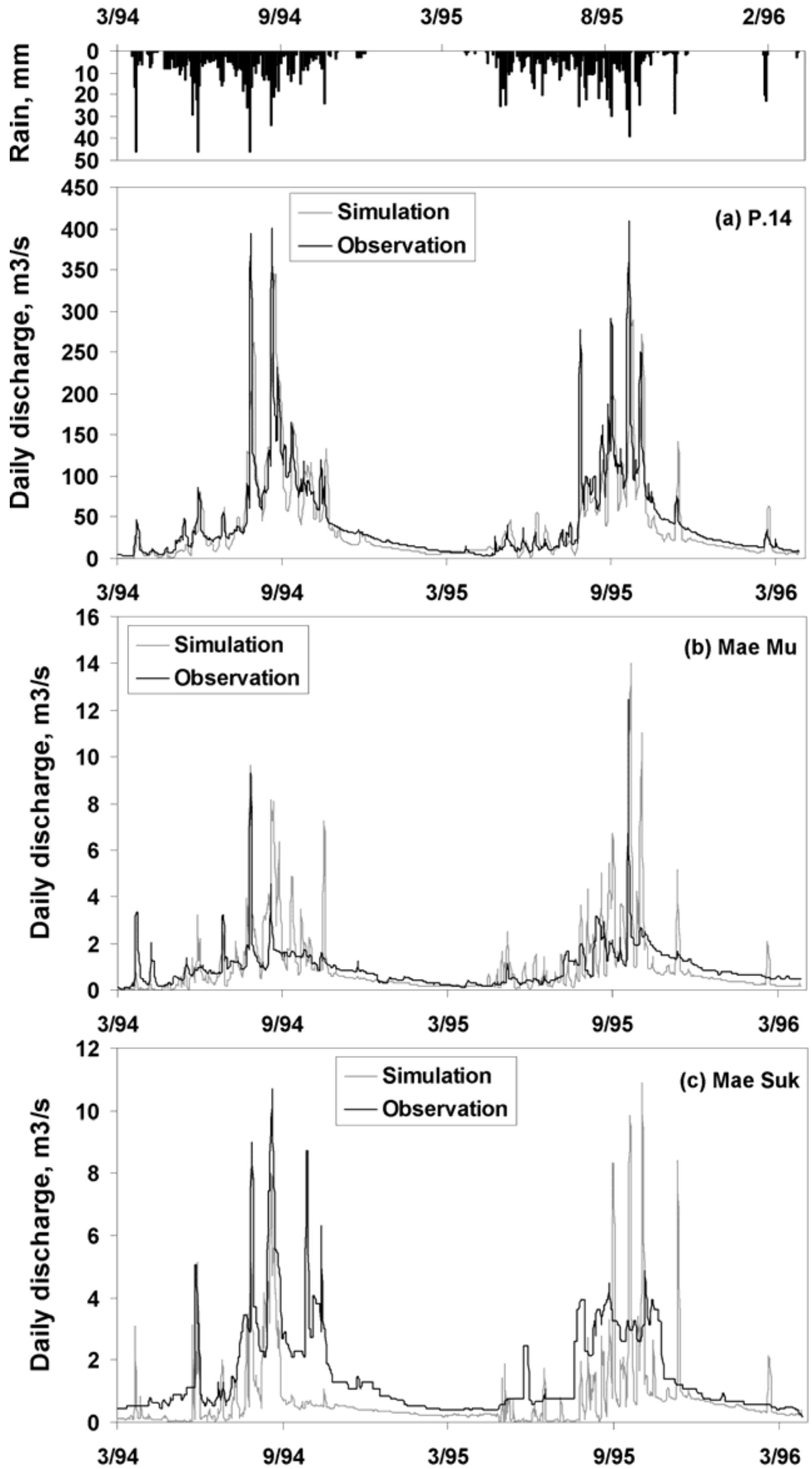

Figure 2.5. Observed and predicted hydrographs simulated using Veg 2000 during calibration period for (a) basin outlet: P.14, (b) Mae Mu subcatchment, and (c) Mae Suk subcatchment.

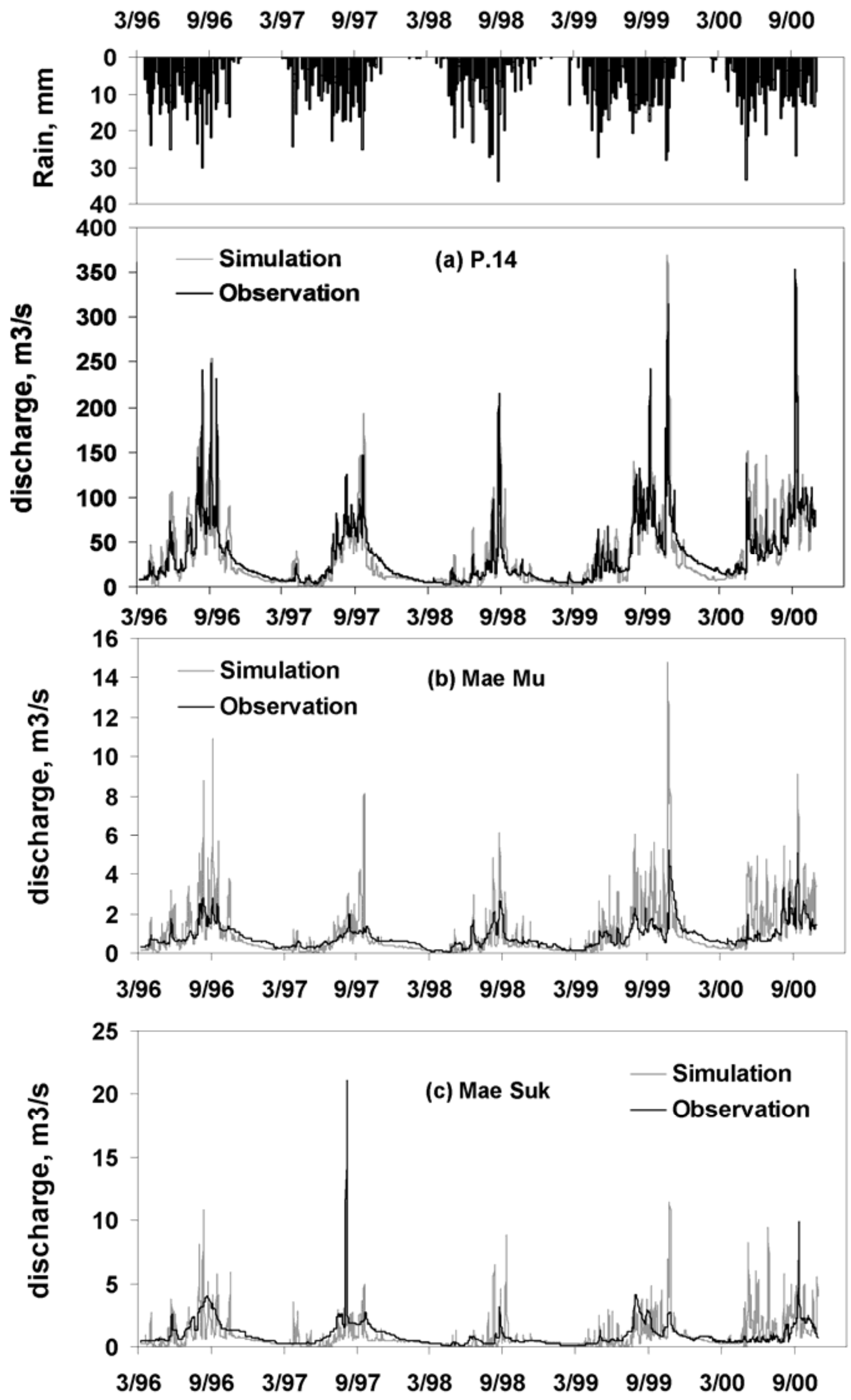

Figure 2.6. Observed and predicted hydrographs simulated using Veg 2000 during validation period for (a) basin outlet: P.14, (b) Mae Mu subcatchment, and (c) Mae Suk subcatchment

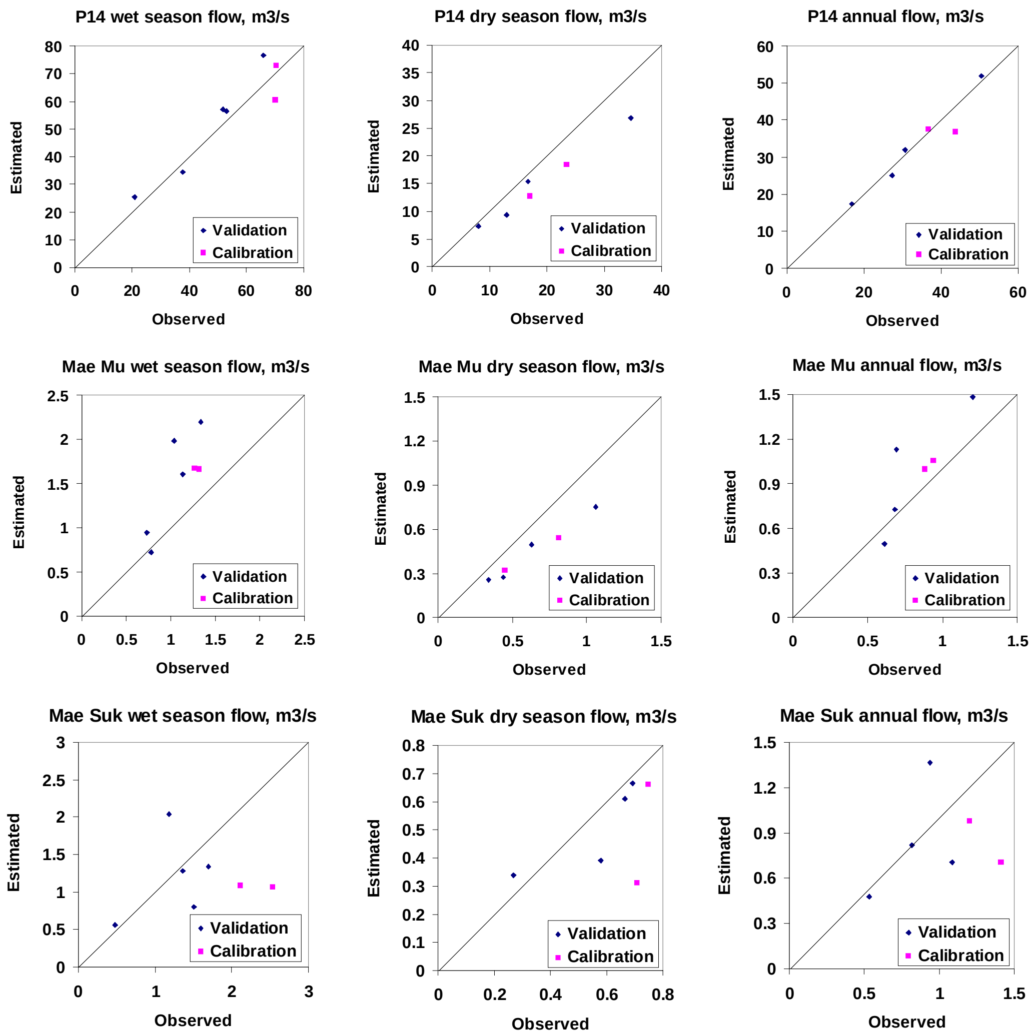

Figure 2.7. Comparison between observed and estimated annual, wet-season, and dry-season discharges for (a) basin outlet: P.14, (b) Mae Mu subcatchment, and (c) Mae Suk subcatchment.

2.4.4: Model performance and sources of errors

Overall, the model at P.14 performed within published ranges (comparable to Nash and Sutcliffe model efficiency -0.76 - 0.5, Cuo *et al.*, 2006; 0.57 - 0.87, Becker and Alila, 2004). That there was greater divergence for the Mae Mu and Mae Suk sub-basins is not surprising, given their small size relative to the overall scale of the basin and data available. The divergence of estimated stream flow from the observed could have been due to:

2.4.4.1: Uncertainty in estimated rainfall distribution within the basin

The shapes of observed wet-season stream flow peaks for the subcatchments are different than that at the main basin outlet, especially in the wet season of 1999 and 2000. Those observed peaks also do not match with basin-wide rainfall (Figure 2.6), indicating that local rainfall events differ from basin-wide events. Rainfall could be overestimated in the higher elevation zone of the two subcatchments. Therefore, rainfall measurement and appropriate basin-wide meteorological data interpolation from weather station records are critical for model performance, especially when the basin has a large elevation range.

2.4.4.2: Water regulation from irrigation

Two aspects regarding irrigation are the percent of croplands being irrigated and the uncertainty in the timing and frequency of irrigation diversion. In the Mae Suk especially, 17% of the subcatchment is crop area. These crop areas are mainly paddy fields near the streams, field crops, and shifting cultivation. The percentage of crop areas in the Mae Suk is 70% higher than that of the whole Mae Chaem basin (10.4%), and the fraction of calculated irrigation diversion accounts for 10-60% of the mean observed flows whereas the estimated irrigation diversion from the main stream flow only accounts for 4-30% of the observed values. Therefore, the channel prediction at Mae Suk is more sensitive to the subtraction of irrigation water than at the main basin outlet (P.14).

2.4.4.3: Dynamics of crop conversion

The simulation from 1994-2000 was performed on a static landcover using Veg 2000 dataset. However, the landcover gradually changes over time, as observed in the original landcover classifications from 1989 and 2000. This shows a cropland area net increase of about 1%. Even though the total increase in the crop area is small, the location of land conversion between crop type subgroups is not represented in the model.

2.4.4.4: Estimated sub-daily climate data

Sub-daily data was interpolated from daily data. This, compounded by the need to estimate missing temperature values for TMD300201 and DO rainfall data, is another source of uncertainty.

2.4.4.5: Preferential flow not represented

The prediction performance also depends on the representation of subsurface and surface flows in the model. The version of DHSVM used in this work does not account for the preferential flow. Cuo *et al*. (2006) discussed the work by Beckers and Alila (2004) which explained the tradeoffs for model accuracy between peak flows versus base flows when the preferential flow was not represented.

2.5: Hydrologic flow paths: current conditions and scenarios

The hydrologic response at the main basin outlet to the current landcover and to the effect of forest-to-crop conversion was evaluated in terms of the water yields and spatial variation of soil moisture and evapotranspiration inside the basin.

2.5.1: Hydrologic dynamics under current conditions

The Mae Chaem River observed runoff ratio is approximately 19% of total rainfall, and 70% of the discharge appears as the wet-season flow (Table 2.6). Predicted annual yields from DHSVM, accounting for irrigation, were about the same as observed values. The runoff ratio was consistent with the 15-25% runoff ratio published in Alford's study of annual runoff in mountainous regions of northern Thailand (1992). However, in this simulation the high flow was overestimated by 9% and the low flow was underestimated by nearly 20%. The magnitude of forecasted flow was sensitive to the estimated irrigation consumption, as discussed earlier in section 2.4.4.

The simulated average annual evapotranspiration was 1016 mm, corresponding to 74% of basin-wide estimated precipitation. Evapotranspiration was highest in the period from May to August and reached minimum values in January and February. The seasonal trend is positively correlated with rainfall seasonality.

The spatial distribution of soil moisture and evapotranspiration was demonstrated in Figure 2.8. Direct observation indicates that soil moisture dynamics may follow spatial variation of rainfall across the basin. To analyze if spatial relationships exist, basin elevation data was categorized into 5 zones, and zonal means of simulated soil moisture and evapotranspiration were computed. Results showed that soil moisture was relatively high near the main channel and on the ridges and decreased towards midlands at 800-1200 m (Figure 2.9). The exception was the soil moisture in the second layer on a dry day (March 9, 1999), which had decreasing soil moisture with increasing elevation. There was no clear correlation between evapotranspiration and elevation zone.

Simulation results were sensitive to soil depths and soil lateral conductivity, indicating that the saturation excess overland flow could be an important mechanism for runoff production. The saturation excess area is expected to occur near the stream channel, with the size of the runoff source areas varying seasonally and during individual storm events. To evaluate the importance of saturation excess runoff, the spatial distribution of depth to the water table during both wet and dry periods (Figure 2.8) was analyzed. During a selected dry period (March 9, 1999), the water table depth intersected the surface (depth to water table < 0.01 m) primarily around the main and tributary channels. On the selected wet days October 30 and December 9, 1999, the saturation excess overland flow is evident on a larger portion of the basin, including wider areas around the main stem, near the basin outlet, and along the ridges, consistent with the higher precipitation. The occurrence of saturation excess overland flow on October 30, 1999 along the ridges is highly unusual. If this occurrence is valid, the flow was probably due to high antecedent moisture conditions caused by several preceding storm events. To determine the runoff mechanism more precisely, field observation should be made. In the absence of such additional observations, this occurrence should be treated as erroneous.

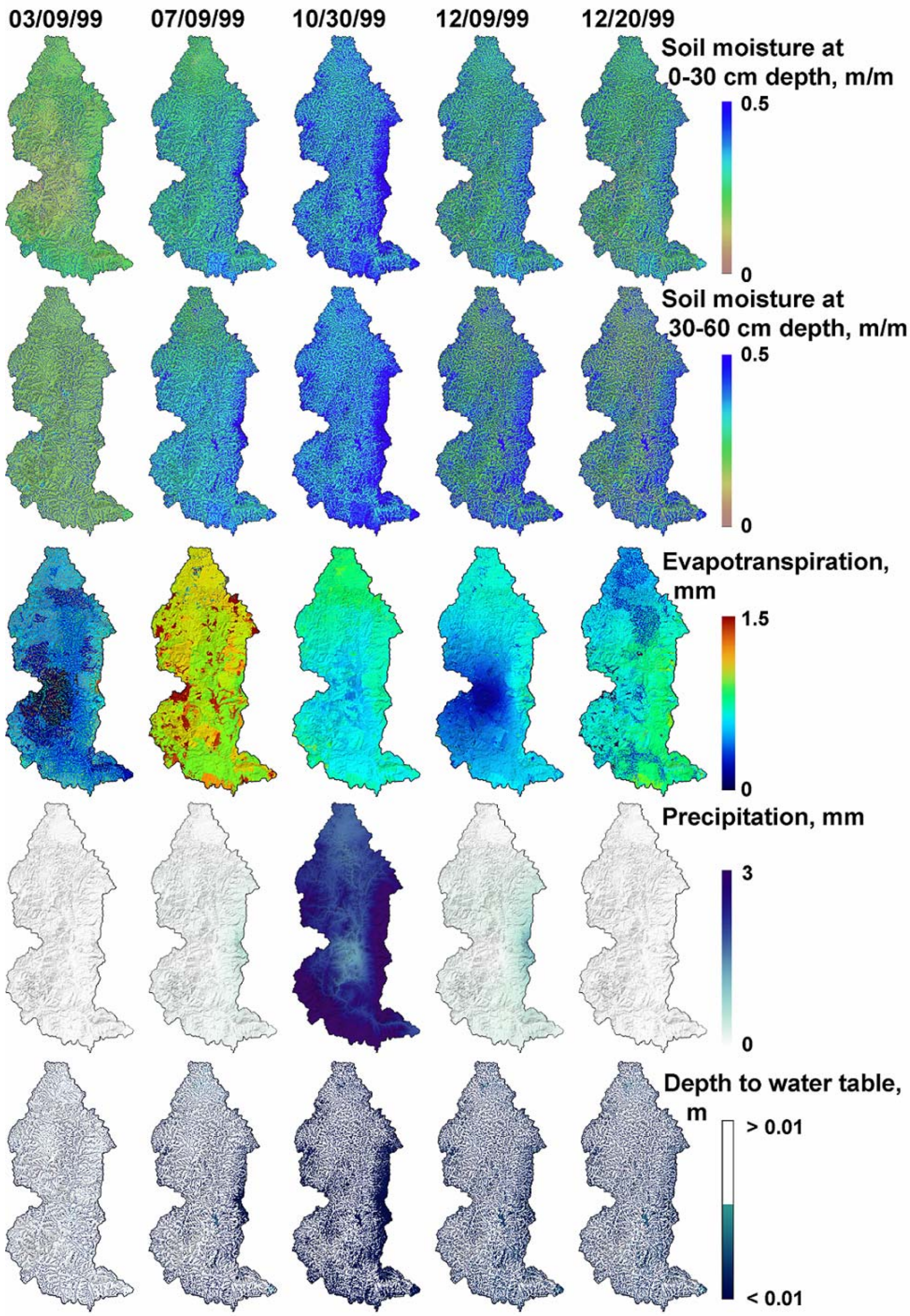

Figure 2.8. Illustration of the underlying dynamics changes in hydrographs, with soil moisture in the root zones at 0-30 cm, 30-60 cm, evapotranspiration, precipitation, and depth to water table (top to bottom). Values are at time = 0:00-3:00 and simulated on Veg 2000.

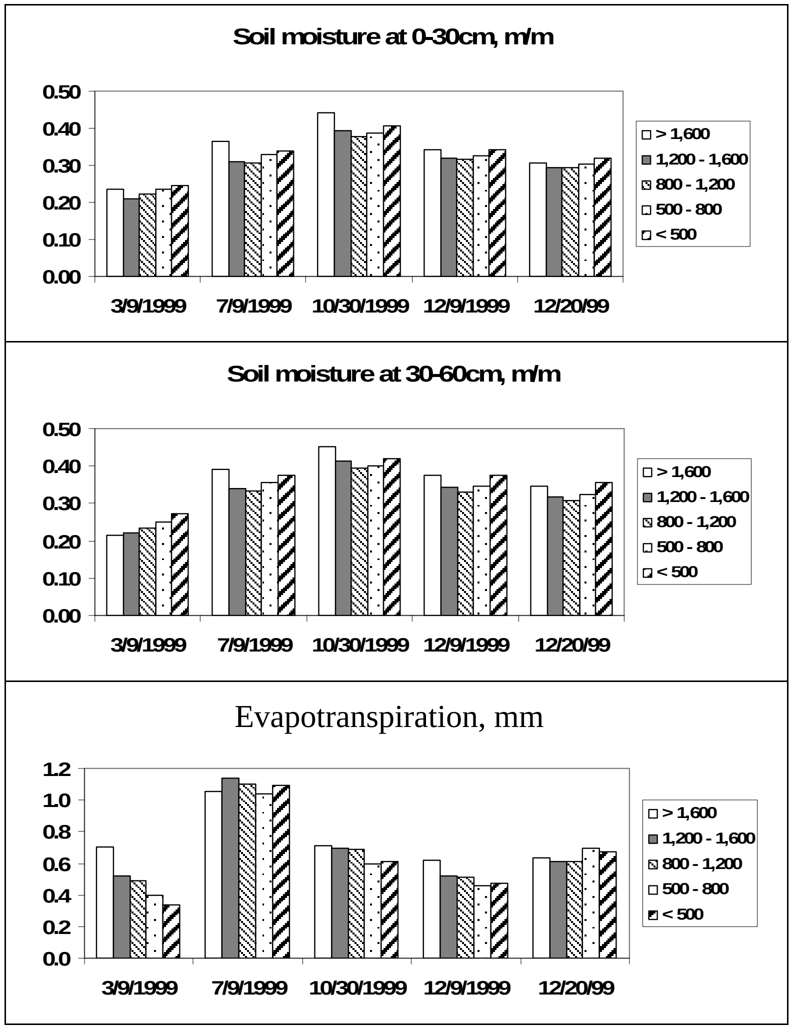

Figure 2.9. Temporal dynamics of evapotranspiration and soil moisture at 0-30 cm and 30-60 cm root depth and their correlations with elevation zone, simulated using Veg 2000.

2.5.2: Effects of landuse change on hydrologic responses

One of the most important concerns regarding forest-to-crop landuse change relates to water availability during the dry season. If the simulated unregulated flows for future scenarios with respect to the referenced Veg 2000 were compared, cropland expansion elevated the dry-season flow by about 4%, and slightly elevated the annual and wet-season flows (Table 2.6). The opposite trend was true when croplands were converted to forests as in Scenario I. The unregulated water yields among Scenarios II, III and IV were about the same although highland crop expansion (Scenario III) yielded slightly higher annual and wet-season flows compared to lowland-midland crop expansion (Scenario IV).

The next step was to consider the effect of irrigation. Under the current set of model parameters, it was demonstrated that increased croplands throughout the basin (Scenario II) caused a reduction in the regulated annual (-9%), wet-season (-6%), dry-season flows (-16%), and increase in evapotranspiration (+3%), compared to the simulation using Veg 2000 (Table 2.6). Scenario III resulted in about the same regulated annual and seasonal water yields as Veg 2000. When compared to Scenario IV, Scenario III yielded higher regulated annual (+8.6%), wet-season (+6%), and dry-season (+16%) flows. Simulations using Scenario II and IV produced about the same water yields.

The magnitude of differences in stream flow behavior among scenarios depends on the approximation of irrigation diversion. Thus, the unregulated water yields provided a reference for potential ranges of stream flows. The regulated to estimated unregulated flows were also compared. Low-season flow was a volatile component and available yields at the basin outlet varied from 77% of unregulated flow under Veg 2000, to 74% under Scenario III, and to 62% on Scenarios II and IV. Wet-season discharge was less sensitive and the flow remaining after diversion was about 90% of unregulated flow in each case. Evapotranspiration was 4% higher than the non-irrigated case for Veg 2000, and about 5-7% higher for Scenarios II - IV.

Table 2.6. Potential value ranges of basin hydrology simulated on different landcover scenarios, with and without irrigation based on water year (November – October).

Landcover scenarios		Average hydrologic components (hydrologic year 1997 – 2000)				
		Annual yield, mm (m^3/s)	High flow, m^3/s	Low flow, m^3/s	Annual evapotranspiration, mm	Runoff ratio b
Observed		257 (31.3)	45.8	18.1	750 c , 1230 d	0.19
Veg 2000	Irrigated	259 (31.6)	50.0	14.7	1016	0.19
	Unregulated	294 (35.8)	54.1	19.1	981	0.21
Scenario I	Unregulated	286 (34.9)	53.1	18.3	988	0.21
Scenario II	Irrigated	237 (29.0)	47.0	12.3	1042	0.17
	Unregulated	300 (36.6)	54.8	19.8	975	0.22
Scenario III	Irrigated	256 (31.2)	49.6	14.2	1020	0.19
	Unregulated	301 (36.8)	55.1	19.8	973	0.22
Scenario IV	Irrigated	235 (28.6)	46.5	12.1	1045	0.17
	Unregulated	297 (36.2)	54.3	19.6	978	0.22

a Based on percentage of irrigated croplands in Table 2. Veg 2000: re-processed 2000; Scenario I: conversion from crops to forest;
Scenario II: double crop areas; Scenario III: more upland crops; Scenario IV: more lowland crops.
b Based on the average 1997-2000 simulated basin-wide rainfall of 1376 mm
c Hill evergreen forest in Chiang Mai (Tangtham,1999) d Typical mountainous watershed, excluding cloud forests (Tangtham,1999)

2.6: Discussion and conclusions

Landuse change in Mae Chaem has largely featured agricultural transformations in different altitude zones. Highland pioneer shifting cultivation has been replaced by expanded permanent fields producing commercial horticultural crops, often with seasonal sprinkler irrigation. While some midland rotational forest fallow shifting cultivation systems remain, others have been replaced by rainfed permanent plots producing subsistence and commercial field crops. Irrigated paddy has expanded where terrain allows, and lowland agriculture has increased dry-season water use for irrigated rice, cash crops and fruit orchards.

Objective 1. Basin hydrologic regime.

The DHSVM hydrology model was used as a tool for analyzing impacts of forest-to-crop conversion, and vice versa, on basin hydrology and water availability at the basin outlet. As would be expected in such a steep basin, topography is the primary factor controlling climatic, vegetation, and, consequently, spatial variation of Mae Chaem's hydrologic components. Saturated overland flow was the predominant flow path for water into streams. That said, this work assumed agricultural practices do not cause significant soil compaction, which would lower infiltration rate and vertical hydraulic conductivity and would induce Horton overland flow. Additional study on the extent and effects of soil compaction may increase the accuracy of the simulation. Irrigation diversion is the most direct influence on discharge magnitude, and it causes vegetation scenario water yields ranges to significantly vary. Discharge magnitude is sensitive to assumptions on the percentage of area irrigated, crop types, and crop water needs. The basin hydrology is sensitive to changes in landcover attributes, with a general pattern of increasing unregulated runoff with migration from trees to crops due to decreasing evapotranspiration. Rainfed upland agriculture, especially in the midland zone, does not appear to result in lower water availabilities downstream. This is in agreement with the conclusion from Walker (2002) that while the forest clearing to agriculture may alter the stream flow pattern, it does not necessarily cause a decline in the dry-season water supply. The net effect depends on whether the benefit of reduced evapotranspiration outweighs the cost of reduced infiltration. Under current irrigation schemes, highland crop expansion (>1,000 m.a.s.l.) may lead to slightly higher seasonal and annual yields than lowland-midland crop expansion.

Objective 2. Assessment of the utility of a distributed, physically-based model as a management tool.

The utility of a spatially-explicit, process-based analytical modeling environment is demonstrated by its ability to reproduce hydrographs across a range of conditions, in a basin where data are relatively sparse. Though the model performance at the two sub-basins is lower, the simulation results at the main basin outlet show that the efficacy of the model as an intelligent data-interpolation engine is clear. That the model does as well as it does basin-wide implies that the constituent dynamics are relatively well-understood over a large and complex watershed and some confidence can be placed in the quantitative implications of the scenarios. This modeling approach can be useful in assessing the influence of spatial configuration or fragmentation of landcovers.

Chapter 3: Spatially distributed modeling of dissolved nitrogen export from watershed: Design and development of D-SEM

3.1: Introduction

Excessive nitrogen (N) loading into streams, rivers, lakes, and coastal water enriches surface water and contributes to the increased bioactivity of primary producers in surface waters. Eutrophication leads to algae blooms and can lead to hypoxic conditions, such as the dead zone in the Gulf of Mexico (Mitsch *et al*., 2001).

Stream N characteristics are a function of anthropogenic activities in the watershed, vegetation, hydrologic control, and in-stream processes. Researchers have used stream N records to address the effects of atmospheric deposition and climate influence (Mitchell *et al*., 1996; Swank and Vose, 1997) and non-point sources from urban and agricultural landuse (Tufford *et al*., 1998; Boyer *et al*., 2002; Brett *et al*., 2005). In forested systems with low atmospheric inputs, N export is influenced by vegetation succession (Cairns and Lajtha, 2005; Liles, 2005). In the Pacific Northwest, indigenous species such as the N-fixing Red Alder (Alnus rubra) take root as early successional species in riparian zones after logging activities. Studies have shown the impact of Red Alder presence along the headwater streams in the Olympic Peninsula (Volk, 2004) and the correlation of annual N export to the total broadleaf cover in the Salmon River basin of the Oregon Coast Range (Compton *et al*., 2003). Newbold *et al*. (1995) studied the relationships between seasonal nitrate concentration and discharges in northwestern Costa-Rica and observed the spikes in nitrate concentration associated with high discharge events. Vanderbilt *et al*. (2003) also found that annual discharge was a positive predictor of stream dissolved organic nitrogen concentrations in watersheds in H.J. Andrews Experimental Forest in Oregon. Peterson *et al*. (2001) illustrated the rapid uptake and transformation of in-stream inorganic nitrogen using $^{15}N^{-}$tracer study in headwater streams throughout North America.

Both statistical and deterministic models are used to aid in understanding the impacts of those factors in the nitrogen export process. Deterministic models simulate known N sources, transport and loss over time. Models such as the Soil Water Assessment Tool or SWAT (Neitsch *et al*., 2000) and Agricultural Non-Point Source Pollution Model (AGNPS) (Young *et al*., 1995) have been developed to aid understanding N in terms of water quality and work well in homogeneous environments with well documented N sources such as agricultural lands. However, these models do not perform well in watersheds with mixed landcover (eg. forests, grasslands, urban) and varied landuse and, therefore, are generally not used for stream N export prediction in mixed ecosystems (Li *et al*., 2004). On the other hand, the biogeochemical model CENTURY (Parton *et al*., 1988) is widely used for N cycling studies and focuses on linking the N biogeochemical processes with the soil organic matter pools which are not easily measurable. In addition, the model is developed at a plot scale and is not easily scaled up spatially.

The statistical approaches such as N export coefficient (Johnes, 1996) are simple to apply; however, they are limited in that the export flux is specific to the location and as such must be customized for each particular site, and do not lend to scalability or scenario analysis.

To better understand the N export process in a watershed-scale of diverse landscape composition, we need a model that captures the landscape heterogeneity. The model described in this chapter, the DHSVM Solute Export Model (D-SEM), was developed in order to generate a viable N export model based on a mixture of heterogeneous inputs such as vegetation cover, soil types and landuse. One of the major benefits to D-SEM is the ability to easily model landuse changes, and forecast the impact of such landuse changes on the N cycle and N export.

3.2: D-SEM structure

The model, D-SEM consists of biogeochemical representations for terrestrial and in-stream systems (Figure 3.1). D-SEM stands for the DHSVM Solute Export Model, DHSVM being the Distributed Hydrology Soil Vegetation Model which was described in Chapter 2 is the hydrologic model used as the base platform on which D-SEM was created.

Terrestrial nitrogen (N) cycling models can generally be categorized into three groups, based on the scale of available laboratory to field data (Parton *et al*., 1996). The microbial growth models simulates N dynamics using explicit representations of microbe and plant activities responsible for nutrient recycling processes such as nitrification and denitrification. Soil structural models describe physical processes such as gas and solute diffusions into the soil aggregates based on detailed advection-dispersion-reaction representations. The first two approaches usually draw on laboratory data to obtain time-series mass transfer rates, microbial dynamics and other physical parameters necessary to test, validate, or parameterize the models. On the other hand, simplified process models represent N cycling processes as a function of soil water, temperature, and pH controls on microbial activities without actually modeling the explicit microbe dynamics. The last category of models is usually used to simulate field experimental data.

In this study, a simplified process-based distributed model representation of carbon-nitrogen interactions in terrestrial and stream systems is developed, and the equations describing biogeochemistry are based on other existing models. The biogeochemical model is then integrated within DHSVM at the same spatial resolution.

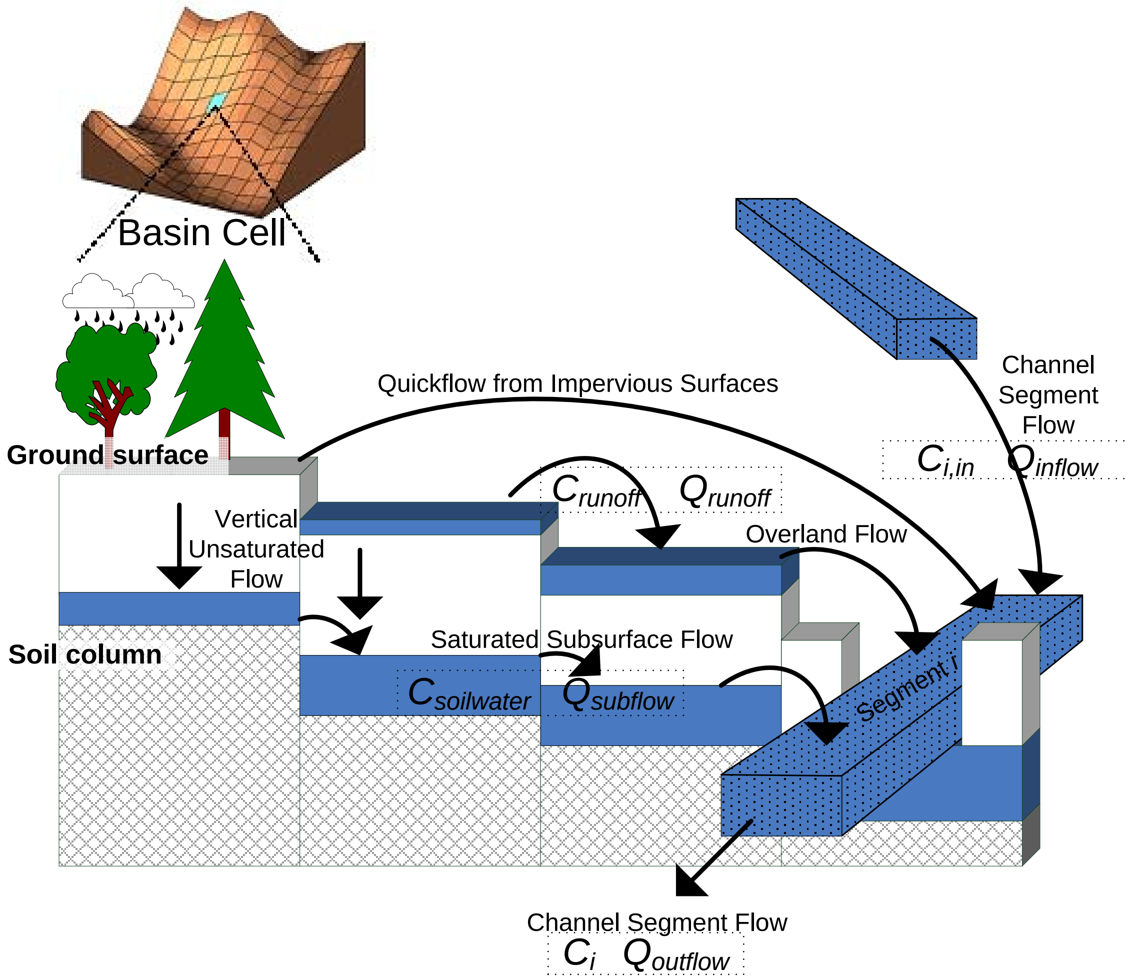

Figure 3.1. D-SEM System representation for terrestrial and stream.

The Terrestrial system is divided into a ground surface and soil column. There are 14 simultaneous ordinary differential equations describing the temporal dynamics of 9 state variables (Table 3.1) in the ground surface, soil column, and stream segment nutrient pools.

Table 3.1: State variables and their presences in ground surface, soil, and segment pools.

State variable	Symbol	Unit	Pool
Metabolic detrital organic carbon mass	$[MetDetrC]$	kg C	Ground surface
Structural detrital organic carbon mass	$[StrucDetrC]$	kg C	Ground surface
Metabolic detrital organic nitrogen mass	$[MetDetrN]$	kg N	Ground surface
Structural detrital organic nitrogen mass	$[StrucDetrN]$	kg N	Ground surface
Dissolved organic carbon mass	$[DOC]$	kg C	Soil Stream
Dissolved organic nitrogen mass	$[DON]$	kg N	Soil Stream
Ammonium mass	$[NH_4]$	kg NH_4	Soil Stream
Nitrite mass	$[NO_2]$	kg NO_2	Soil Stream
Nitrate mass	$[NO_3]$	kg NO_3	Soil Stream

3.2.1: Terrestrial system representation

The terrestrial system consists of 2 nutrient reservoirs which are the ground surface layer and soil column. The state variables are the total mass of constituents in each reservoir.

Instead of having multi-layered soil nutrient reservoirs like the multi-layered soil water pools in the hydrologic computation, all soil layers, excluding the deep soil below the root zones, are considered a single nutrient reservoir. The values of soil attributes and soil moisture from all layers are averaged and used as representative values for a specific pixel.

The major input variables required for D-SEM are soil temperature, soil moisture, and water fluxes obtained from the DHSVM. Nutrient forcing is described in the following section and other requirements are described later in section 3.

3.2.1.1: Nutrient inputs

Four major nutrient sources are represented in D-SEM: litterfall, atmospheric deposition, anthropogenic point and non-point sources, and biological N fixation. The first 3 sources are described in this section whereas N-fixation is described in section 3.2.1.3.

The ground surface pool of litterfall provides the nutrients from the leachate of decomposed litterfall. An additional source of nutrients comes from atmospheric deposition, which is enriched as precipitation moves through plant canopies, (Dalva & Moore, 1991; Koprivnjak and Moore, 1992, McDowell and Likens, 1988). The load of atmospheric inputs was calculated based on monthly values of basin-wide throughfall-enriched atmospheric concentrations. If no information on the enrichment ratio was available, then, the load of each species was equal to the product of actual atmospheric concentration and precipitation.

These input sources are mixed with the rainfall and snowmelt to determine the concentrations in water infiltrating and running off the ground surface. If the water balance results in a net flow of water into the soil surface, then the actual amount entering the soil column is the product of that concentration and the water inflow.

In addition to vegetation and atmospheric inputs, non-point and point sources can also be included. Non-point sources, such as septic loads are represented on a per pixel basis. The mechanism relies on having dynamic maps of population density, source type maps, and a time-series characterization of the source properties associated with corresponding source types. At each time step, the non-point load added to the soil of each pixel is the product of constituent concentration, effluent volume per capita, and the size of population. The point source loads are also based on time-series of water and the concentration of species, but the loads are added to specific locations in the landscape. The size of soil nutrient reservoir after accounting for the transfer to or from the ground is the base value for calculations of other internal processes described below.

Once the nutrients enter the soil, they are subjected to mass change due to the biogeochemical processes described in sections 3.2.1.2 and 3.2.1.3. After the biogeochemical transformation for the time step is completed, the dissolved portion of the constituents moves into the stream network with the surface and sub-surface runoff.

3.2.1.2: Terrestrial carbon cycle

The carbon cycle is included because of its interrelationship with the nitrogen cycle via stoichiometric constraints on microbial processes. This section and section 3.2.1.3 provide descriptions of how each biogeochemical process is represented. The actual mathematic representation is included in Appendix 1.

The carbon-nitrogen cycle (Figure 3.2, Figure 3.3) is based on a modification and combination of existing models including the Riparian Ecosystem Management Model (REMM) (Inamdar *et al*., 1999 (a,b)), which is largely based on CENTURY, and SWAT. Vegetation residue pools from litterfall are divided into a recalcitrant structural and a quickly decomposable metabolic residue pool, each with different decay rates and carbon to nitrogen (C/N) ratios. Instead of focusing on the 3 different humus pools of different decay rates, our interest is in the mobile dissolved organic carbon pool. Plant litter from overstory and understory is added to these residue pools on a sub-daily basis. The partitioning of the fresh litter into structural or metabolic pools is determined by the lignin-to-nitrogen ratio of the litter (Inamdar *et al*., 1999-b).

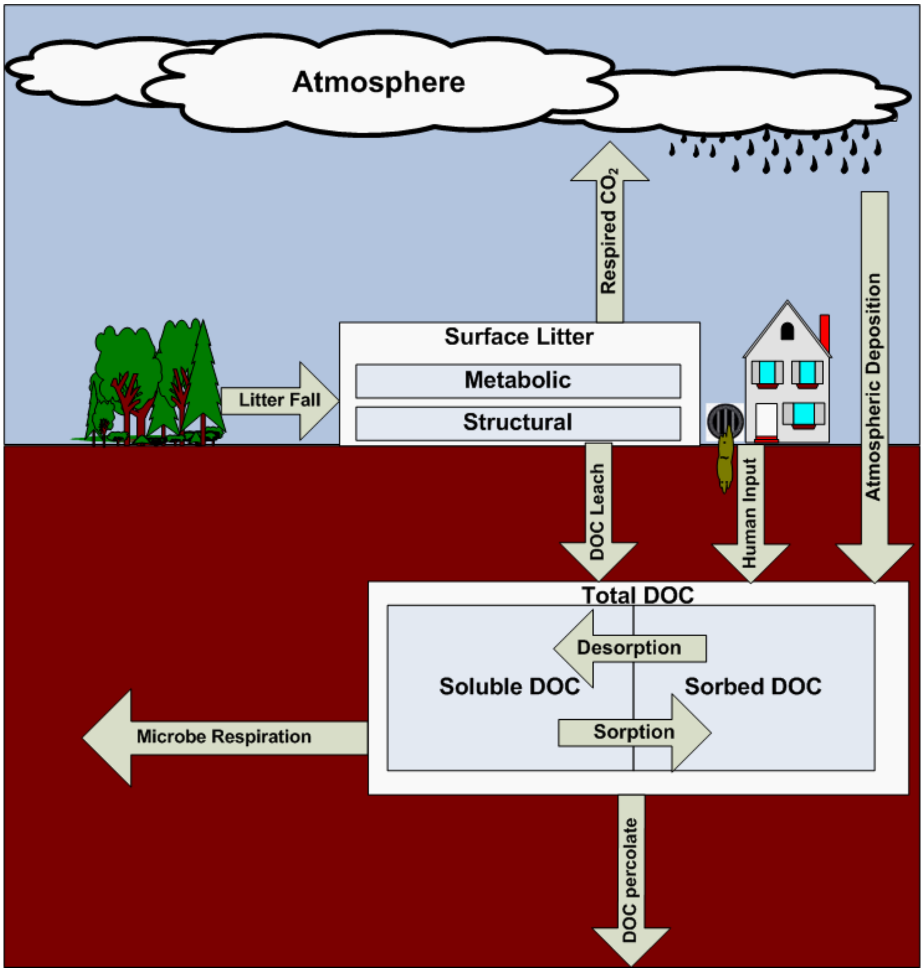

Figure 3.2: Terrestrial carbon cycle representation

Decomposition of the detrital pools is simulated with a first order rate equation, controlled by soil temperature and soil moisture of the top soil layer, both of which were computed during the hydrologic simulation. For metabolic pools, the rate was also influenced by the availability of nitrogen in the litter and the soil inorganic nitrogen in the top soil layer. As decomposition of the litter takes place, a portion of the C is mineralized and lost as CO_2 to the atmosphere. The other part of decomposed detrital organic C turns into DOC and leaches into the soil column. The partitioning between the DOC leachate and the mineralized CO_2 was based on the work by Currie and Aber (1997).

In the soil column, biological consumption of DOC as well as physical sorption processes were considered. The microbe aerobic respiration of DOC is also first-order rate controlled by soil temperature and soil moisture.

Studies have shown that DOC sorption follows an initial mass isotherm (Nodvin *et al.*, 1986; Neff and Asner, 2001) and is also controlled by the hydrologic flux through the soil ((Neff and Asner, 2001). The extent of sorption also depends on the soil organic carbon content, with lower sorption at higher organic content due to competition for sorption sites and because organic carbon has a higher affinity to mineral sites. Because of this, a simplified scheme to represent sorption as a function of soil type and saturation extent (which was chosen as a representative of how fast water flows through the soil column) was developed. The major assumption was the instantaneous equilibrium relationship between soluble and sorbed forms of DOC at each time step. Therefore, instead of tracking the pools of soluble and sorbed DOC explicitly, the effect of sorption on the soluble fraction of DOC was calculated only when DOC was removed out of the soil column in a soluble form. The soluble fraction was calculated by multiplying the maximum soluble fraction, the value of which is dependent on soil type, by the soil water saturation extent. In addition, the maximum solubility of DOC in water was set. This sorption function is intended to be the key for simulating the flushing effect of nutrients during fall quarter.

3.2.1.3: Terrestrial nitrogen cycle

The atmospheric inputs of dissolved inorganic and organic nitrogen are computed the same way as for the carbon pool, and also enter the soil column with infiltration from rainfall and snowmelt (Figure 3.3).

Detrital and dissolved organic nitrogen pools are complementary to the carbon pools, and the sizes of the nitrogen pools are dependent on the size of the carbon pools and their respective C/N ratios. Mineralized detrital and dissolved organic nitrogen is added to the ammonium pool, in proportion to transformations of C and C/N ratios.

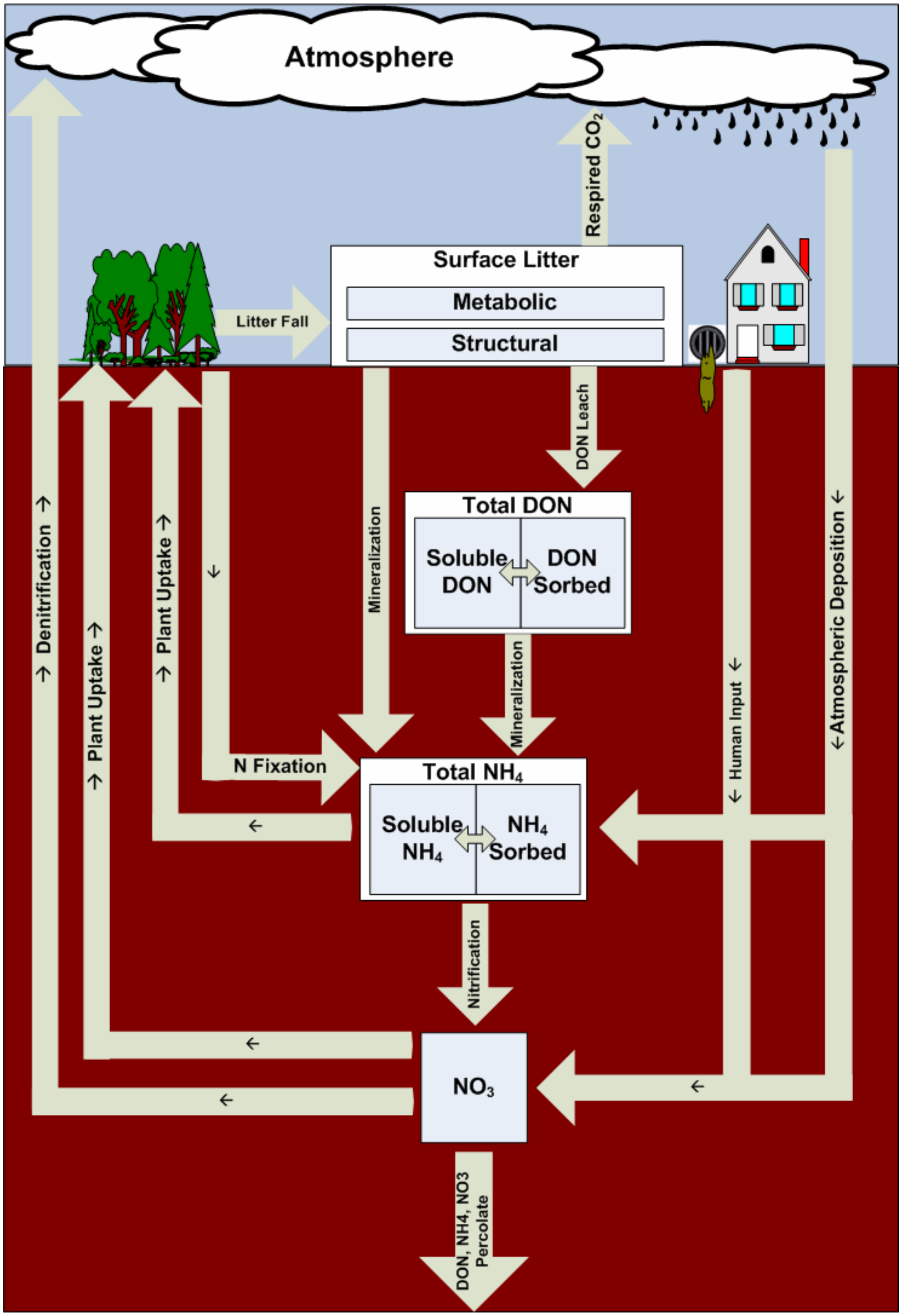

Figure 3.3. Terrestrial nitrogen cycle representation

N-fixation by bacteria living in root nodules of trees contributes inorganic nitrogen by converting atmospheric nitrogen to ammonia. For the model, it is assumed that N-fixation occurs primarily due to Red Alder. Nitrogen fixation by Red Alder is controlled by sunlight, soil moisture level, temperature, phosphorus availability, stand density, and symbioses (Binkley *et al*., 1994). It is not conclusive that nitrogen fixation in forests is suppressed by the increasing soil nitrogen level (Pastor & Binkley, *et al*., 1998). The range of nitrogen fixation under Red Alder is 50-100 kg/ha-yr in mixed stands and 100-200 kg/ha-yr in pure stands (Binkley *et al*., 1994). Sharma *et al*. (2002) reported N-fixation in mixed stands of of Himalayan Alder-cardamom increased from 52 kg/ha-yr for a 5 year-old stand to 155 kg/ha-yr in a 15 year-old stand, and then declined to 58-59 kg/ha-yr for 30- and 40-year-old stands. Red Alder N-fixation increases with plant maturation but then slow downs as the plant ages above 50 years (Edmonds, personal communication). Based on these studies, the formula for N-fixation was developed as a multiplication of referenced N-fixation values of pure Red Alder stands and factors accounting for the control on rates by average stand age, fraction of N-fixing trees in the land pixel, and the temperature (for seasonality).

Based on the Soil and Water Assessment Tool or SWAT model, the total amount of nitrification and ammonia volatilization is calculated and then partitioned between the two processes, using a combination of the methods developed by Reddy *et al*. (1979) and Godwin *et al*. (1984). Nitrification is a function of soil temperature and soil water content while ammonia volatilization is a function of soil temperature and depth.

Denitrification is a process in which NO_3 and other nitrogen oxides are reduced to nitrogen gas via anaerobic fermentation of organic substrates (Parton *et al*., 1996). The D-SEM representation of denitrification is modified from Hénault and Germon (2000) as a multiplicative function of soil potential denitrification flux and dimensionless factors for temperature, soil moisture, anaerobic condition, and nitrate availability.

Michealis-Menton saturation kinetics are assumed to be the mechanics of plant NH_4 uptake. For NO_3 uptake, the model used is a modified yield based approach from Hydrologic Simulation Program-Fortran (HSPF) (Bicknell *et al*., 1993). In the original yield-based approach, which is meant for crops, the annual target crop N need is specified, and then is divided into monthly N needs based on the growing season period. The actual nitrogen uptake per time step is computed by down-sampling the aggregate monthly rates. A modified yield-based approach was chosen due to the benefits of unified equations that can be applied to both crop and forest type vegetations. Normally for crop type vegetation, the known information about the crop uptake is the start date of growing season, the duration of rapid growth period, the time it takes for the crop to reach maximum N uptake rate, and the maximum N accumulation in the biomass (Figure 3.4-a). Using this information, N-uptake flux was represented by Gaussian distribution functions (Figure 3.4-b) with the magnitude proportional to the maximum N accumulation in the crop, the location of N uptake peak corresponding to the time required to reach the maximum N uptake rate, and the location of the tails proportional to the duration of rapid crop growth phase. The equation was formulated and tested by plotting the daily N and cumulative N uptake in Excel (Microsoft Corporation) and comparing to N uptake profiles given for winter wheat, hops, and broccoli, which are common Pacific Northwest crops (Sullivan *et al*., 1999).

In the case of forest vegetation, the Gaussian distribution represents the annual seasonality in N uptake. Thus, the maximum N accumulation would be equivalent to the total annual nitrogen uptake rate.

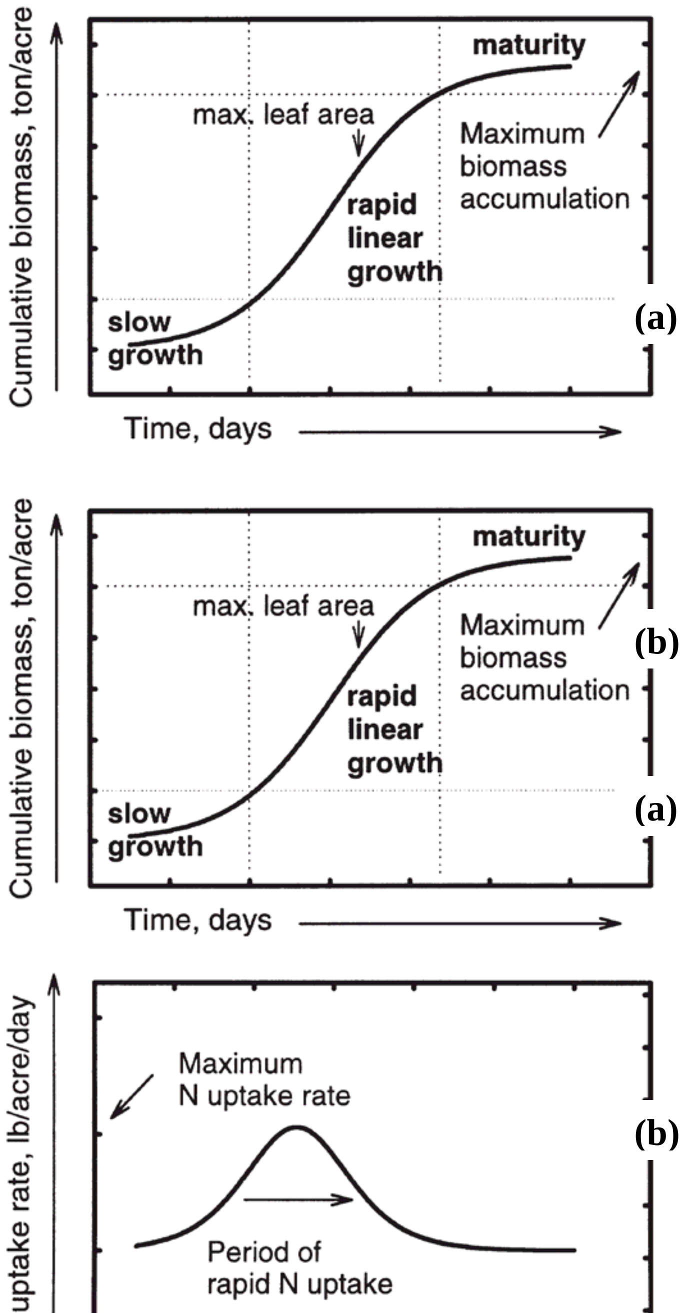

Figure 3.4. Schematic diagram to represent Gaussian distribution of NO_3 uptake rate (Sullivan *et al.*, 1999)

Although studies have shown some plants can also uptake DON directly, specifically amino acids, without relying on microbial mineralization (Neff *et al*., 2003; Lipson and Näsholm 2001; Nordin *et al*., 2001), this study assumed no DON uptake by vegetation.

The sorption of DON was represented by the same approach as that of DOC. Studies have shown that the hydrophobic dissolved organic matter (DOM) is preferentially sorbed over more N-enriched hydrophilic DOM (Murphy *et al*., 2000; Neff *et al*., 2003) and the net sorption results in lower C/N in non-sorbing DOM (Kaiser and Zech, 2000). Therefore, the maximum soluble fraction of DON will be set at a higher value than that of DOC to represent the preferential sorption. Matschonat and Matzner (1995) found that the pattern of ammonium sorption also fits the initial mass isotherm. Consequently, the same sorption representation that was used for DOC and DON was applied for NH_4. On the other hand, nitrate is generally highly mobile due to the weak tendency of NO_3 to form surface complexes. However, the work by Strahm and Harrison (2006) has shown that nitrate sorption could occur in acidic soil containing variable charge minerals, such as in soils under the coniferous forest of the Pacific Northwest. In D-SEM, sorption of NO_3 was expressed by setting the maximum soluble fraction to less than 1.

3.2.1.4: Terrestrial mass balance equations

In each grid cell, mass balances of metabolic and structural detrital organic carbon and nitrogen in the ground surface pools are calculated, along with the mass balance of DOC, DON, NO_2, NO_3, and NH_4 in the soil column.

$$
\begin{aligned}
\frac{d\left[MetDetrC\right]_G}{dt} &= MetDetrCLitterInput - MetDetrCDecomp \\
\frac{d\left[StrucDetrC\right]_G}{dt} &= StrucDetrCLitterInput - StrucDetrCDecomp \\
\frac{d\left[MetDetrN\right]_G}{dt} &= MetDetrNLitterInput - MetDetrNDecomp \\
\frac{d\left[StrucDetrN\right]_G}{dt} &= StrucDetrNLitterInput - StrucDetrNDecomp \\
\frac{d\left[DOC\right]_L}{dt} &= M_{[DOC],atm} + M_{[DOC],PS} + M_{[DOC],NPS} + LitterLeachedDOC - soilDOCresp \\
\frac{d\left[DON\right]_L}{dt} &= M_{[DON],atm} + M_{[DON],PS} + M_{[DON],NPS} + LitterLeachedDON - soilDONmineraliz \\
\frac{d\left[NH_4\right]_L}{dt} &= M_{[NH_4],atm} + M_{[NH_4],PS} + M_{[NH_4],NPS} + soilDONmineraliz + N_2\,fixation \\
&\quad + MineralizMetDetrN + MineralizStrucDetrN - NitriAndVolatilz - NH_4PlantUptake \\
\frac{d\left[NO_3\right]_L}{dt} &= M_{[NO_3],atm} + M_{[NO_3],PS} + M_{[NO_3],NPS} + Nitri - NO_3lsDetrDecomp - NO_3PlantUptake - Denitrif \\
\frac{d\left[NO_2\right]_L}{dt} &= M_{[NO_2],atm} + M_{[NO_2],PS} + M_{[NO_2],NPS}
\end{aligned}
$$

$[i]_G$ and $[i]_L$ are the ground surface pool and soil pool of species *i* (see Table 3.1 for units). $M_{[i],atm}$, $M_{[i],PS}$, and $M_{[i],NPS}$ are nutrient inputs of species *i* from atmospheric deposition, point source, and non-point source respectively. The rest of the terms are the mass change of species due to biogeochemical processes. Their descriptions and the mathematical representation are in Appendix 1.

Mass balance of each species was done on a basis of mass of chemical species. However, all the input concentrations, reported terrestrial nitrogen loads, and reported stream nitrogen loads and concentrations are presented in mass as carbon and mass as nitrogen, for carbon and nitrogen species respectively.

3.2.2: Stream system

The channel routing of constituents is based on a finite volume (box model) approach with individual stream segments as individual control volumes. Constituent inflow to each channel segment at each time step consists of the constituent entering from the upstream segment and the lateral terrestrial inputs (Figure 3.1).

3.2.2.1: In-stream carbon and nitrogen cycles

In-stream biogeochemical processes are simplified (Figure 3.5), by modifying the carbon and nitrogen representations from the QUAL2K model, developed by the Environmental Protection Agency (EPA). The presence of floating and attached algae was neglected as well as the exchange of constituents with the benthic sediments or suspended particulate matters. Instead of doing a mass balance of dissolved organic matter in terms of biochemical oxygen demand, dissolved organic carbon and dissolved organic nitrogen concentrations are computed explicitly. Stream temperature was computed based on energy balance. The temperature-dependent rate constants follow Streeter-Phelps formulation.

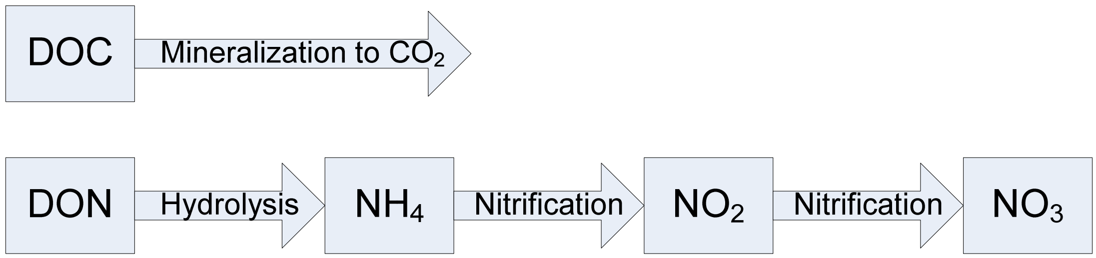

Figure 3.5. Simplified in-stream carbon and nitrogen cycles

3.2.2.2: In-stream mass balance equations

$$\frac{d[DOC]_S}{dt} = M_{[DOC],INFLOW} + M_{[DOC],LATINFLOW} - M_{[DOC],OUTFLOW} - streamDOCresp$$

$$\frac{d[DON]_S}{dt} = M_{[DON],INFLOW} + M_{[DON],LATINFLOW} - M_{[DON],OUTFLOW} - streamDONhydr$$

$$\frac{d[NH_4]_S}{dt} = M_{[NH_4],INFLOW} + M_{[NH_4],LATINFLOW} - M_{[NH_4],OUTFLOW} + streamDONhydr - streamNitri1$$

$$\frac{d[NO_2]_S}{dt} = M_{[NO_2],INFLOW} + M_{[NO_2],LATINFLOW} - M_{[NO_2],OUTFLOW} + streamNitri1 - streamNitri2$$

$$\frac{d[NO_3]_S}{dt} = M_{[NO_3],INFLOW} + M_{[NO_3],LATINFLOW} - M_{[NO_3],OUTFLOW} + streamNitri2$$

where $[i]s$ is the mass of species *i* in the segment pool (see Table 3.1 for units),

$M_{[i],INFLOW}$ is the mass rate of inflow of species *i* from the upstream segment in $\frac{kg}{timestep}$,

$M_{[i],OUTFLOW}$ is the mass rate of outflow of species *i* to the downstream segment in $\frac{kg}{timestep}$, and $M_{[i],LATINFLOW}$ is the total mass rate of lateral inflow of species *i* from the watershed (from subsurface and surface runoffs) in $\frac{kg}{timestep}$. $streamDOCresp$ represents the rate of respiration of DOC, $streamDONhydr$ is the rate of mineralization of DON to

NH_4, $streamNitri1$ is the rate of nitrification conversion from NH_4 to NO_2 and $streamNitri2$ is the rate of nitrification conversion from NO_2 to NO_3. The units of all in-stream rates of reactions are in $\frac{kg}{timestep}$. Detailed process representation is in Appendix 1.

3.3: Input requirements

In Chapter 2 section 2.3, detailed explanation of input requirements for the hydrology part is given. For the chemistry side, input data includes spatial characteristics data, anthropogenic forcing, global constants, and initial mass of each constituent in the ground surface, soil, and stream segment pools.

Spatial characteristics data vary by grid cell, but remain constant throughout the simulation. They include attributes associated with the same vegetation and soil type maps used for the water balance computation (Table 3.2 and Table 3.3). In the actual modeling application, those attribute values will be derived from or based on field data or literature values. The anthropogenic forcing includes temporally varying source input rates and source properties (composition) for point-source and non-point sources (Table 3.4). For point-source loading, specific locations in the landscape need be indicated, whereas monthly maps of population density and a source-type map are given for non-point loading calculation.

Global constants (Table 3.5) are rate constants for kinetics-controlled processes, and monthly concentrations of atmospheric depositions of all constituents. Initial concentration or mass of constituents in the terrestrial system and stream segments also need to be specified.

Table 3.2. List of vegetation attributes for individual vegetation types.

Parameter	Description*
Fraction alder	Fraction of stand that is Red Alder (0-1) for each layer
Average stand age	Average stand age for each layer, year
Lignin nitrogen mass ratio	Lignin to nitrogen mass ratio for each layer, $\frac{mgLignin}{mgN}$
Overstory litter carbon fraction	Mass fraction of carbon (0-1) in each pool of overstory litter
Overstory DOC leachate fraction	Fraction (0-1) of decomposed detrital organic carbon that turns into DOC for each pool of overstory litter
Understory litter carbon fraction	Mass fraction of carbon (0-1) in each pool of understory litter
Understory DOC leachate fraction	Fraction (0-1) of decomposed detrital organic carbon that turns into DOC for each pool of understory litter
Annual litterfall mass	Annual litterfall mass flux for each layer, $\frac{kg}{m^2 - yr}$
Overstory DON leachate fraction	Fraction (0-1) of decomposed detrital organic nitrogen that turns into DON for each pool of overstory litter
Understory DON leachate fraction	Fraction (0-1) of decomposed detrital organic nitrogen that turns into DON for each pool of understory litter
Overstory litter CN ratio	Carbon to nitrogen mass ratio for each pool of overstory litter
Understory litter CN ratio	Carbon to nitrogen mass ratio for each pool of understory litter
Nitrogen fixing reference rate	Nitrogen fixing reference rate, $\frac{kgN}{ha - yr}$
Growing season start day	Start day of growing season in Julian day of the year
Growing season length	Rapid growing season length in number of days

Table 3.2 continued

Parameter	Description*
Maximum nitrogen uptake delay	For crop type: number of days from crop seedlings or transplanting until the crop reaches the maximum nitrogen uptake rate For forest type: number of days from the start of growing season until the high nitrogen uptake season
Maximum nitrogen accumulation	Maximum nitrate-nitrogen accumulation, $\frac{kgN}{m^2}$
Maximum ammonium uptake constant	Michaelis-Menten maximum ammonium intake flux, $\frac{kgN}{m^2-3h}$
Half-rate ammonium uptake constant	Michaelis-Menten constant at half-maximum ammonium intake flux, $\frac{kgN}{m^3}$
Overstory monthly litter fraction	Fraction of annual flux of overstory litterfall for each month (January – December)
Understory monthly litter fraction	Fraction of annual flux of overstory litterfall for each month (January – December)

*If parameters are required for each vegetation layer, the first value is for the overstory, the second for the understory. If the parameters are specific to either overstory or understory, the first and second values are for the metabolic and the structural pools respectively.

Table 3.3. List of soil attributes for individual soil types.

Parameter	Description
DOC sorption coefficient	Dimensionless sorption coefficient for DOC (0-1) for each soil layer
DON sorption coefficient	Dimensionless sorption coefficient for DON (0-1) for each soil layer
Ammonium sorption coefficient	Dimensionless sorption coefficient for ammonium (0-1) for each soil layer

Table 3.4. List of time-series source properties for point and non-point sources.

Parameter	Description
Effluent water rate	Effluent input rate for point source or for non-point source, $\frac{m^3}{capita - timestep}$
Temperature	Temperature in Celsius
DOC concentration	DOC concentration, $\frac{mgC}{L}$
DON concentration	DON concentration, $\frac{mgN}{L}$
NH_4 concentration	NH_4 concentration, $\frac{mgN}{L}$
NO_3 concentration	NO_3 concentration, $\frac{mgN}{L}$
NO_2 concentration	NO_2 concentration, $\frac{mgN}{L}$

Table 3.5. List of global rate constants for processes and the throughfall concentrations

Parameter	Description
Metabolic detrital organic carbon decomposition rate	Base value of metabolic detrital organic carbon decomposition rate, $\frac{1}{3h}$
Structural detrital organic carbon decomposition rate	Base value of structural detrital organic carbon decomposition rate, $\frac{1}{3h}$
Decomposition rate constant of DOC	Based value decomposition rate constant of DOC, $\frac{1}{3h}$
C:N for microbial decomp of DOM	Carbon to nitrogen mass ratio of dissolved organic matter being decomposed
Potential denitrification flux	Potential denitrification flux, $\frac{kg\ N}{m^2-3h}$
Nitrate reduction half saturation constant	Nitrate reduction half saturation constant, $\frac{kg\ N}{kg\ Soil}$
Denitrification saturation threshold	Saturation extent above which the condition favors denitrification (0-1)
OptimumT for N fixation	Optimum temperature for N fixation, ^oC
Optimum T for litter decomposition	Optimum temperature for litter decomposition, ^oC
Optimum T for DOC decomposition	Optimum temperature for DOC decomposition, ^oC
Optimum T for nitrification	Optimum temperature for nitrification, ^oC
In-stream DOC mineralization rate constant	Rate constant for organic carbon mineralization to CO_2(aq) at 20 ^oC, $\frac{1}{3h}$
In-stream DON hydrolysis rate constant	Rate constant for the hydrolysis of dissolved organic nitrogen to NH_4 at 20 ^oC, $\frac{1}{3h}$
In-stream nitrification rate constant 1	Rate constant for the nitrification process to convert from NH_4 to NO_2 at 20 ^oC, $\frac{1}{3h}$
In-stream nitrification rate constant 2	Rate constant for the nitrification process to convert from NO_2 to NO_3 at 20 ^oC, $\frac{1}{3h}$

Table 3.5 continued

Parameter	Description
Atmospheric DOC concentration	Enriched atmospheric DOC concentration due to the passage through canopy, $\frac{mgC}{L}$ for each month (January – December)
Atmospheric DON concentration	Enriched atmospheric DON concentration due to the passage through canopy, $\frac{mgN}{L}$ for each month (January – December)
Atmospheric NH_4 concentration	Enriched atmospheric NH_4 concentration due to the passage through canopy, $\frac{mgN}{L}$ for each month (January – December)
Atmospheric NO_3 concentration	Enriched atmospheric NO_3 concentration due to the passage through canopy, $\frac{mgN}{L}$ for each month (January – December)
Atmospheric NO_2 concentration	Enriched atmospheric NO_2 concentration due to the passage through canopy, $\frac{mgN}{L}$

3.4: D-SEM model implementation and integration within DHSVM

3.4.1: Implementation

The solute export model (SEM) for a single pixel was initially prototyped in the modeling software SIMILE (Simulistics Ltd.) to help understand the behavior of individual processes and the influences of environmental factors that control the processes such as soil moisture and temperature. Afterwards, the model equations were implemented in C language and were built with GMake on Linux, and with Visual Studio 2005 (Microsoft Corporation) on Microsoft Windows XP.

To take the advantage of the existing routing scheme in DHSVM, (SEM) was integrated within DHSVM, resulting in D-SEM. The numerical solutions to the governing equations were approximated using Euler’s method. Within each time step, the pools of constituents were adjusted dynamically by each individual biogeochemical process or water transport adding/removing mass. The sequence of computation was in the following order. First, the point source and non-point source nutrient inputs were applied to the correct locations. Then, for each pixel, the litterfall and decomposition of litterfall added nutrients to the soil pools. Additional inputs from atmospheric deposition entered the soil. Next, DOC and DON respiration was computed, followed by nitrification, denitrificaiton, and nitrogen fixation. Thus, plant uptake of ammonium and nitrate was estimated. After the pool adjustment due to in-pixel processes was completed, sub-surface flow, overland flow and the nutrients were routed to adjacent cells according to the selected routing scheme (either based on topographic gradient or based on water table depth gradient). The concentration of nutrients in the surface and sub-surface flow was equal to the soil water nutrient concentration which was calculated from the soluble fraction of soil nutrient pool right before exporting the nutrient mass out of the cell. Afterwards, the dissolved nutrients were routed into stream channel segments. Lastly, the segment pools of nutrients were adjusted by the in-stream mineralization, the DON hydrolysis and the channel nitrification. The detailed DHSVM function call sequence is in Appendix 2.

3.4.2: D-SEM code analysis and verification

To facilitate the development and the tuning of D-SEM, a number of “troubleshooting” steps were taken. This was logically separated into five phases.

The first phase was to build and execute the model, D-SEM’s original C code in Microsoft’s Visual Studio 2005. Executing D-SEM from within Visual Studio gave access to rich run-time debugging tools, the usage of which will be described in phase four. As the DHSVM code has traditionally been compiled and executed on UNIX and LINUX systems with GMake (a command-line C compiler), this phase makes DHSVM and D-SEM specifically cross-platform. Due to the traditional use of GMake, many rich debugging features were not available to the original developers of the model. Therefore, this first phase made it easier to address code problems such as un-initialized variables which had previously caused unpredictable results (especially variables approaching infinity) during model execution.

During the second phase, D-SEM's execution was scoped down to receive no chemistry inputs. At this step soil and stream reaction processes were disabled. This phase make it possible to confirm that there were really no additional inputs or processes that may have otherwise been overlooked. If there were areas overlooked, they would have caused anomalous results when executing the "bare bones" model.

Phase three involved improving source-code readability by adding the unit of measurements to the variables. Important variables and their usage in the source-code were analyzed one-by-one to ensure that the units were consistent and any unit conversion bugs in the source codes were detected.

During the fourth phase, the components of D-SEM's, inputs and/or processes were enabled in a meticulous, one-at-a-time fashion. This made it possible to gauge the relative contributions of each component to the model execution. When errorneous results were detected, additional debug code was constructed to inspect the functions. This debug code checks every important variable, for values that are out of expected range such as soil moisture saturation extent (which should range from 0 to 1). If during D-SEM's execution, variables exceed their pre-specified bounds, the program's execution halts, and the developer is able to perform a multitude of actions. These can include inspecting all contributing variables, re-running the suspect code line-by-line (to better understand the problem causes), or modifying problematic code while D-SEM is still executing, so that bug-fixes can be tested on-the-fly, without having to re-run D-SEM from the beginning. Advanced debugging features such as memory-breakpoints were also used, to track where specific variables were modified in the source code, essentially allowing the developer to trace code execution without stepping through the executing code line-by-line.

The fifth phase is D-SEM's calibration, which will be explained in Chapter 4.

3.5: Summary of D-SEM

The physically-based distributed dynamic biogeochemical solute export model, as outlined in this chapter, was developed and coupled with the hydrology model DHSVM, resulting in the DHSVM Solute Export Model (D-SEM). This was done to create a tool for estimating the movement of water and dissolved nitrogen species across the landscape into the stream network. D-SEM is intended to evaluate the influence of landuse and landcover patterns on watershed nitrogen export, using the advantage that processes are represented as a function of the landscape attributes and the hydrologic condition.

The system requirements of D-SEM are very low, as the application itself uses less than 20MB of RAM. However, due to the computational intensity of the model, the faster the computer, the faster D-SEM will run. D-SEM was developed and run on a 2.5GHZ, dual-processor machine with 2GB RAM, running Windows XP. On this computer, the Big Beef Creek scenario (3454 ha in size) completes 15 years in approximately 2 hours. Runtime increases approximately linearly with basin size (spatial resolution is 150m). Please note that at this time, D-SEM is single-threaded, meaning that it does not benefit from having multiple CPU's in a machine.

The next chapter will discuss the test application of D-SEM to help solve a real-life problem.

Chapter 4: D-SEM application: Nitrogen load estimation from sub-basins in Hood Canal, Washington.

4.1: Introduction

Hood Canal is a 110-km-long fjord in the western portion of Puget Sound in Washington State. It has a width of 2 to 4 km, a maximum depth of 175 m and a shallow 50-meter sill at it's entrance (Paulson *et al*., 2006). Low dissolved oxygen (DO) concentration in the deep marine water, especially in the southern half of the canal, during the late summer has been observed since the 1920s (Osborne, 2006). Typically, the DO seasonal cycle is characterized by relatively high concentrations in the spring, a decline to minimum levels in late summer, and increasing throughout the fall and winter (Hull and Bryan, 2005). However, hypoxic conditions have become more severe in recent years, leading to lower concentrations of spring DO, a narrower range of seasonal recovery, and larger areas affected by hypoxia (Hull and Bryan, 2005). This resulted in fish kills in the summer and fall of 2002 and 2003, and the late summer of 2006.

The major cause of the low oxygen is the fjord's morphometric characteristics which naturally cause poor water circulation. This results in surface phyloplankton that deplete the bottom water oxygen level as they decompose. DIN is delivered to Hood Canal via four routes: atmospheric deposition onto its surface, marine flow over the sill at the fjord's entrance, direct surface runoff and groundwater discharge from drainage basins, and surface stream water from regional watersheds (Paulson *et al*., 2006).

The magnitude of the various N sources and how the fjord's physical characteristics influence DO levels, are being investigated by the Hood Canal Dissolved Oxygen Program (HCDOP). This group works with the governmental policy makers to evaluate potential corrective actions to restore and maintain suitable DO levels using a combination of computer modeling and marine and freshwater monitoring.

The goal in this chapter is to use D-SEM (described in Chapter 3) in combination with freshwater monitoring data to aid in scenario analyses of the processes controlling terrestrial nitrogen export into Hood Canal (Figure 4.1), and its contribution to the DO problem. Further in this chapter, D-SEM will be applied on the North Fork Skokomish River and Big Beef Creek (Figure 4.2) as a test-of-concept, and the preliminary results will be discussed. These sub-basins were chosen because their qualities make a representative sample of the majority of Hood Canal sub-basins. Big Beef Creek represents a watershed with relatively high impact of human activity whereas North Fork Skokomish River is pristine. In addition, these basins have relatively few missing field sampling data, have long-term observed stream discharge, and yielded relatively good fits in the stream flow calibration conducted by Wiley (2006).

To achieve the goals of this study, the first objective is to estimate the terrestrial nitrogen loading from selected sub-basins and to calculate the relative contributions of nitrogen loads from septic, vegetation, and atmospheric sources. The second objective is to evaluate the seasonal patterns of terrestrial biogeochemical processes and in-stream nutrient concentrations and loads of dissolved nitrogen species and DOC. The third objective is to assess the potential impact of anthropogenic non-point sources by simulating the relative N input loads and in-stream nutrient profiles using two scenarios for septic N loads.

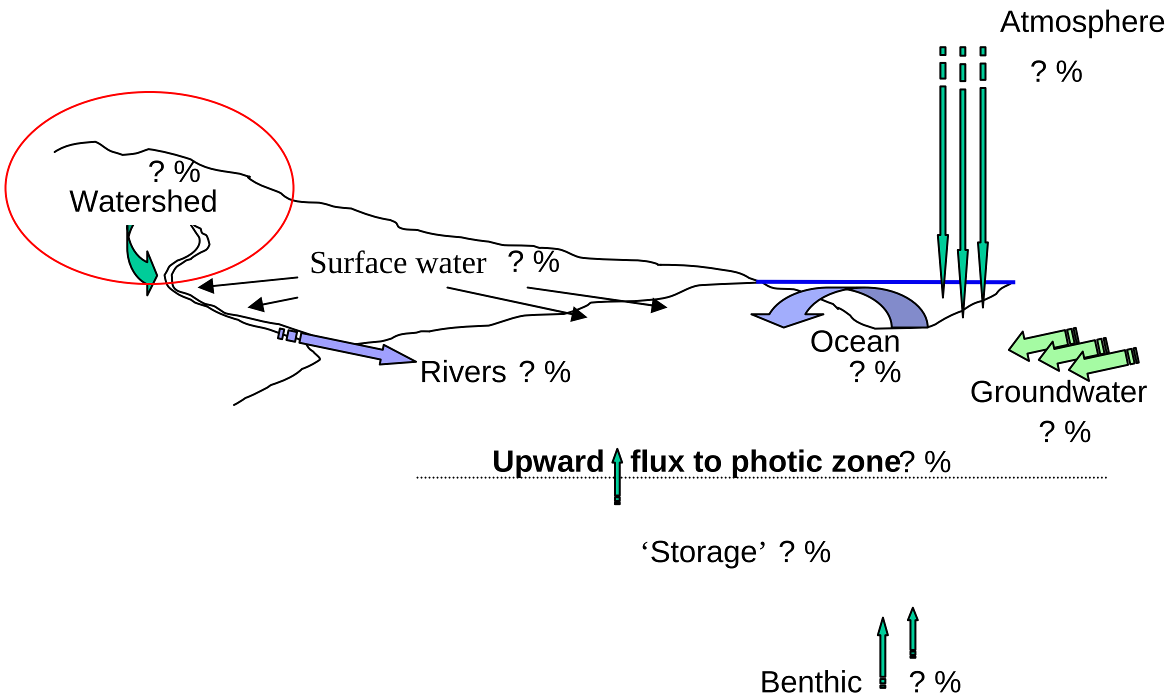

Figure 4.1. The focus area of this research (inside red circle) with respect to all the contributing factors for the Hood Canal DO problem. The question marks indicate that the quantitative effects are being investigated by various groups.

Figure 4.2. Selected sub-basins in Hood Canal from left to right: (NFSK) North Fork Skokomish River (above Lake Cushman) and (BBEE) Big Beef Creek

4.2: Site description

4.2.1: Big Beef Creek

The 38 km^2 Big Beef Creek watershed is located in Kitsap County on the east shore of Hood Canal on Kitsap Peninsula. Its headwaters are at 500 m elevation and the stream flows northward to the Hood Canal for a total of 18 stream km, 8 km upstream and 10 km downstream of William Symington Lake, a 32 ha man-made impoundment built in 1965. In the upper watershed, the main stream is very flat (0.2% gradient) and is connected to 0.6 km-wide riparian wetlands (Quinn and Peterson, 1996; http://www.cofs.washington.edu/bbc/florafauna.html). Below Symington Lake, the slope of the stream gradually decreases from 1.5% to 0.5% near the mouth.

Second- and third-growth conifer, deciduous, and mixed forest, inter-tidal wetlands, and freshwater wetlands characterize Big Beef Creek (http://www.cofs.washington.edu/bbc/florafauna.html). In the climax or sub-climax forests, dominant tree species are Douglas-fir (*Pseudotsuga menziesii*), Western Hemlock (*Tsuga heterophylla*), Western Red Cedar (*Thuja plicata*), and Red Alder (*Alnus rubra*). Most of the forest in this watershed are in early successional stages, and the regenerated forests consist of higher percentages of deciduous than coniferous trees. Deciduous forests consist primarily of Red Alder, Big-Leaf Maple (*Acer macrophyllum*), and Vine Maple (*Acer circinatum* Pursh). The majority of stream flow is derived from rains between November and March (Quinn and Peterson, 1996).

In terms of landuse, this watershed has a history of logging since the early 1900's and extensive road construction and housing development. Residential development in the upper-central watershed has occurred since 1965 with the most significant development located around Symington Lake (http://www.cofs.washington.edu/bbc/florafauna.html). However, the headwaters and the lower watershed are still predominantly forested.

The Big Beef Creek watershed has the highest total population and the highest estimated average population density in Hood Canal based on the 2000 census block level data. 16.4% of the total area in Big Beef Creek basin is classified as mixed forests and deciduous forests (percentage of deciduous forests for individual sub-basins ranges from 0.1 to 35%). Red Alder is a primary tree species in the Big Beef basin. Because Red Alder is usually associated with land disturbance, Big Beef is a watershed representing high anthropogenic impact.

4.2.2: North Fork Skokomish River

The North Fork Skokomish River is located in Mason County on the southeast corner of Olympic National park, and flows southeastward into Lake Cushman, a 1,620 ha reservoir with 2 dams constructed downstream (Brenkman *et al*., 2001). At these dams, 90% of the North Fork's flow is routed directly to Hood Canal for hydropower production, reducing the Skokomish's main stem flow by 40% (Stover and Montgomery, 2001). Below the dams, the river joins with the larger South Fork Skokomish River, and continues as the Skokomish River before entering the south of Hood Canal. The study area is the river system upstream from Lake Cushman, with a total drainage area of 148 km^2, and is the area we refer to when discussing the North Fork Skokomish River.

Mature conifers, mainly Douglas-fir and Western Red Cedar characterize the North Fork Skokomish basin (Brenkman *et al*., 2001). The headwaters are at 1,622 m elevation and steep montane topography in basaltic bedrock is associated with high-gradient tributaries. The elevation drops to 225 m at Lake Cushman.

Because the North Fork Skokomish River is still very pristine, it is selected as representative of natural signals or low anthropogenic impact. The understanding of natural variability or processes that govern the trend of stream nitrogen loading will be essential to provide a baseline for comparisons with other basins with anthropogenic influences.

4.3: Development of the geospatial model of the Hood Canal sub-basins

4.3.1: Topography and flow network

Topography for the Hood Canal sub-basins was acquired as a 1^{o} x 2^{o} 10-meter digital elevation model (DEM) of western Washington, constructed by the University of Washington Puget Sound Regional Synthesis Model (PRISM) initiative, Seattle, WA. The original source data of the DEM are the U.S. Geological Survey 7.5-minute quadrangles for Washington State. This 10-meter DEM was then aggregated to 150-meter resolution (Figure 4.3), re-projected and clipped to the basin boundaries. Stream networks (Figure 4.3) were derived from the 150-meter DEM and subsequently verified against the Washington State Department of Natural Resources (DNR) statewide stream network and watershed GIS layers. Soil depth was generated by DHSVM, based on slope, upstream contributing area, and elevation; with the maximum soil depth set at 2.25 m.

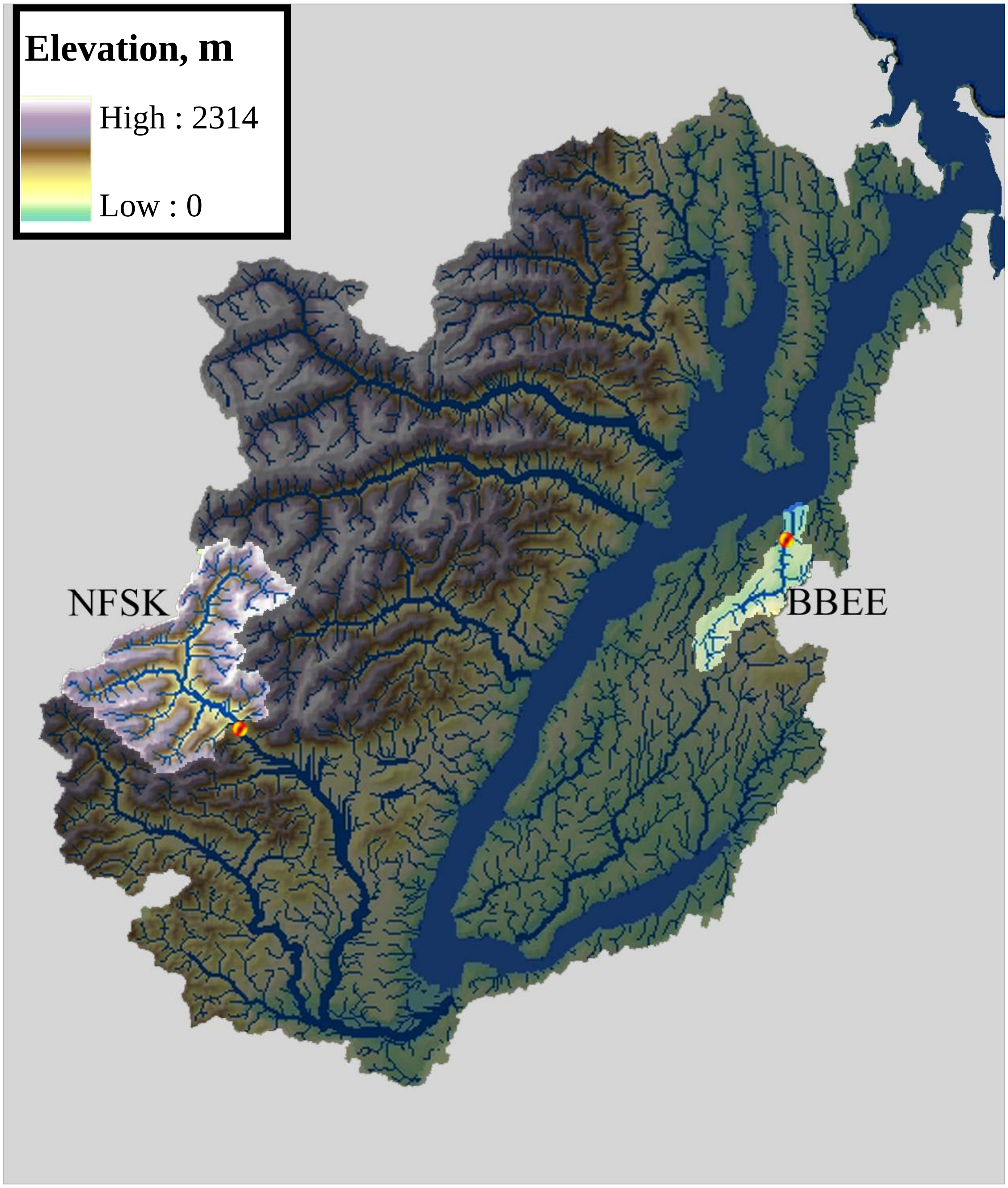

Figure 4.3. Digital Elevation Model (DEM) of Hood Canal, represented by the 150-meter resolution.

4.3.2: Soil map

The soil map, developed by HCDOP, was initially defined using the Washington State DNR soil survey data and was classified into texture categories based on the percentage of fine particulates. The soil type in areas with missing data was estimated using a multi-parameter regression model described in Wiley (2006). The inputs are surficial geology, pixel slope, and upstream contributing area (combined into a single soil depth index), and a coarse scale soil definition derived from the U.S. General Soil Map (STATSGO) database maintained by The Natural Resources Conservation Service (NRCS), U. S. Department of Agriculture. The regression model was applied to the entire area of Washington State and the soil classification output was verified against the actual DNR soil data in the area where actual data is available. In the final 150-meter soil map (Figure 4.4), the regression model output was used only to fill missing data.

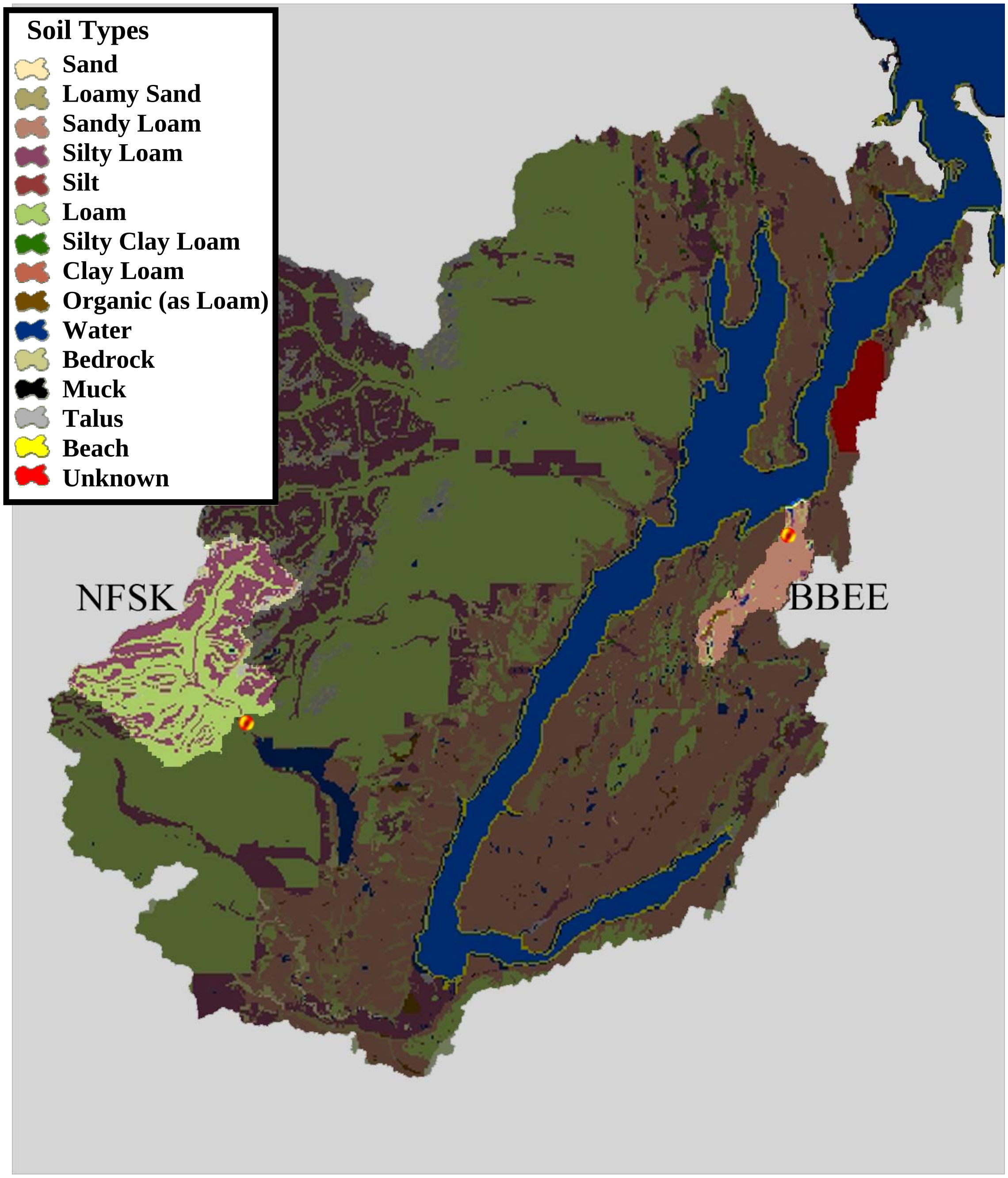

Figure 4.4. Soil map of Hood Canal represented by 150-meter resolution

4.3.3: Landcover

The 30-meter 2001 landcover data layer was obtained from the National Oceanic and Atmospheric Administration (NOAA) Coastal Change Analysis Program (C-CAP), and was subsequently aggregated to 150-meter resolution by Matthew Wiley. The final map (Figure 4.5) is a reclassification of C-CAP vegetation classes into smaller groups of eleven hydrologically distinct classes (Wiley, 2006). The landcover composition in each sub-basin is presented in Table 4.1.

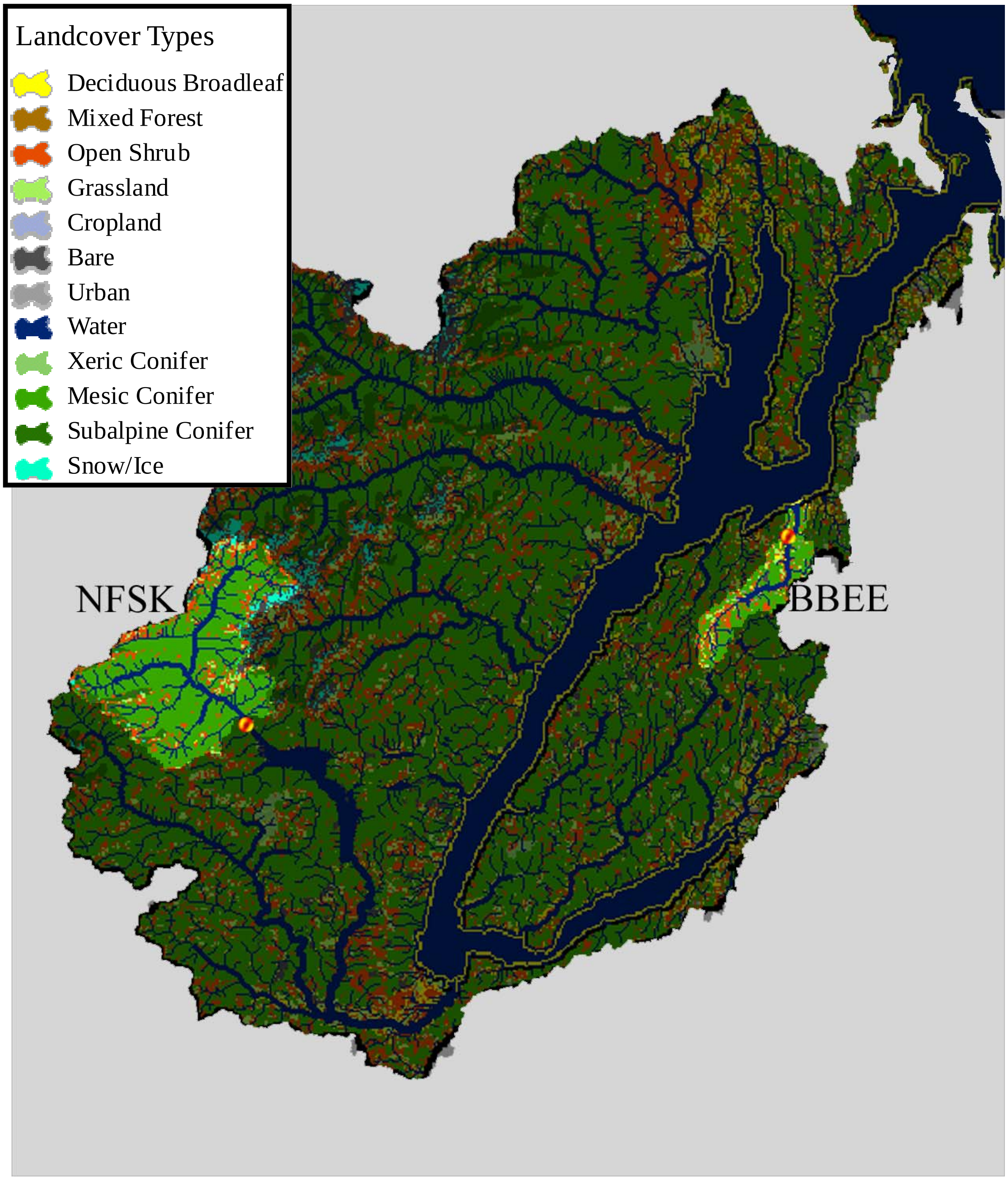

Figure 4.5. Vegetation types and compositions of Big Beef Creek and North Fork Skokomish River basin

Table 4.1. Landcover composition in (BBEE) Big Beef Creek and (NFSK) North Fork Skokomish River

Landcover type	Percentage of total basin area	
	BBEE	NFSK
1. Deciduous Broadleaf	4.43	0.08
2. Mixed Forest	11.92	0.04
3. Open Shrub	15.50	15.00
4. Grassland	6.58	4.22
5. Bare	0.91	4.59
6. Urban	1.56	0
7. Water	0.52	0.36
8. Mesic Conifer Forest (Wet)	58.57	65.05
9. Subalpine Conifer Forest	0	7.27
10. Ice	0	3.39

4.3.4: Climate forcing and hydrology

Daily climate records including total precipitation, minimum and maximum air temperature from October 1990 – June 2006 are available from seventeen climate stations (Figure 4.6) operated by the National Climatic Data Center (NCDC), US Department of Commerce. This daily data, along with elevation, geographic location of the stations, and wind record from at least one nearby station, is used by Matthew Wiley to prepare the 3-hourly meteorological data using the method in the work by Waichler *et al*. (2004).

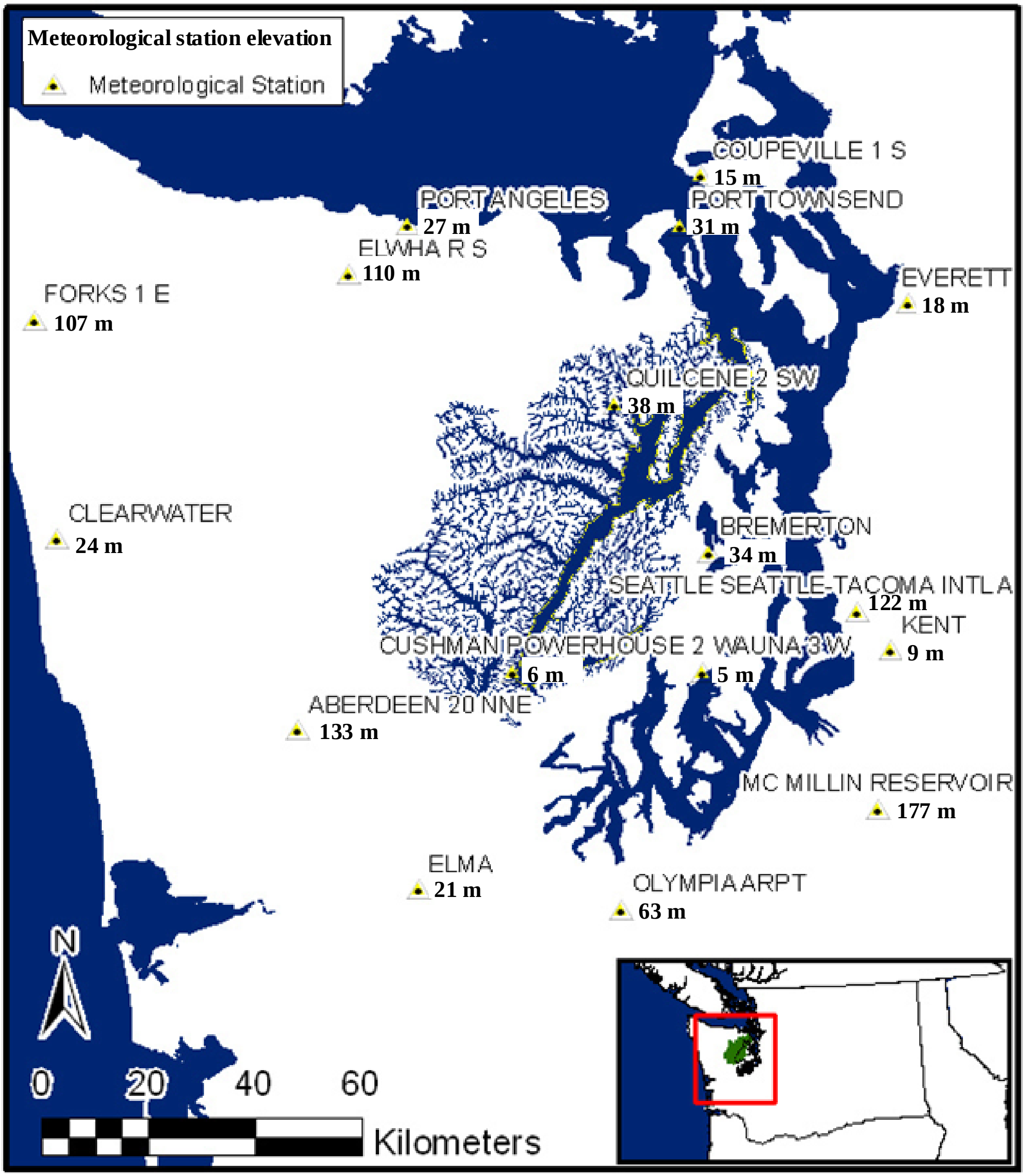

Figure 4.6. Location of meteorological stations used in the Hood Canal DHSVM application (Wiley, 2006)

The North Fork Skokomish River is at a relatively high elevation and is rain and snow dominated with 2 major peaks reflecting rainfall in the fall through the early winter and snowmelt runoff in the spring through the early summer. Big Beef Creek is rain-dominated with the characteristic winter peak flow in the annual hydrograph. The water year is defined to be from October of the previous year to the end of September in the current year. Refer to section 4.5.2.1. for a detailed description of the hydrology for both sub-basins.

The observed mean daily discharges from October 1991 – June 2006 were obtained from two USGS stream flow gauges (Figure 4.2). Gauge 12056500 is located on the North Fork Skokomish River 1.93 km upstream from Lake Cushman with a 148 km^2 drainage area. The gauge on Big Beef Creek is located 3.06 km east of the town of Seabeck, with 35.7 km^2 of contributing area.

4.3.5: Nutrient forcing

4.3.5.1: Litterfall input

To estimate the annual flux and monthly distribution of litterfall, dominant vegetation species in each landcover type were identified and used as representative species for that landcover type. Literature values of annual fluxes and seasonal distribution were then selected from sites with similar vegetation in approximately the same geographic region (Pacific Northwest).

Based on ground truthing of the landcover data by Lauren McGeoch, personal communication, the dominant coniferous overstory species are Western Hemlock and Douglas-fir in mature stands and Fir in young conifers and regrowth stands. The major understory species are Salal, Fir saplings, and fern. For deciduous and mixed forests, the major overstory species are Red Alder and Bigleaf Maple, and understory species are Salal, Indian Plum, and Fir saplings. In the subalpine forests, Pacific Silver Fir is the dominant species.

Using this ground truth information, annual overstory litterfall fluxes and seasonal litterfall distribution from Edmonds and Murray (2002)'s Olympic National Park data was used, their lower-elevation site data selected for mesic and xeric conifer forests, whereas the higher-elevation site was used for the subalpine conifer class. Red Alder litterfall data from Gessel and Turner (1974) and Roberts (2006) were used for deciduous broadleaf and mixed forest categories. For all types of forests, the understory litterfall flux was assumed to be at 20% of the overstory litterfall flux and the understory litterfall was assumed to distribute evenly throughout all months. The shrub litterfall characterization was based on the work by Benfield (1997). Urban litterfall data was taken from Puget Sound lowland sites with high disturbance (Roberts, 2006). The actual values are listed in Table 4.5.

4.3.5.2: Atmospheric deposition input

Monthly wet-deposition concentrations of NH_4 and NO_3 were taken from average monthly precipitation-weighted concentrations from 1980 to 2005 from the National Atmospheric Deposition Program (NADP) at the Hoh Ranger Station in Washington. Geomean values were used for July because one of the years having abnormally high values compared to other years. Since only inorganic nitrogen data is available at the Hoh Ranger Station, bulk precipitation concentrations of DOC and DON were taken from Solinger *et al*. (2001) as single average values. In order to apply a seasonal effect for data from Solinger *et al*., a seasonal multiplier was developed based on the assumption that DOC and DON seasonal deposition trends were the same as that of NO_3. First, the average annual concentration of NO_3 was calculated by averaging the monthly concentrations from NADP. Next, a ratio between each month's concentration and the annual concentration was computed. These monthly ratios are seasonal multipliers and are used with the average DOC and DON concentrations to get the monthly concentrations for both species. NO_2 concentrations were assumed to be about 10-15% that of NH_4 as N equivalent. Final values of atmospheric composition are in Table 4.2.

Table 4.2. Composition of wet atmospheric deposition used in this study

Species concentration	Jan	Feb	Mar	Apr	May	Jun	Jul	Aug	Sep	Oct	Nov	Dec
NH4, $\frac{mgN}{L}$	0.014	0.012	0.016	0.016	0.02	0.013	0.018	0.021	0.02	0.011	0.01	0.01
NO2, $\frac{mgN}{L}$	0.002	0.001	0.002	0.002	0.002	0.001	0.002	0.002	0.002	0.001	0.001	0.001
NO3, $\frac{mgN}{L}$	0.019	0.024	0.028	0.028	0.037	0.033	0.033	0.034	0.039	0.02	0.017	0.017
DOC, $\frac{mgC}{L}$	1.423	1.808	2.177	2.177	2.825	2.561	2.509	2.649	2.972	1.534	1.284	1.280
DON, $\frac{mgN}{L}$	0.135	0.172	0.207	0.207	0.269	0.244	0.239	0.252	0.283	0.146	0.122	0.122

The load of atmospheric deposition was calculated as the product of precipitation and the atmospheric concentration of species. Dry deposition of nutrients was not included in this study. Because the information on throughfall enrichment ratio of nutrients is not available, the enrichment ratio is set equal to 1 for all species (no enrichment).

4.3.5.3: Non-point source input

The only non-point input considered in this study is septic effluent N loading from the population in the sub-basins, assuming that gravity-drain septic tanks are the primary method of sewage management in these households. This septic load estimation excludes any contribution of septic loads from houses on shoreline that drain directly into the canal.

Monthly maps of population density per 150-meter pixel were developed by HCDOP based on census block population data from the 2000 US Census, the 2002 landcover map developed by the Puget Sound Regional Synthesis Model (PRISM) at the University of Washington, a Normalized Difference Vegetation Index (NDVI) layer obtained from a

July 30, 2000 LANDSAT image, and seasonal traffic data obtained from the Washington State Department of Transportation. Total estimated population in the Big Beef Creek basin is lowest in January, about 3100, and is higher in the summer months, with the peak of 4900 in August due to seasonal residents. The population then decreases in the fall. This trend holds true for the entire Hood Canal watershed. For example, the map of population in August is shown in Figure 4.7.

To assess the effect of population on septic loads, two dissimilar scenarios were developed based on different septic load characteristics (Table 4.3) and population data. The first scenario represents the average septic loads by using the current population and using median reported domestic water consumption and average values of reported septic effluent N concentrations per capita. The second scenario demonstrates an extreme low septic load by setting the population in the watershed to be 5% of the current population. This was done uniformly throughout the watershed by dividing the population per pixel by 20. Then, a set of effluent quality for more conservative water use or better onsite treatment system was assigned. For both scenarios, the characterization of septic loads was based on septic tank effluent prior to entering the subsurface soil. The average value of effluent nutrient concentrations were the values used in the septic load computation by Akanda *et al*. (2006), which set the total nitrogen concentration to 87 mg N/L. The lower bound load was estimated using the US EPA household wastewater quality, reported in Akanda *et al*., with total nitrogen of 26 mg N/L. It was assumed that 50% of total organic nitrogen in the effluent is in the dissolved form. The carbon to nitrogen ratio of waste product was assumed to be 4:1. The effluent water flow rates were taken from McCray *et al*. (2005). The values of household waste water flow rates, compiled by McCray *et al*. (2005), at the 50^{th} and 10^{th} percentiles were used for both average and minimal septic load scenarios.

Table 4.3. Two characterizations of septic loads used in this study

Scenario	Flow rate per capita $\frac{L}{day}$	DOC $\frac{mgC}{L}$	DON $\frac{mgN}{L}$	NH4 $\frac{mgN}{L}$	NO2 $\frac{mgN}{L}$	NO3 $\frac{mgN}{L}$
Average septic load	235	52	14	59	0.03	1.0
Minimal septic load	132.5	26	6.5	13	0	0

Using the above effluent quality, the input septic effluent loads are equivalent to 6.3 and 0.94 kg N/capita-yr for average and minimal septic scenarios.

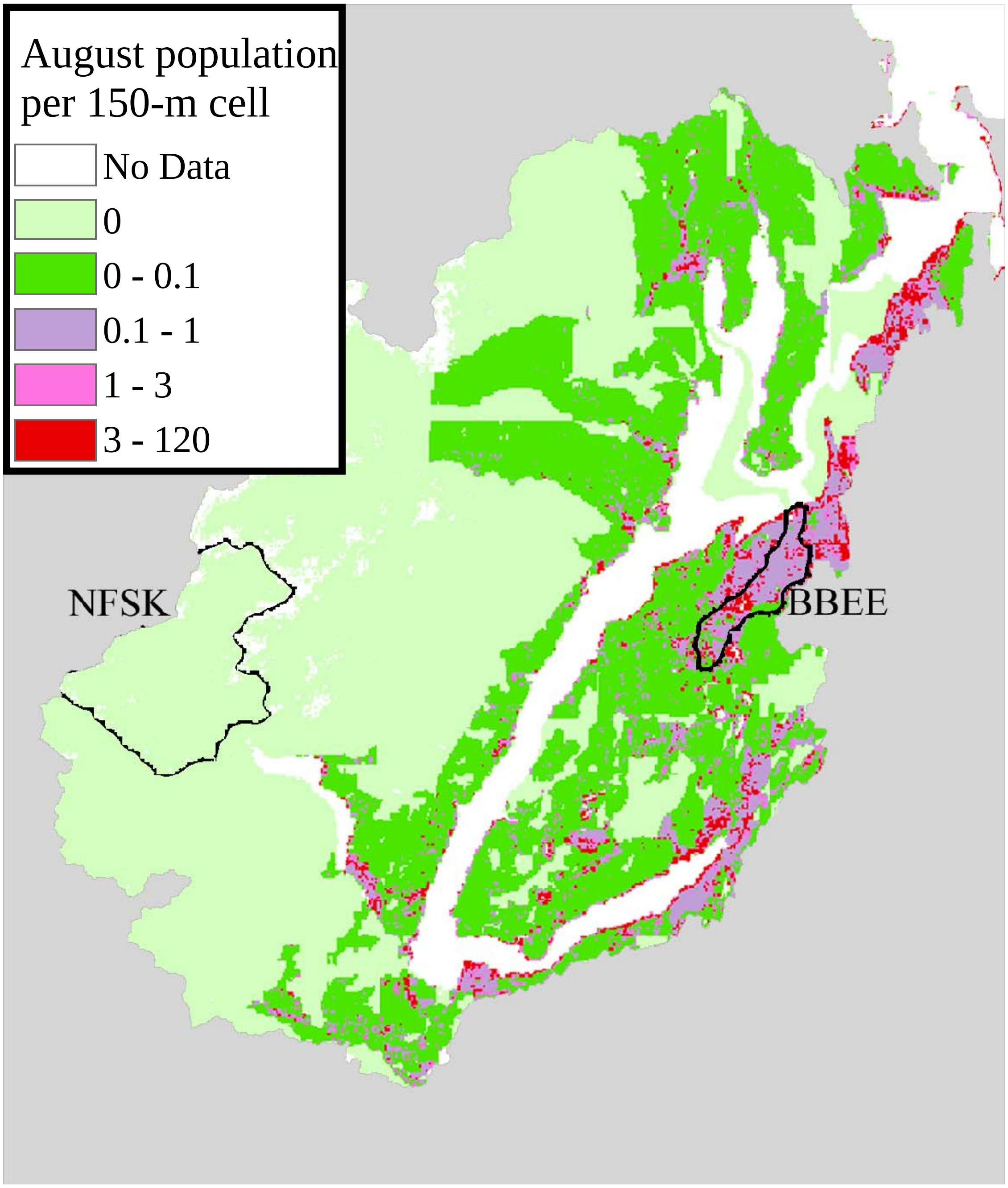

Figure 4.7. Population density per 150-meter pixel in August.

4.3.5.4: Nitrogen fixation by Red Alder

Based on the ground truthing by Lauren McGeoch, personal communication, the fraction of Red Alder in each pixel was set to 0.5 and 0.75 for mixed forest and broadleaf vegetation respectively. For the mesic conifer forest, the fraction of Red Alder was assumed to be 0.001, based on Volk (2004) who found that conifer-dominated watersheds in Olympic Peninsula in Washington has less than 0.1% Red Alder coverage. In other landcover classes where no groundtruth data was available, the fraction of Red Alder was assumed to be from 0.01 to 0.05. The referenced rate of annual N fixation by pure stands of Red Alder was set at 200 kg N/ha-yr based on data from Binkley (1992). The stand age of Red Alder was assumed to be 40-45 year-old.

With the current assumption, the total coverage of Red Alder in Big Beef Creek and North Fork Skokomish is 10.3% and 1% of the basin areas respectively.

4.3.6: Surface water quality data

Monthly instantaneous dissolved nutrient data from HCDOP was available from January 2005 – June 2006. The sampling protocol and nutrient analysis were described in Osborne (2006). Additionally, gauge 12060500 for the North Fork Skokomish River has monthly instantaneous dissolved nitrogen data available from March 1996 – July 2005 (downloaded from the USGS website in September, 2006). Washington Department of Ecology (DOE) also has nutrient data for Big Beef Creek at site 15F050, located approximately the same location as the USGS gauge 12069550, from Oct 2004 – August 2006. These three sources of observed data will be used for comparison with the simulation data further in this chapter. Note that the water quality data from USGS and DOE are only verified until the end of the 2005 water year, and the preliminary 2006 data is used due to an otherwise lack of sufficient field samples to analyze D-SEM against. The use of this preliminary data may result in anomalous field readings being compared to the simulated results. Through the remainder of this chapter, the assumption is made that the preliminary data is accurate, and a re-analysis of D-SEM’s results should be performed once the 2006 data is finalized.

4.4: D-SEM setup and operations

4.4.1: Simulation conditions

The spatial resolution, for inputs such as population density, vegetation cover, and soil types, was 150-meter. The temporal resolution or the time step of the simulation, is 3-hour. The soil profile was divided into 3 root zones, 0-10 cm, 10-35 cm, and 35-75 cm. Lateral subsurface flow was calculated using a water table gradient. In the routing scheme, roads were not included, and stream classification was based on Strahler stream order and segment slope, derived from the DEM. Although the groundwater component of the DHSVM was available at the time D-SEM was being developed, further research into its integration is needed before this component can be added to the biogeochemical model.

For the initial state of D-SEM, the amount of residue on the ground and the stream nutrient concentrations were set to zero (no metabolic and structural detrital pools). Initial mass concentrations of DOC, DON, NH_4, NO_3, and NO_2 were set at an arbitrary values, and the model was run from October 1, 1991 for 10 years. Then, the output states were used as the initial states for the model re-run from October 1, 1991 to June 20, 1006. On the model re-run, the first five years were the start-up period for the soil to reach equilibrium, and the results from October 1, 1996 to June 2006 were used for analysis.

4.4.2: Parameter estimation

The parameter estimation and calibration of the hydrologic simulation was performed by Matthew Wiley. The precipitation lapse rate was a constant of 0.0018 m/m. Monthly temperature lapse rates in a range from -0.0060 to -0.0075 ^{o}C/m were used. The basic vegetation parameters necessary for computing the hydrologic simulation are listed in Table 4.4.

Litter nutrient compositions of leaf and needle litter, including carbon content, lignin to nitrogen ratio, carbon-to-nitrogen ratio were compiled from Edmonds (1980) and Edmonds (1987). For terrestrial process rate characteristics, the initial metabolic and structural detrital decomposition rates were taken from REMM default values and were compared to in-stream litter decomposition rates (Richardson *et al.*, 2004), a representative of a higher-bound value, and to a range of aboveground litter decomposition rates summarized by Edmonds (1980), Edmonds (1987). The initial values used in this study appeared relatively high, compared to literature ranges. However, these values are maximum values, and the actual rates were influenced by soil temperature and moisture condition, as described earlier in section 3.2.1.2. The initial values of fraction of DOC leachate from the decomposition of litter was based on the work by Currie and Aber (1997). The DOC and DON mineralization rates were approximated from the litter decomposition rates. The high end of observed annual denitrification flux given in a literature compilation by Barton *et al*. (1999) was selected to be the potential denitrification flux in D-SEM, for the same reason as choosing the high value for litter decomposition rates.

The maximum soluble fraction for DOC was set at 0.4 based on the data of Nodvin and Likens (1986), and the same soluble fraction was used for DON. Soluble fractions of NH_4, NO_3, and NO_2 were set at 50%, 90%, and 90% respectively. Sorption, especially dissolved organic matter, depends on soil Fe and Al oxide/hydroxide content, clay minerals and clay content, and total organic content in the soil (Kalbitz *et al.*, 2000; Neff and Asner, 2001). Therefore, it was originally designed that the soluble fraction of each species will be quantitatively tied to those soil chemical properties. However, most of the areas in the Hood Canal, including these two sub-basins are dominated by loamy soils (sandy loam for Big Beef and loam for North Fork Skokomish). While providing hydraulic differentiation, the soil textural classification alone does not provide enough information to assign specific chemical properties. Therefore, the values of maximum soluble fractions of all species provided above were applied as constants.

Michaelis-Menten kinetics information for the plant uptake of NH_4 from Hangs *et al*. (2003) was used. The seasonal distribution of the NO_3 uptake was approximated from Nadelhoffer *et al*. (1984) and maximum N accumulation for conifer and Red Alder-conifer were taken from the publication by Binkley *et al*. (1992).

In-stream rate constants for nitrification at 20 ^oC were taken from the default values in QUAL2E model. DOC and DON mineralization rates were modified from QUAL2K, which gives lump rates for mineralization of organic carbon and nitrogen.

Table 4.4. Final vegetation parameters for hydrologic simulation

Parameter	Overstory (Class 1, 2, 6, 8, 9)	Understory (Class 1-4, 6, 8, 9)
Fractional trunk space height	0.4-0.5	N/A
Height, m	20 – 50	0.5 - 1
Aerodynamic attenuation coefficient	0.5 - 2.0	N/A
Radiation attenuation coefficient	0.15 – 0.20	N/A
Maximum stomatal resistance, s/m	5000	600 - 3000
Minimum stomatal resistance, s/m	600 -667	120 - 200
Vapor pressure deficit threshold, Pa	4000	4000
LAI	2.0 - 10.0 (Broadleaf) 12.0 (Conifer)	0.5 – 7.0
Albedo	0.15 – 0.20	0.12 – 0.20
Root fraction in layer 1,2, and 3	0.2 0.4 0.4	0.4 0.6 0.0

Table 4.5. Final vegetation parameters for biogeochemical computation

Parameter	Landcover type		
	Mesic conifer	Mixed/deciduous broadleaf (class 3, 4)	Open shrub and grassland
Fraction alder	0.001	0.50 - 0.75	0.01 – 0.05
Average stand age	40	45	45
Annual litterfall mass, $\frac{kg}{m^2-yr}$ Overstory Understory	 0.3 0.06	 0.50 - 0.55 0.12 - 0.18	 N/A 0.1 – 0.2
Lignin nitrogen mass ratio, $\frac{mgLignin}{mgN}$ Overstory Understory	 40 19.0	 9.45 19.0	 N/A 14
Overstory litter carbon fraction Metabolic Structural	 0.468 0.467	 0.48 0.47	 N/A
Overstory DOC leachate fraction Metabolic Structural	 0.1 0.2	 0.1 0.2	 N/A
Understory litter carbon fraction Metabolic Structural	 0.468 0.467	 0.48 0.48	 0.48 0.48
Understory DOC leachate fraction Metabolic Structural	 0.1 0.2	 0.1 0.2	 0.1 0.2
Overstory DON leachate fraction Metabolic Structural	 0.15 0.3	 0.15 0.3	 N/A
Understory DON leachate fraction Metabolic Structural	 0.15 0.3	 0.15 0.3	 0.15 0.3
Overstory litter CN ratio Metabolic Structural	 40 200	 31.5 195	 N/A
Understory litter CN ratio Metabolic Structural	 35 150	 40 150	 37 150
Nitrogen fixing reference rate, $\frac{kgN}{ha-yr}$	200	200	200
Growing season start day	0	0	0
Growing season length	210	210	210

Table 4.5 continued

Maximum nitrogen uptake delay	180	180	180
Maximum nitrogen accumulation, $\frac{kgN}{m^2}$	3.73e-3	3.39e-3	1.00e-3
Maximum ammonium uptake constant, $\frac{kgN}{m^2-3hr}$	3.1e-4	2.3e-4	2.3e-4
Half-rate ammonium uptake constant $\frac{kgN}{m^3}$	2.88e-3	2.88e-3	2.88e-3
Overstory monthly litter fraction (Jan – Dec)	0.0436 0.0436 0.0436 0.085 0.085 0.0848 0.1416 0.1416 0.1416 0.0632 0.0632 0.0632	0.056 0.022 0.017 0.013 0.034 0.045 0.078 0.112 0.135 0.151 0.174 0.163	N/A
Understory monthly litter fraction (Jan – Dec)	0.083 0.083 0.083 0.083 0.083 0.083 0.083 0.083 0.083 0.083 0.084 0.084	0.083 0.083 0.083 0.083 0.083 0.083 0.083 0.083 0.083 0.084 0.085 0.084	0.083 0.083 0.083 0.083 0.083 0.083 0.083 0.083 0.083 0.083 0.083 0.083

Table 4.6. Final global constants for chemistry

Parameter	Value used in this study
Metabolic detrital organic carbon decomposition rate	0.00425 $\frac{1}{3h}$
Structural detrital organic carbon decomposition rate	0.0008 $\frac{1}{3h}$
Decomposition rate constant of DOC	0.005 $\frac{1}{3h}$
C:N for microbial decomposition of DOM	24
Potential denitrification flux	7x10^{-6} $\frac{kgN}{m^2 - 3h}$
Nitrate reduction half saturation constant	5 X10^{-7} $\frac{kgN}{kgSoil}$
Denitrification saturation threshold	0.60
Optimum temperature for N fixation	22 ^{o}C
Optimum T for litter decomposition	35 ^{o}C
Optimum T for DOC decomposition	35 ^{o}C
Optimum T for nitrification	35 ^{o}C
In-stream DOC mineralization rate constant	0.0125 $\frac{1}{3h}$
In-stream DON hydrolysis rate constant	0.01 $\frac{1}{3h}$
In-stream nitrification rate constant 1	0.0188 $\frac{1}{3h}$
In-stream nitrification rate constant 2	0.094 $\frac{1}{3h}$

4.4.3: Model analysis and calibration

D-SEM was applied on the individual sub-basins separately. To assess the goodness of model fit (the DHSVM component) for hydrology, the model efficiency, RMSEs, and Pearson's correlation r were computed.

Analysis of the D-SEM test-run was conducted using Big Beef Creek due to its smaller basin size and shorter simulation run time. To test the routing scheme for nutrients, a run with initial soil concentration and no nutrient inputs was performed to ensure that all the constituents were properly flushed out with the runoff. D-SEM was then tested with only one type of input at a time and the stream concentration response was observed.

The model parameters were divided into 3 groups based on how much information is known about the parameters. The first group is the parameters with well known range of values for all vegetation types (for vegetation parameters) and for range of condition occurs in the Hood Canal (for global constants) such as literfall rates, decomposition rates, and carbon to nitrogen ratios. The second group is the parameters with some known literature values, but the information was known for a limited range of conditions. Example parameters in this category are DOC and DON leachate fractions, of which the values are known for humid montane forests (Currie and Aber, 1997). The last category is the parameters with the least information, such as fraction of sorption of each chemical species on different soils.

Consequently, rather than performing vigorous model sensitivity analysis of all parameters, the sensitivity analysis was performed on parameters in the first and second categories. The parameters that the model was more sensitive were first identified and then the optimization was done based on trial and error; one parameter was adjusted at a time. For parameters in the first category, the adjustment of parameter values from the initial estimation was confined to be within the published ranges. The parameters in the third categories are assigned constant values for all vegetation types or all soil types, based on whether they are vegetation or soil parameters.

The preliminary model sensitivity analysis showed that the model is sensitive to DOC and DON leachate fraction, the initial nutrient pool in the soil. The stream nutrient seasonality was influenced by the soluble fraction of each nitrogen species. The litter decomposition rates only affect the soil pool of nutrients during the first few years of the run, but the soil nutrient pool reaches new equilibrium, and the actual nutrient release was limited by the litter fall input. The in-stream concentration was not sensitive to the stream reactions, especially for nitrate. Final parameter set was reported in Table 4.5 and 4.6.

During the parameter adjustment step, the average septic load scenario was used as a reference case, and the simulated nutrient concentrations were compared to the monthly instantaneous field sampling concentrations from the HCDOP and DOE for Big Beef Creek. After parameter adjustment was completed, D-SEM was also re-run for the minimal septic load scenario.

Because the observed water quality data was available for only a relatively short period (18 months for HCDOP, and 2 years for DOE), it was not practical to divide the observed data into 2 periods for model analysis and model evaluation. Instead, the final parameter set obtained from the model analysis in Big Beef Creek was applied to the North Fork Skokomish application as a way to test D-SEM’s reusability. The simulated results for North Fork Skokomish River was compared to osbserved values from HCDOP and USGS. A limitation of USGS stream water quality data is the minimum level of nutrient detection at 50 or 100 ug N/L, which is above or at the same concentration as commonly observed in the HCDOP data. Therefore, no seasonality of data is available because the data is mostly shown as less than detection limit for USGS. However, this data set is still useful as a guideline for the maximum concentration expected in the simulation results.

Big Beef Creek and North Fork Skokomish River differ substantially in the underlying geology, catchment slope, catchment size and composition of land disturbance. Big Beef Creek is very flat, is rain-dominated and the size is about 4 times smaller than North Fork Skokomish. Steep terrain and rain-on-snow dominates North Fork Skokomish. The underlying soil parent material for Big Beef Creek is glacial drift and glacial till whereas marine sedimentary deposits dominate in North Fork Skokomish, based on the geology map developed by HCDOP from data from the Washington State Department of Natural Resources Division of Geology and Earth Resources. Therefore, if the simulation results appear comparable to the observation, some confidence can be placed in D-SEM's mechanics.

4.5: Results and discussion

In the terrestrial system, the interest is on the annual and seasonal loads and relative contributions of major nitrogen input sources in the North Fork Skokomish River and in Big Beef Creek. For the latter basin, the results from 2 scenarios of septic loads will be examined. In addition, annual and seasonal loads of other processes in the N cycle are reported. Together, these results will help understand the seasonal profiles of the in-stream nutrients and will be used to assess D-SEM's performance by comparing with literature values.

For the stream system, the monthly stream flows were compared against USGS flow samples to verify the parameter set used for hydrologic representation in the DHSVM. After that the loads and concentrations of each chemical species will be compared with the field data and uncertainty and limitation of the simulations will be discussed.

4.5.1: Terrestrial N cycling

4.5.1.1: Relative magnitudes of terrestrial N inputs

The four major sources of terrestrial N inputs are vegetation litter decomposition, atmospheric deposition, the septic effluent before entering the soil column, and the nitrogen fixation by Red Alders. The loads include contributions from both dissolved organic and inorganic nitrogen.

For the undisturbed North Fork Skokomish natural forest ecosystem upstream of Lake Cushman, annually the main terrestrial N input source to the system was vegetation litter (Figure 4.8), followed by atmospheric deposition, with an insignificant contribution of nitrogen fixation. There was no septic contribution due to the estimated zero population in this sub-basin. In Big Beef Creek, vegetation litter was also the highest N contributor, followed by the nitrogen fixation, septic load, and then atmospheric deposition (Figure 4.10). Total N load in Big Beef Creek was higher than that in North Fork Skokomish River basin.

Comparing the annual flux of each input source between the two sub-basins, the N flux from atmospheric deposition in the North Fork Skokomish River was higher than that of Big Beef Creek. This is due to a higher precipitation in the North Fork Skokomish. Approximately 20% of the atmospheric deposition was dissolved inorganic nitrogen (DIN) (Table 4.2), so the annual flux of DIN was 1.07 and 0.54 kg N/ha-yr for the North Fork Skokomish and Big Beef Creek respectively. This was comparable to the reported NADP wet deposition of less than 1.6 kg N/ha/yr at 8 of 10 monitor sites in the Pacific Northwest (Fenn *et al*., 2003). Nitrogen fixation in Big Beef Creek was contributed by the presence of Red Alder, mostly in the mixed forest and deciduous broadleaf landcover types, with an estimated total coverage of 10.3% in the basin. In contrast, estimated Red Alder presence in North Fork Skokomish River was 1%; consequently, the N fixation input is much less than the input in Big Beef Creek.

The monthly loads of all terrestrial N inputs, except atmospheric deposition, were highest from late spring through summer and were lowest from December to February (Figure 4.9 and 4.11), resulting in the total N loads peaking in summer and reaching the minimum in winter months. For the vegetation inputs, the litter fall rate was generally highest in the fall. However, the actual release of nutrients peaked during spring and summer because the warmer months provided more suitable condition for the microbial decomposition. The N fixation by alders is also a biotic process; therefore, the input is higher in spring and summer. The septic load contribution was highest in the summer months when the population is highest due to additional seasonal residents. The atmospheric deposition had an inverse monthly trend and peaked in fall and winter, corresponding to the precipitation profile (Figure 4.16 and 4.17). Consequently, the relative contribution of atmospheric deposition is more significant in the fall and winter.

Note that the input flux from each process is a basin-wide average. The actual flux within each landcover type differs. For example, the estimated N fixation flux in the deciduous broadleaf class was actually 74.6 kg N/ha-yr, which is consistent with the published values (Binkley *et al*., 1992; Binkley *et al*., 1994), whereas the N fixation flux in the mesic conifer class was 0.1 kg N/ha-yr.

4.5.1.2: Comparison of septic loads based on anthropogenic scenarios in Big Beef Creek

The estimated total septic input of 7.07 kg N/ha/yr from the average septic load scenario is 136 times greater than the low septic load case, resulting in the difference in the relative contribution from 17% of total terrestrial N in the first scenario to almost 0% in the minimal load scenario (compare Figure 4.10 to 4.12, and Figure 4.11 to 4.13). The difference is mostly in terms of the ammonium load, and, to some extent, the amount of nitrate. The difference in the water volume added into the soil was not expected to alter the hydrograph significantly.

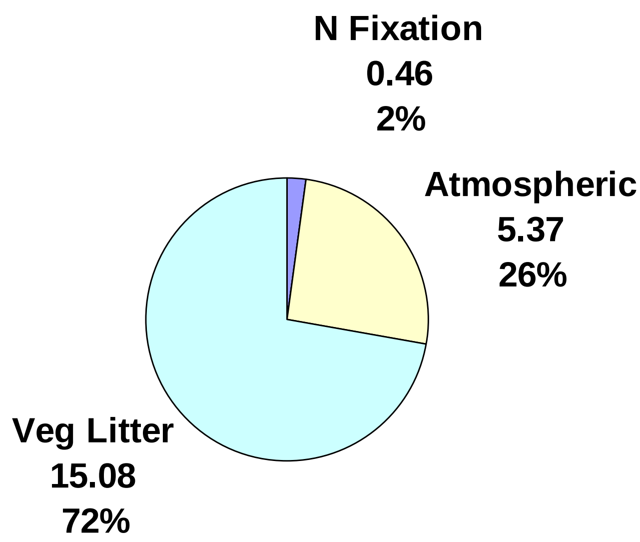

Sources of terrestrial inputs	Annual load (metric tons N /yr)	Annual flux (kg N/ha-yr)
Vegetation litter	255.11	15.08
N fixation	7.84	0.46
Septic	-	-
Atmospheric	90.85	5.37
Total	353.8	20.9

Figure 4.8. Basin-wide North Fork Skokomish average annual loads of terrestrial nitrogen (both inorganic and organic) inputs from water year 1998 – 2005

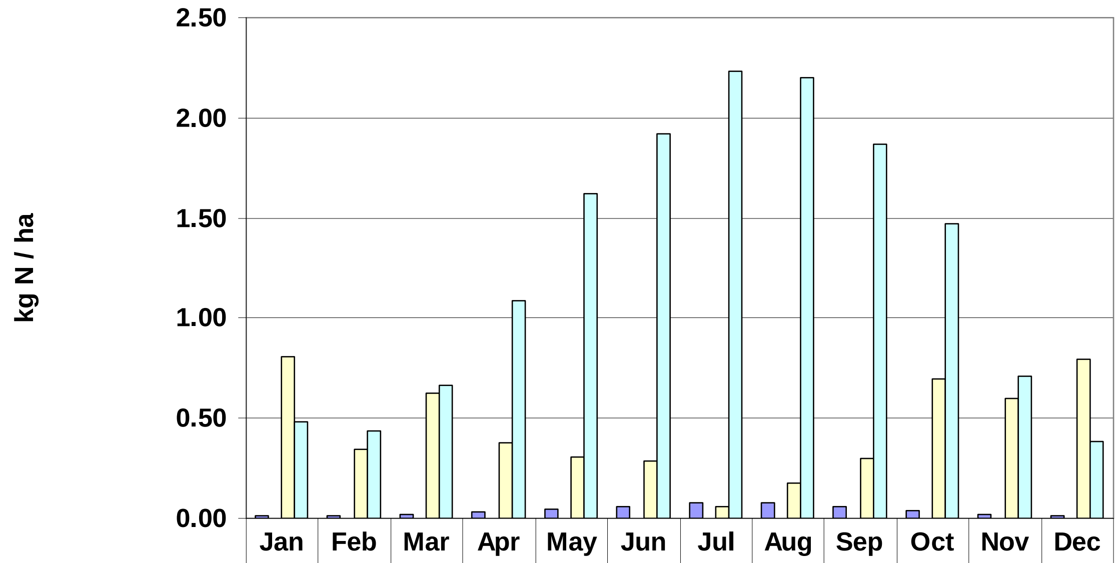

	Jan	Feb	Mar	Apr	May	Jun	Jul	Aug	Sep	Oct	Nov	Dec
N Fixation	0.01	0.01	0.02	0.03	0.04	0.06	0.08	0.08	0.06	0.04	0.02	0.01
Septic	0.00	0.00	0.00	0.00	0.00	0.00	0.00	0.00	0.00	0.00	0.00	0.00
Atmospheric	0.80	0.34	0.63	0.38	0.31	0.28	0.06	0.18	0.30	0.70	0.60	0.79
Veg Litter	0.48	0.44	0.66	1.09	1.62	1.92	2.23	2.20	1.87	1.47	0.71	0.38

Figure 4.9. Basin-wide North Fork Skokomish River average (water year 1998 – 2005) monthly loads of terrestrial input nitrogen

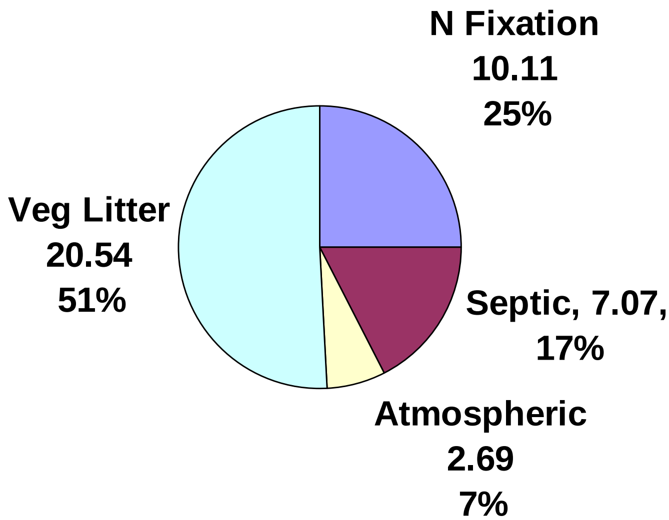

Sources of terrestrial inputs	N Fixation	Septic	Atmospheric	Veg Litter	Total
Annual load (metric tons of N/yr)	34.93	24.41	9.30	70.94	139.58
Annual flux (kg N/ha/yr)	10.11	7.07	2.69	20.54	40.41

Figure 4.10. Basin-wide Big Beef Creek average annual loads of terrestrial nitrogen (both inorganic and organic) inputs from water year 1998 – 2005. Scenario I: average septic load

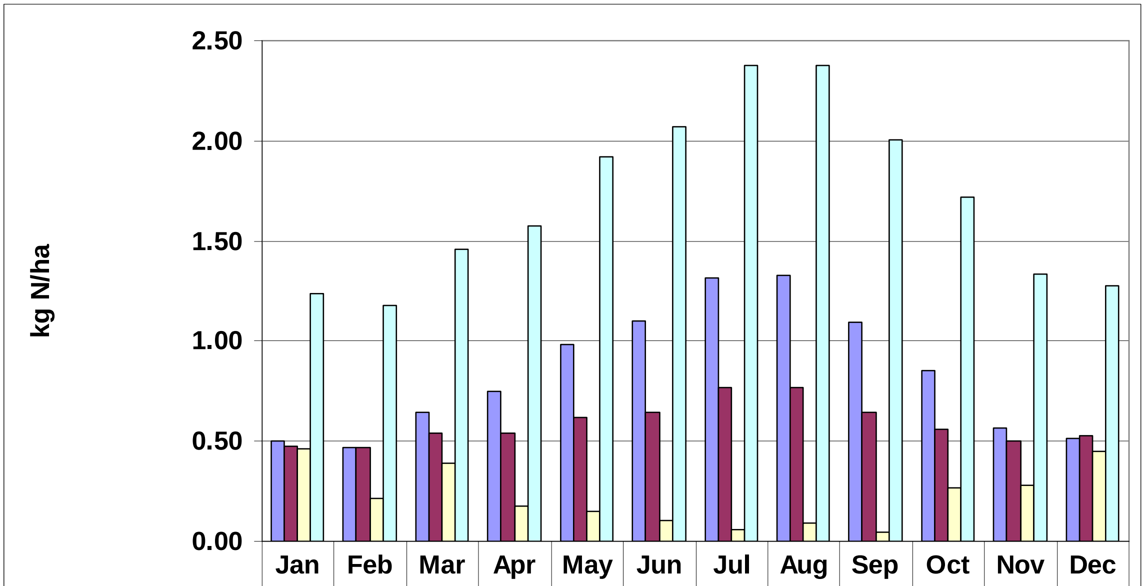

	Jan	Feb	Mar	Apr	May	Jun	Jul	Aug	Sep	Oct	Nov	Dec
N Fixation	0.50	0.47	0.65	0.75	0.98	1.10	1.31	1.33	1.10	0.85	0.57	0.51
Septic	0.48	0.47	0.54	0.54	0.62	0.65	0.77	0.77	0.64	0.56	0.50	0.53
Atmospheric	0.46	0.22	0.39	0.18	0.15	0.11	0.06	0.09	0.05	0.27	0.28	0.45
Veg Litter	1.24	1.18	1.46	1.58	1.92	2.07	2.38	2.37	2.01	1.72	1.34	1.28

Figure 4.11. Basin-wide Big Beef Creek average (water year 1998 – 2005) monthly loads of terrestrial input nitrogen – scenario I: average septic load

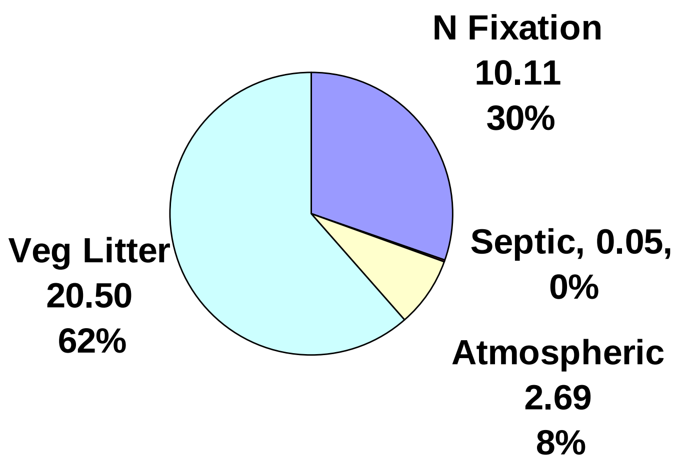

Sources of terrestrial inputs	N Fixation	Septic	Atmospheric	Veg Litter	Total
Annual load (metric tons of N/yr)	34.93	0.18	9.30	70.81	115.22
Annual flux (kg N/ha/yr)	10.11	0.05	2.69	20.50	33.35

Figure 4.12. Basin-wide Big Beef Creek average annual loads of terrestrial nitrogen (both inorganic and organic) inputs from water year 1998 – 2005. Scenario II: minimal septic load

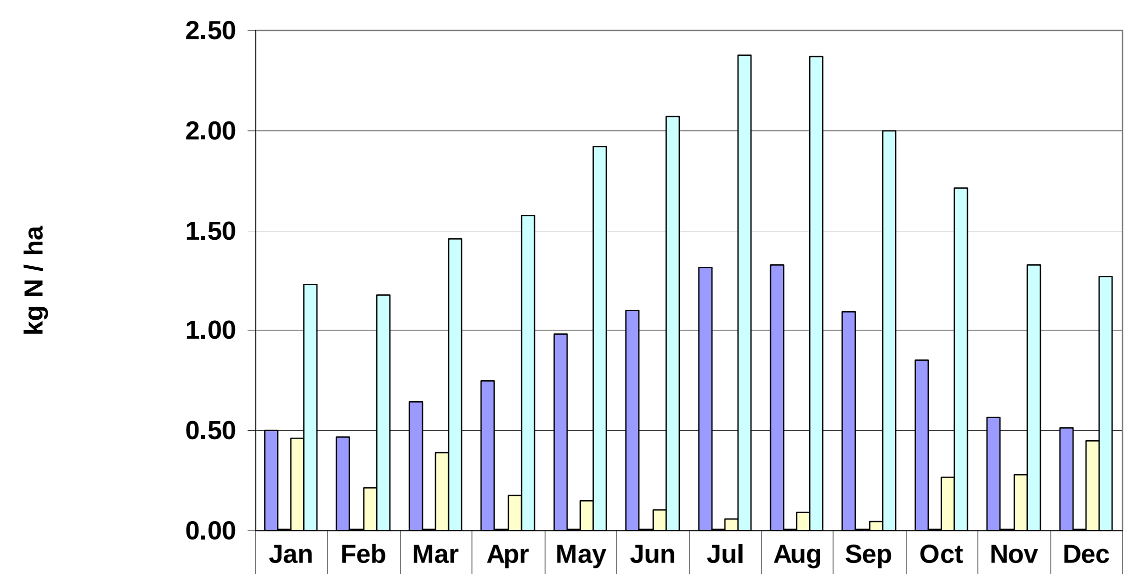

	Jan	Feb	Mar	Apr	May	Jun	Jul	Aug	Sep	Oct	Nov	Dec
N Fixation	0.50	0.47	0.65	0.75	0.98	1.10	1.31	1.33	1.10	0.85	0.57	0.51
Septic	0.00	0.00	0.00	0.00	0.00	0.00	0.01	0.01	0.00	0.00	0.00	0.00
Atmospheric	0.46	0.22	0.39	0.18	0.15	0.11	0.06	0.09	0.05	0.27	0.28	0.45
Veg Litter	1.23	1.18	1.46	1.58	1.92	2.07	2.38	2.37	2.00	1.71	1.33	1.27

Figure 4.13. Basin-wide Big Beef Creek average (water year 1998 – 2005) monthly loads of terrestrial input nitrogen – scenario II: minimal septic load

4.5.1.3: Annual and seasonal N budgets

The major factors controlling the magnitude and seasonality of the biochemical processes in the N cycle in the current mathematical representation are temperature, moisture regime, and landcover type. Mineralization and nitrification rates peak in the late spring and summer when the temperature and soil moisture regime is at the optimum condition for microbe activities (Figure 4.14 and 4.15). In natural forested systems, the relative nitrification (the ratio of mineralized N that is nitrified) is less than 1 and the value ranges from 0.01 – 0.71 (Fenn et al., 2005, Lavoie and Bradley, 2003; Turner et al., 1993). The relative nitrifications in Big Beef Creek and in the North Fork Skokomish River are 0.95 and 0.29 respectively.

The denitrification rate in Big Beef Creek was higher than in North Fork Skokomish River (Table 4.7). In both basins, the annual denitrification flux falls within published ranges (<0.21 – 2.4 kg N/ha-yr for undisturbed conifers and < 0.3 – 28 for undisturbed deciduous trees, Barton et al., 1999; 0.08-0.21, Binkley et al., 1992). Plant uptake inclined during spring and summer and was lower in the late summer through winter.

Table 4.7. Summary of basin-wide average annual flux of each process in N-cycle.

	Average basin-wide annual flux, kg N/ha/yr			
	Denitrification	Mineralization	Nitrification	Plant Uptake
Big Beef (average septic load scenario)	0.14	23.06	21.88	32.93
North Fork Skokomish	0.04	15.52	4.46	13.60

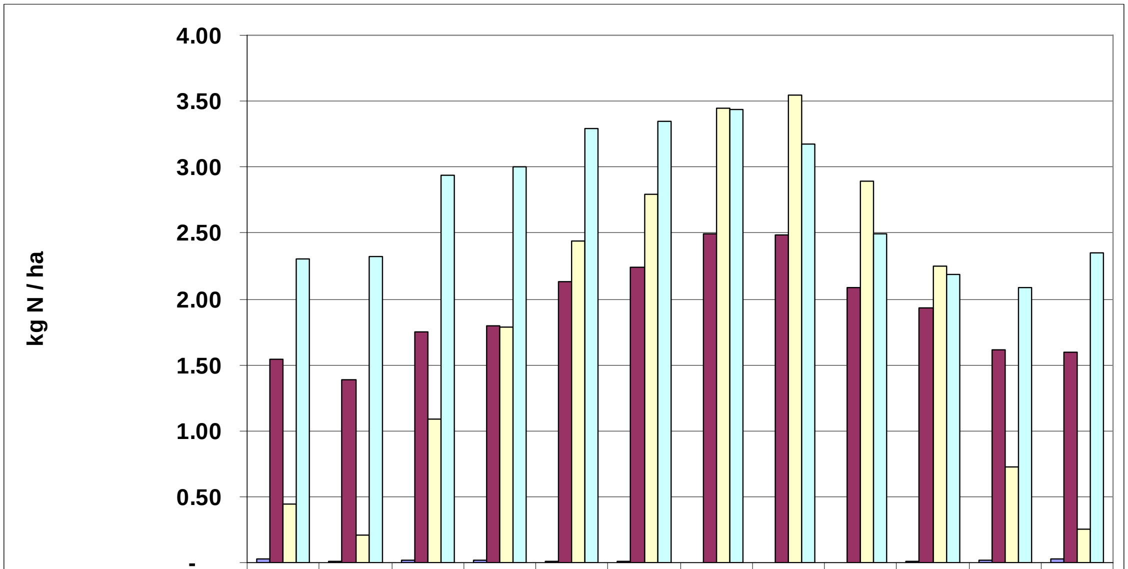

	1	2	3	4	5	6	7	8	9	10	11	12
Denitrification	**0.02**	**0.01**	**0.02**	**0.02**	**0.01**	**0.01**	**0.00**	**0.00**	**0.00**	**0.01**	**0.01**	**0.02**
Mineralization	**1.54**	**1.39**	**1.75**	**1.80**	**2.13**	**2.24**	**2.49**	**2.48**	**2.09**	**1.93**	**1.61**	**1.60**
Nitrification	**0.45**	**0.20**	**1.09**	**1.79**	**2.44**	**2.80**	**3.44**	**3.55**	**2.90**	**2.25**	**0.72**	**0.26**
Plant Uptake	**2.31**	**2.32**	**2.94**	**3.00**	**3.29**	**3.35**	**3.44**	**3.17**	**2.49**	**2.18**	**2.09**	**2.35**

Figure 4. 14. Big Beef Creek average 1998 - 2005 seasonal variation in the biogeochemical processes, under the average septic scenario

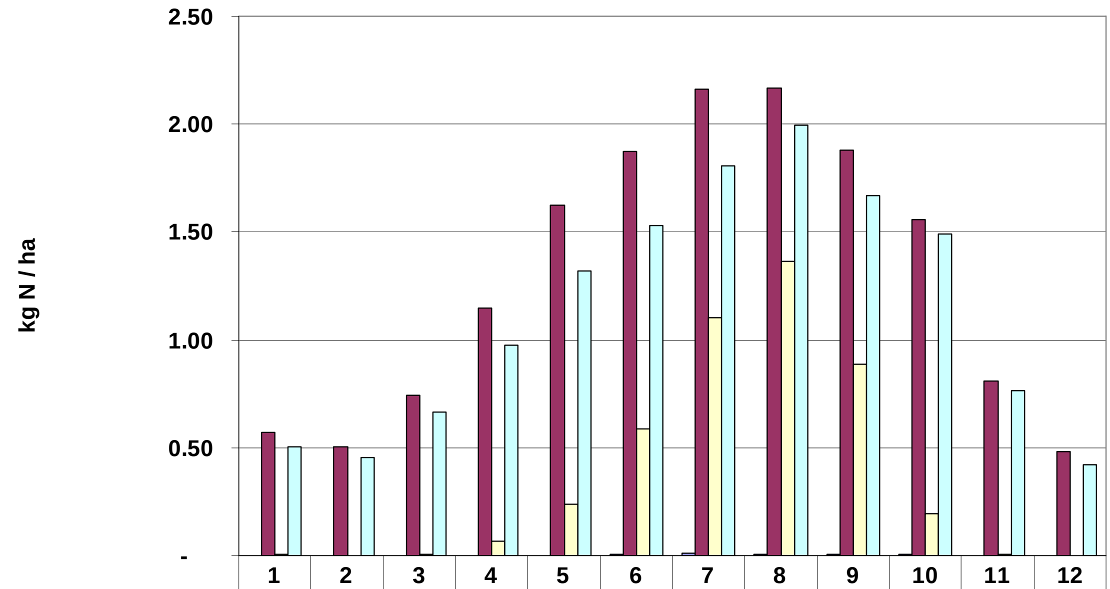

	1	2	3	4	5	6	7	8	9	10	11	12
Denitrification	0.00	0.00	0.00	0.00	0.00	0.01	0.01	0.01	0.00	0.00	0.00	0.00
Mineralization	0.57	0.50	0.74	1.15	1.62	1.87	2.16	2.17	1.88	1.56	0.81	0.48
Nitrification	0.00	0.00	0.01	0.07	0.24	0.59	1.10	1.36	0.89	0.20	0.01	0.00
Plant Uptake	0.50	0.45	0.66	0.98	1.32	1.53	1.81	1.99	1.67	1.49	0.77	0.42

Figure 4.15. North Fork Skokomish River average 1998 - 2005 monthly variation in the biogeochemical processes

4.5.2: Hydrologic dynamics and N export

4.5.2.1: Hydrologic dynamics

With the current parameter setting, the DHSVM component of D-SEM performed relatively satisfactorily for the stream flow simulation for both sub-basins (Figure 4.16, 4.17 and Table 4.8). The model efficiency is consistent with the published ranges, previously mentioned in Chapter 3.

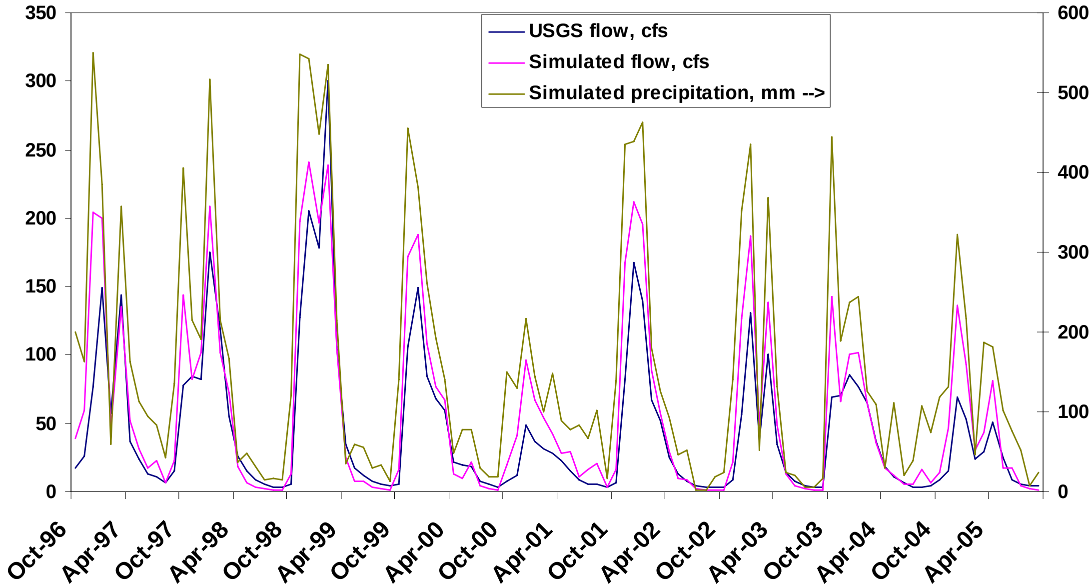

Figure 4.16. Simulated monthly precipitation, observed, and predicted average monthly flows from water year 1997 to June 2006 for Big Beef Creek.

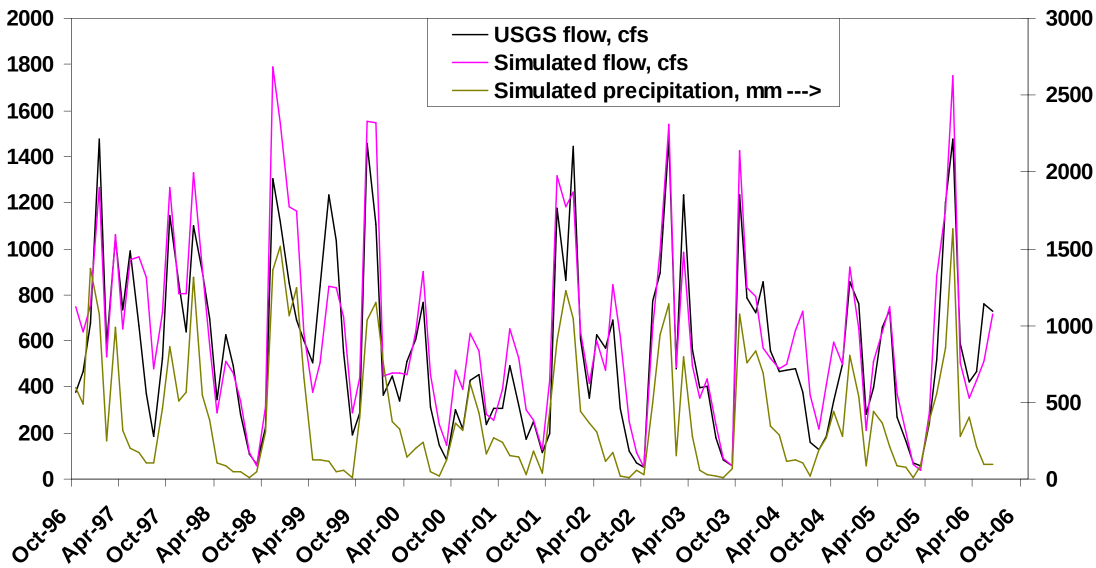

Figure 4.17. Simulated monthly precipitation, observed, and predicted average monthly flows from water year 1997 to June 2006 for North Fork Skokomish River.

Table 4.8. Hydrologic simulation performance for Big Beef Creek and North Fork Skokomish at the USGS gauges from water year 1997 – June 2006

	Gauge location	
Goodness of model fit	BBEE (12069550)	NFSK (12056500)
Nash and Sutcliffe E	0.7168	0.76
RMSE, cfs	28.61	178.0
Pearson's correlation, r	0.93	0.90

4.5.2.2: Stream N load and concentrations

The understanding of how the stream N loads and concentrations were obtained differently between simulation and observation is important for the interpretation of results. Nitrogen loads is defined as the mass flow rate of nitrogen species and is a product of stream flow rate and nitrogen concentration. For the observed stream nutrient data, the nitrogen concentration analyzed from instantaneous grabbed samples in each month was used as representative monthly concentration. The observed monthly load was calculated as a product of instantaneous concentration and the monthly USGS flow rate. In contrast, the simulated monthly load of nitrogen species is the aggregate of the 3-h estimated loads, and the simulated monthly concentration is the flow-weighted average value of 3-h results.

For Big Beef Creek, the estimated nutrient loads of nitrogen species were within a comparable range as the observed values from HCDOP and DOE (Table 4.9, Figure 4.22 – 4.29), with a difference of less than a factor of 2.

In terms of seasonality, it is expected that the stream nutrient concentration is highest in the late fall during the rise of the high-season flow, due to the flushing of nutrients that have been built up during the dry summer. If the basin is rain-on-snow dominated, the second peak with smaller magnitude is also expected during spring melt. On the other hand, in summer, terrestrial biotic demand is high and there is not much water to flush out the nutrients from the soil column. Therefore, stream nutrient concentration is expected to be low during summer. The trend described above was demonstrated most clearly by both the simulated and observed stream concentrations of nitrate, the most mobile dissolved nitrogen species (Figure 4.24 - 4.25). For dissolved organic nitrogen, the higher concentration in the late fall was also observed (Figure 4.22 – 4.23), but the difference between the highest and lowest concentrations was not as varied as that of nitrate. The monthly trend of the estimated load of NO_3, as well as those of other species, is more dominated by stream flow, rather than by concentrations, leading to the similar trend as the stream flow (Figure 4.30).

The estimated nutrient loads and concentrations from North Fork Skokomish River were not as close to observed values, compared to Big Beef Creek (Figure 4.31 – 4.38). The estimated 2005 annual load of DON was in the same range as observed values whereas the estimated DIN loads were different from the observation by a factor of 3 and 6 for ammonium and nitrite plus nitrate, respectively (Table 4.10). For nitrate, the peak of estimated load and concentration appeared towards the beginning of the high-season flow (Figure 4.33 – 4.34). For ammonium, the seasonality of the estimated concentration seemed to have a six-month lag in the peak time compared to the peak time of stream flow (Figure 4.37 – 4.38), indicating that the sorption estimation for this basin was not well represented. Further analysis on why the model performance on the North Fork Skokomish was not satisfactory will be discussed in section 4.5.3.2.

The estimation of annual DON load in both basins was close to observation than the estimated load of dissolved inorganic nitrogen. Based on the current representation of N cycle, the major source of DON was the vegetation litter decomposition. As mentioned earlier in section 4.4.3, the litter fall rate and litter composition data were the parameters with the most known information. Therefore, this may contribute to the higher accuracy in the estimated dissolved organic nitrogen compared to the inorganic nitrogen. For the inorganic species, the uncertainty in the estimation was compounded by the uncertainty of estimated mineralization and nitrification.

Comparing the stream N concentrations and loads in Big Beef Creek between 2 scenarios of septic loads (Table 4.11), the average annual concentration and load of NO_3 are the most impacted parameter, followed by the load and concentration of NH_4. The stream nutrient profiles of the low septic scenario appear the same as those of the average septic load scenario.

Table 4.9. Comparison of annual load estimated in Big Beef Creek from simulation and from HCDOP field data.

	2005 annual nutrient load, kg N/yr (Jan - Dec 2005)		
Source	DON	$NO_2 + NO_3$	NH_4
HCDOP	2,714	9,262	290
DHSVM	2,145	15,684	513
% of observed value	79%	169%	177%

Table 4.10. Comparison of annual load estimated in North Fork Skokomish from simulation and from HCDOP field data.

	2005 annual nutrient load, kg N/yr (Jan - Dec 2005)		
Source	DON	$NO_2 + NO_3$	NH_4
HCDOP	20,572	10,551	815
DHSVM	16,136	1,479	2,258
% of observed value	78%	14%	277%

Table 4.11. Comparison of average annual simulated loads and concentrations of nutrients between average septic and minimal septic load scenarios for Big Beef Creek.

Scenario	DON	NH_4	NO_3	NO_2
Average septic load				
kg/yr	3,492	163	2,624	28
ug/L	670	31	503	5
Minimal septic load				
kg/yr	3,281	138	2,085	27
ug/L	634	27	403	5
Difference				
kg/yr	(211)	(25)	(539)	(1)
% load difference	-6.04%	-15.06%	-20.54%	-2.99%
ug/L	36	4	100	0
% concentration difference	-5.31%	-14.40%	-19.93%	-2.24%

4.5.3: Model performance, uncertainty, and limitation

4.5.3.1: Discrepancy between simulated and observed results

As explained at the beginning of section 4.5.2.2, the monthly load and water flow that D-SEM reports was aggregated up from 3-hourly values that the simulation records The simulated monthly concentrations were flow-weighted, calculated from total monthly load and water flow. Conversely, the field samples that D-SEM compares to are all instantaneous samples taken once per month, that are then up-sampled into monthly representative values. This is an inherent difference in quantitative methods, the importance of which should not be understated.

To illustrate the inherent difference between single discrete data points from the field sampling and the monthly average simulated concentration, Figure 4.18 and 4.19 were constructed for comparison of NO_3 concentrations in Big Beef Creek and in North Fork Skokomish respectively. The pink line represents the simulated monthly average of the preceding and following 15 days, 30 days total. This line approximates what is reported as the monthly value in the other figures of this chapter. The light green colored area above and below the pink line shows the standard deviation of data points, from the monthly average values, over the month. The simulated instantaneous flow (black line), while labeled as such, is actually the average value over a 3-hour time step. This is as close to instantaneous as D-SEM allows, and is sufficient to compare volatility with the field-samples. As shown in Figure 4.18, the simulated instantaneous concentration is comparable to the values given by the field-samples in regards to range. However, when the simulation results are presented in the monthly average values, the extreme low and extreme high values of concentrations in the sub-daily or inter-daily variations will be filtered out.

Another issue in the comparison between simulation and observation is the minimum detection limit of nutrient concentrations, as encountered in the field sampling data from USGS and DOE. Because streams in western Washington are generally low in inorganic nitrogen concentrations, compared to streams on the eastern USA coast, the USGS measuring devices are not sensitive to the degree necessary to obtain discrete measurements. However, this field data still provides a base line of maximum value the modeled results should not exceed. A clear example is in Figure 4.19. The USGS minimum data points (green squares) show that the observed concentrations are below those points. The remaining USGS data points (blue squares) are estimated values. For North Fork Skokomish River, one sample point from HCDOP in July 2005 exceeds the USGS 60 ug/L detection limit. This may be due to the difference in the methods of nutrient composition analysis between the two sources.

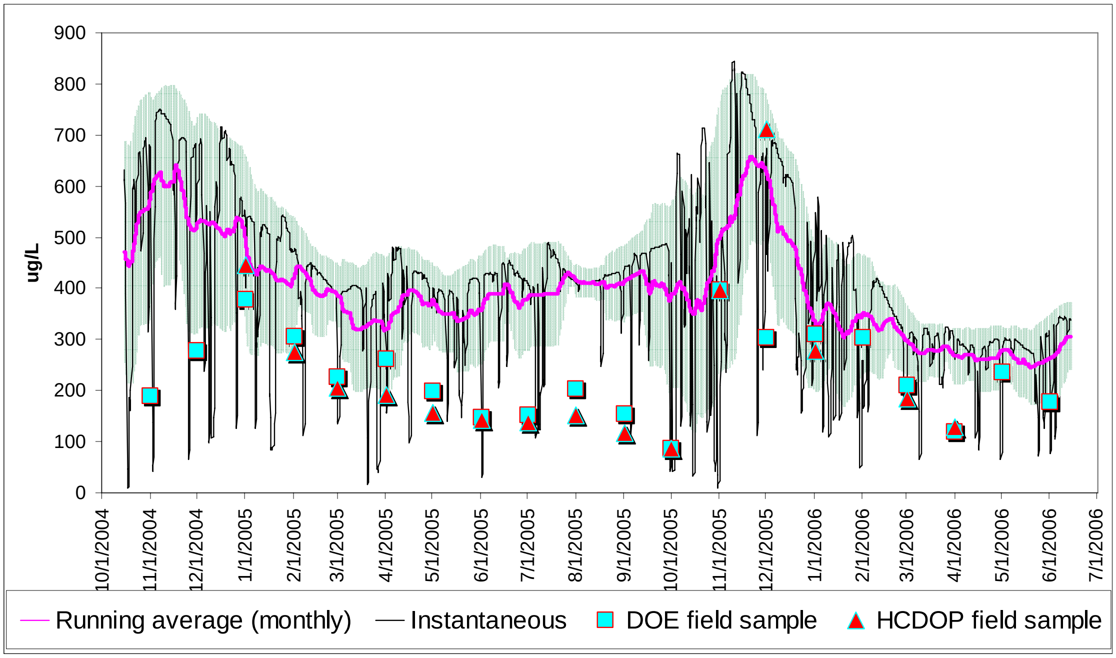

Figure 4.18. Big Beef Creek, discrepancy between instantaneous field sampling data and continuous data from modeling

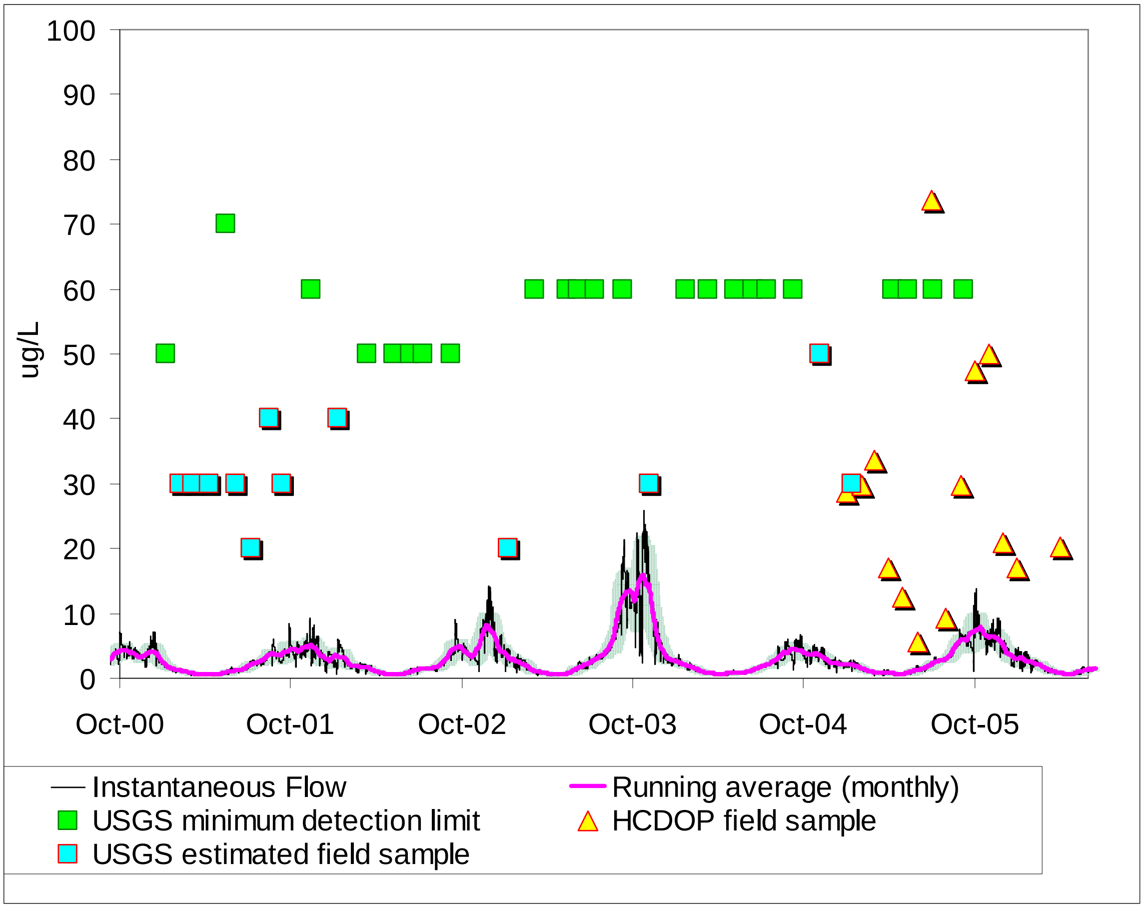

Figure 4.19. North Fork Skokomish discrepancy between instantaneous field sampling data and continuous modeling data

Although Figure 4.18 and 4.19 was intended for demonstrating the difference between observation and simulation, the 3-h result was also beneficial for evaluating the model performance. In Figure 4.18, the sub-daily and inter-daily variability in the simulated 3-h concentrations during certain periods, such as at the beginning of November, 2004, was dramatic and was not commonly observed (Michael Brett, personal communication). As D-SEM is a simulation, there are a number of areas that, on close inspection, do not model real-life very exactly. Examples of this include homogeneous soil layers, 150-m topographic representation, and these concentration spikes. This is because the focus of D-SEM is on long-term averages, and components must be simulated in an approximation. Thus, the extreme cases will not always fit well on close inspection. While D-SEM concentrates on the long-term results, it is valid, and very desirable to improve on the underlying processes as much as possible, as this will help improve the efficiency of D-SEM as a whole. Therefore, the next section is the discussion on the uncertainty and current model limitation.

4.5.3.2: Model uncertainty and limitation

Model is an approximation of the real world, and how close it is to represent real world behavior depends on the input data availability and the processes being represented or not being represented.

4.5.3.2.1: The limitation in input data availability

Soil chemistry data

As mentioned earlier, the current soil map is characterized by hydraulic property differentiation, as in how fast water moves through the soil. While this is useful for hydrologic simulation, it is less useful for chemistry modeling. A more refined soil map or a separate map using additional information on the soil order and soil parent material would be helpful in deriving chemical properties such as soil organic content, clay content, mineral type, and pH ranges. These chemical property data will be useful in refining the sorption process representation, the pool size of nutrient reservoirs, and other biotic processes in the nitrogen cycle. Statistic relationships from soil field sampling, rather than soil column-experiment data will also be helpful in defining the sorption behavior.

Soil temperature

Major control factors of most biogeochemical processes are biotic, hydrologic, and physical processes such as sorption. Of these three factors, hydrologic is the one most known and was proven to be reasonably represented, on most conditions. The terrestrial biotic control depends mostly on temperature and moisture conditions of the soil, and the stream biotic control depends on stream temperature. Therefore, the accuracy in the estimated stream nutrient loads and concentrations is dependent on the temperature.

Currently the soil temperature of each soil layer was estimated empirically from the air temperature. During the winter months, the simulated soil temperature becomes negative. However, the work by Edmonds et al. (1998) demonstrated that the temperature of the top 50 cm of soil in a watershed in Olympic National Park never gets below about 3 ^{o}C (Figure 4.20) even when the air temperature gets below freezing point. However, in the simulation, the soil temperature during the colder months is less accurate and the values are below freezing points whenever the air temperature is below zero (Figure 4.21). This contributed to the underestimation of nitrate in North Fork Skokomish because the magnitude of mineralization and nitrification may be underestimated. An example is the zero value of monthly nitrification during the late fall and winter months (Figure 4.15). Additional information on soil surface temperature or actual soil temperature measurement data will be helpful in improving the scheme for estimating soil temperature.

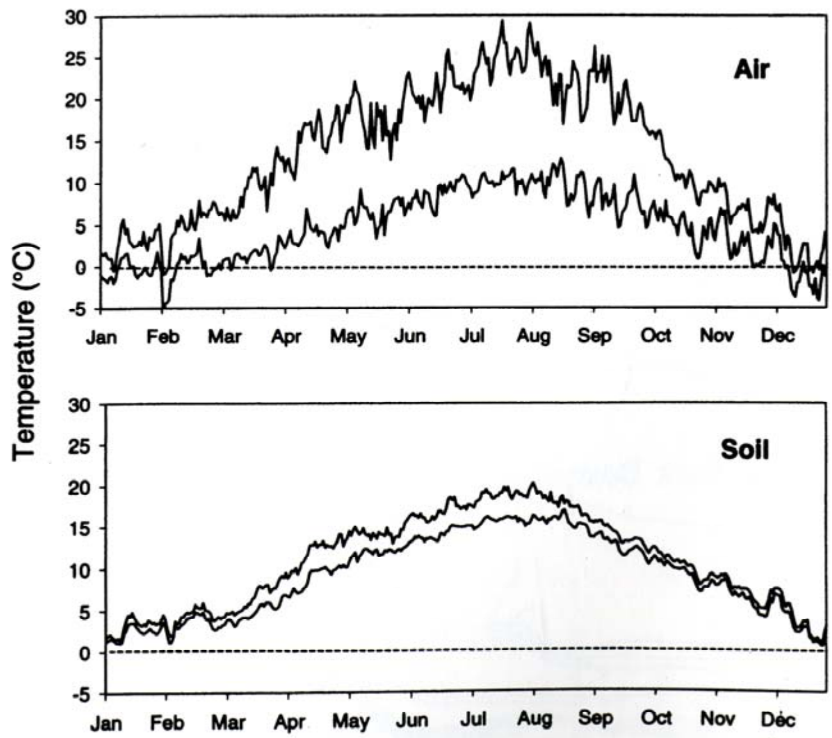

Figure 4.20. Average 1984-1993 daily maximum and minimum air and soil temperatures in the West Twin Creek in Olympic National Park, WA (Edmonds *et al*., 1998)

For stream temperature, D-SEM tends to underestimate the winter temperature (Figure 4.39 and 4.40) in both sub-basins. However, these two streams are cold and the difference in the winter temperature factor due to a few degree differences in the temperature range of 2-6 ^{o}C should not cause significant impact on the in-stream process rates. The preliminary sensitivity analysis also indicates that the model is not very sensitive to the in-stream reaction rates.

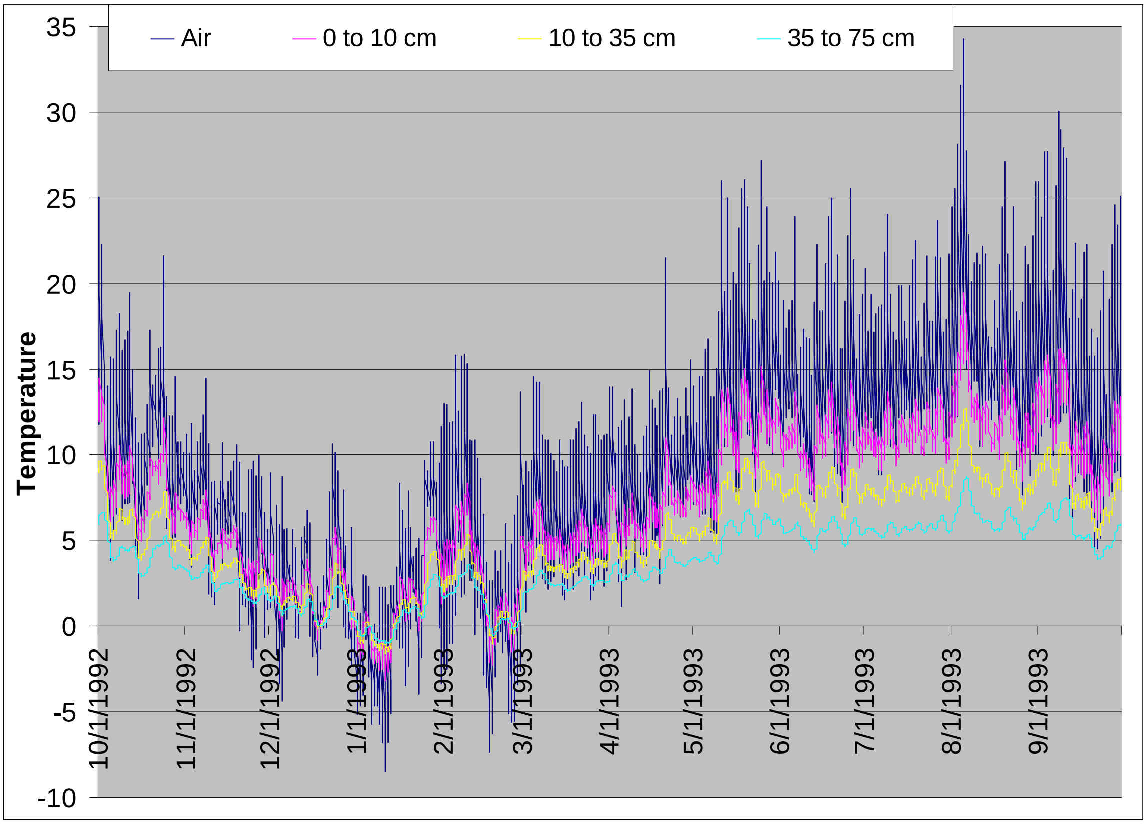

Figure 4.21. Simulated soil temperature for the top soil (0-10 cm), second layer (10-35 cm), and third layer (35 – 75 cm)

4.5.3.2.2: Process representation

The version of DHSVM used in this study does not simulate sediment erosion and transport or groundwater. These two components are additional sources of nutrient export. In terms of sediment erosion and transport, this component will add to dissolved nutrients in an amount based on the partitioning with the particulate nutrients getting into the streams. This additional input may be significant in an area with high disturbance because such a situation is more prone to erosion.

The groundwater contribution of nutrients will be highest in the summer, when the contribution of groundwater to the stream flow is highest. In addition to being another source of nutrient, the groundwater representation will also improve hydrologic simulation. Wiley (2006) indicated that DHSVM tends to underestimate the dry-season stream flow, and in the past, this issue has been addressed using statistical, bias correction approaches.

The inclusion of the groundwater component should also improve the accuracy of the simulated concentration during the extreme flow periods. The internal mechanisms of D-SEM use chemical mass, not concentration, as the means of computation, mass-balance, and export. When concentrations are needed, it is computed dynamically, based on total available mass and the amount of water. Therefore, the simulated concentrations are strongly tied to the accuracy of the hydrology model. During most time periods, the hydrology model is relatively accurate (Figure 4.16, Figure 4.17). However during periods of extreme water flow (very low in summer or very high in winter), the simulated hydrology is less predictive of actual flows, and as such the simulated chemical concentrations are less predictive of actual concentrations.

Another source of model uncertainty comes from the terrestrial nutrient reservoir representation. Currently, each soil column, excluding the deep soil below the root zones, is considered a homogeneous reservoir of nutrients. The magnitude of estimated biotic processes is dependent on the average condition, such as soil moisture and soil temperature, within the top 75 cm of the soil. In reality, the soil nutrient level, organic content and biotic activity are highest on the surface soil and decreases with depth. Physical processes such as sorption also vary with soil depth. An example is a discussion in the work by Neff and Asner (2001) that the patterns of soil DOC fluxes and concentrations with soil depth are controlled mainly by sorption rather than by biotic control, and sorption depends on the soil organic content which varies with depth.

The final model limitation is on the selected scheme of sorption representation. Local instantaneous linear sorption equilibrium is currently assumed in the system. However, the scheme does not work well in North Fork Skokomish River. In addition to having more refined input soil chemistry data, a modification of sorption representation to be explicit first order kinetics is believed to help adjust the timing of nutrient export from the soil and should be an item for future improvement.

4.6: Conclusion

The DHSVM Solute Export Model (D-SEM) was created to help understand the terrestrial and hydrological processes occurring in a targeted watershed, and how these processes influence nutrient export into associated streams.

Performance-wise D-SEM performs its testing functions adequately, giving results well within the same order of magnitude as field observations, and has demonstrated a potential for portability to multiple watersheds with no additional tuning needed. With these results it is clear that with additional refinement of the methods and additional field samplings (see further below), D-SEM will be able to be leveraged for all of the Hood Canal basins.

For Big Beef Creek, the scenarios of average versus low anthropogenic input have shown that human inputs such as septic loads can change the stream chemistry by increasing the inorganic nitrogen levels in the stream. The extent of the impact, however, may not be as sensitive as might be first imagined. This is because between the two scenarios, while the input factor was increased by about 140 times, the actual loads that reached the stream channel translated to approximately a 15% increase in NH_4, and a 20% change in NO_3. Again, these stated results, while compelling, are from the test run of D-SEM. Once the model has been refined, these scenarios will be re-run, and the conclusions revisited.

To qualify the D-SEM’s performance more significantly, additional field observations, over a longer period of time, are needed for comparison purposes. Reciprocally, additional observation data is needed to further adjust and improve D-SEM performance. As of November 2006, the HCDOP is proceeding with field sampling of the Hood Canal watersheds that will provide the data points necessary to further adjust and analyze D-SEM performance. Other organizations that are in the process of providing similar field samples include the Washington State Department of Ecology, and the USGS. Additional field data sources should be investigated to determine what current or future data could be used in tuning D-SEM, both in terms of soil and stream sampling. For example, HCDOP storm sampling data, while short in duration, provides field-samples on a much more granular level compared to the monthly samples that have traditionally been used. The capture of storm data for the Hood Canal region has recently started, and as such is another source that should be investigated in the future.

After D-SEM is further tuned, it can be applied to the entirety of Hood Canal, and all the watersheds it contains. One of the many benefits this application will provide is the simulation of stream concentrations for watersheds that do not have recorded field observations and will aid in the estimation of canal loads from terrestrial systems. This will then aid in the estimates of nutrient loads within Hood Canal itself, the marine cycle, and assist in the solution to the problem of the low oxygen level.

As D-SEM is tuned and improved, it will also provide a powerful tool to help decision makers assess the different scenarios of land management options. In turn, the water quality issues this model will help solve will benefit everyone.

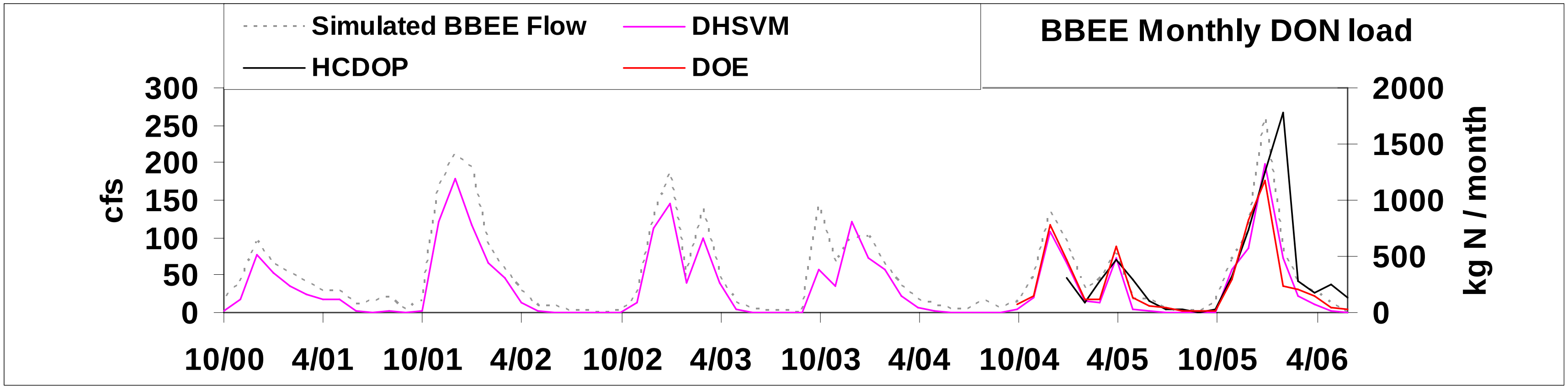

Figure 4.22. Comparison of Big Beef Creek monthly DON loads from the simulation on average septic load scenario and field observation.

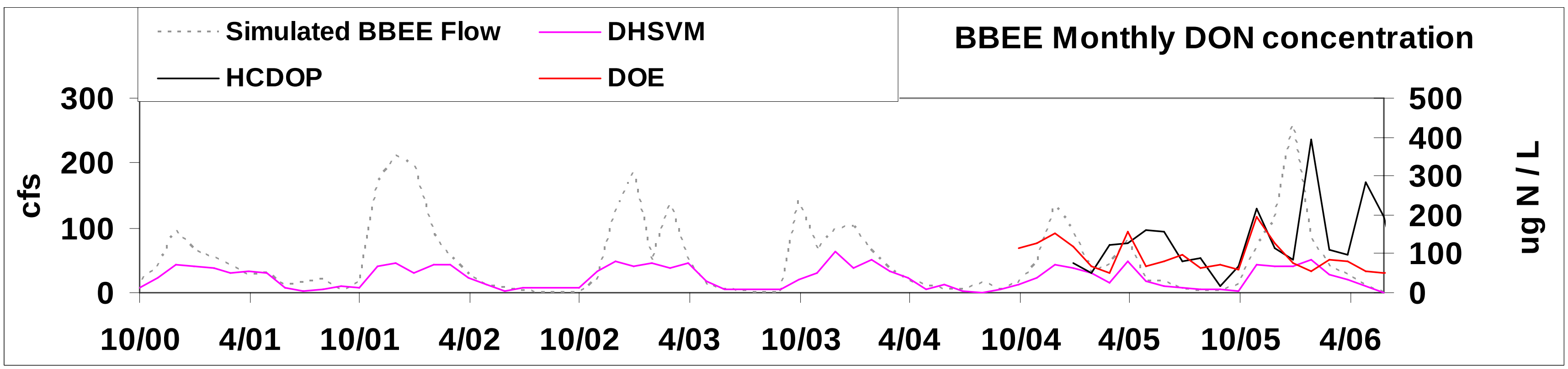

Figure 4.23. Comparison of Big Beef Creek monthly flow-weighted DON concentration from the simulation on average septic load scenario and instantaneous observed DON concentration.

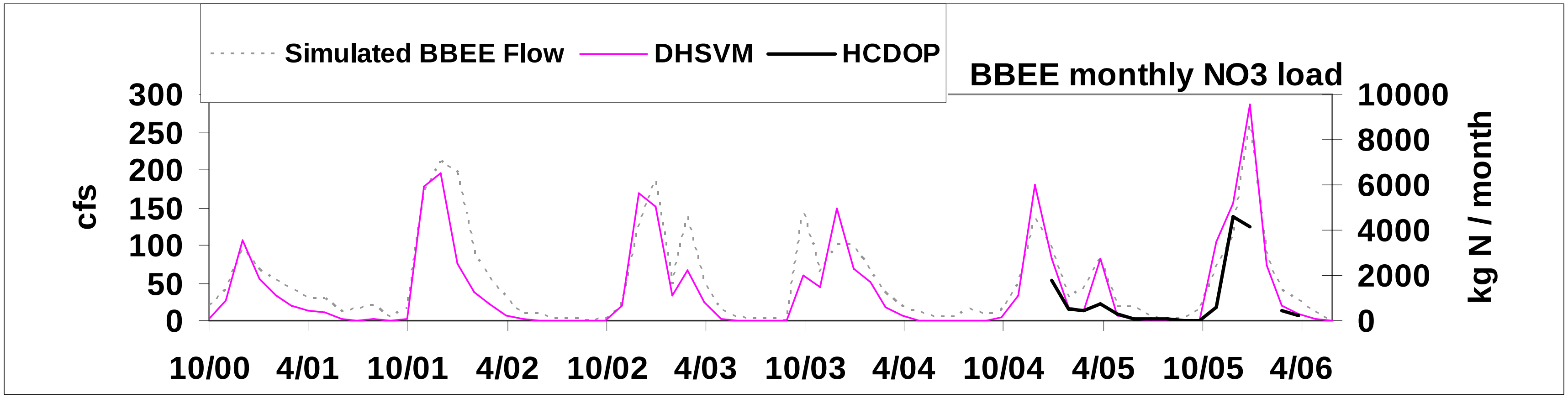

Figure 4.24. Comparison of Big Beef Creek monthly NO_3 loads from the simulation on average septic load scenario and field observation.

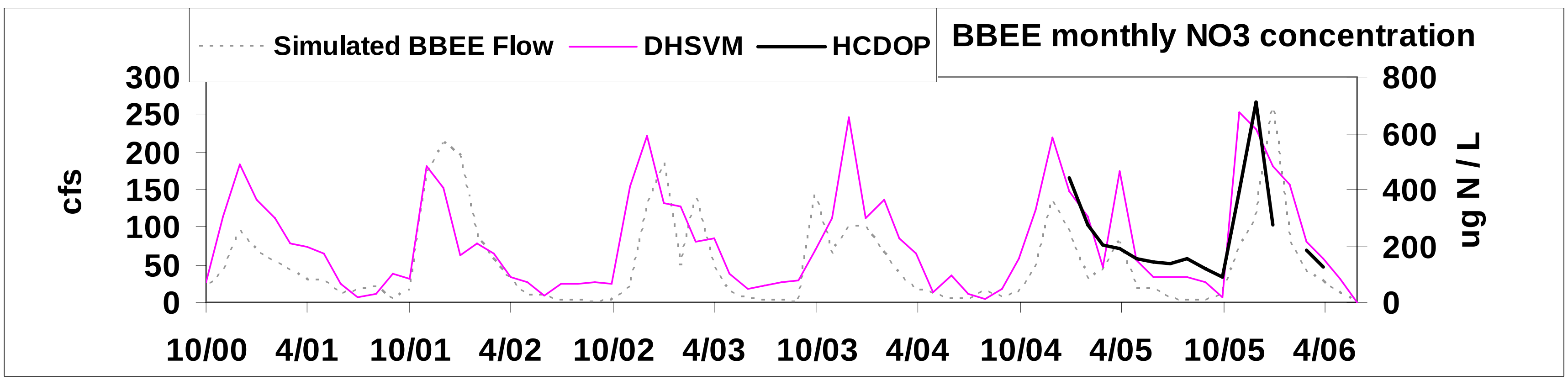

Figure 4.25. Comparison of Big Beef Creek monthly flow-weighted NO_3 concentration from the simulation on average septic load scenario and instantaneous observed NO_3 concentration.

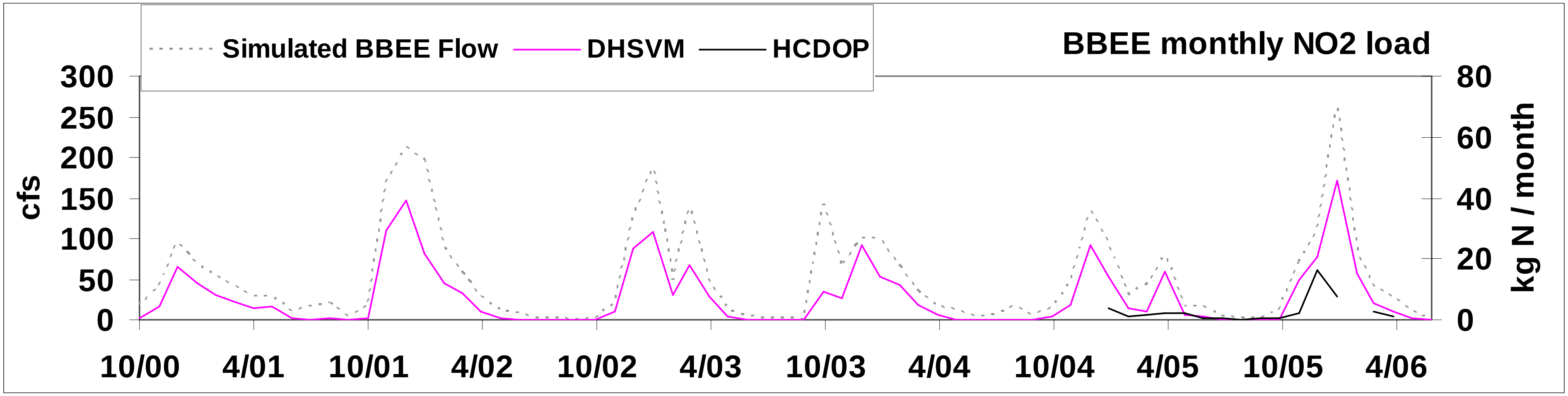

Figure 4.26. Comparison of Big Beef Creek monthly NO_2 loads from the simulation on average septic load scenario and field observation.

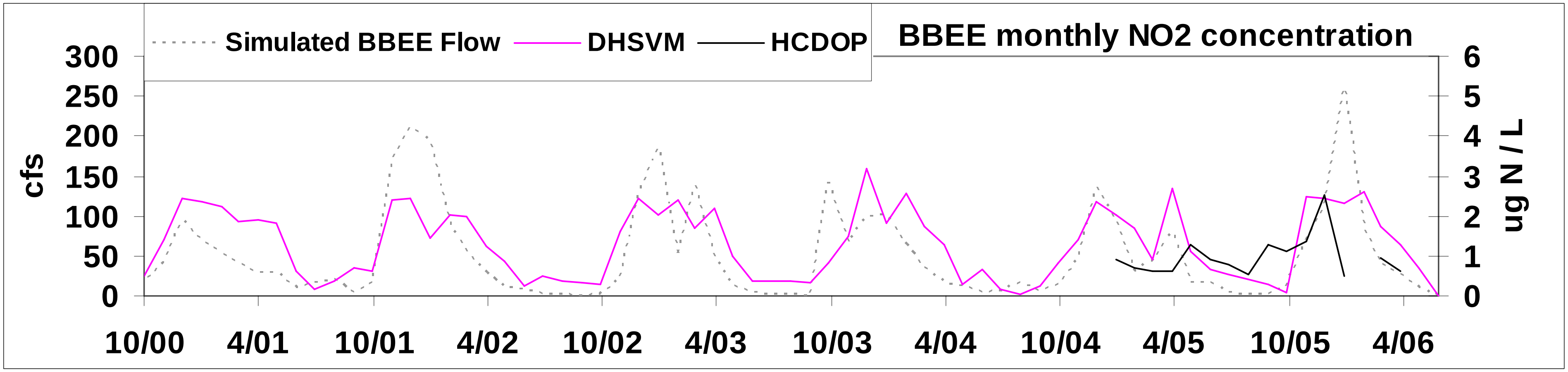

Figure 4.27. Comparison of Big Beef Creek monthly flow-weighted NO_2 concentration from the simulation on average septic load scenario and instantaneous observed NO_2 concentration.

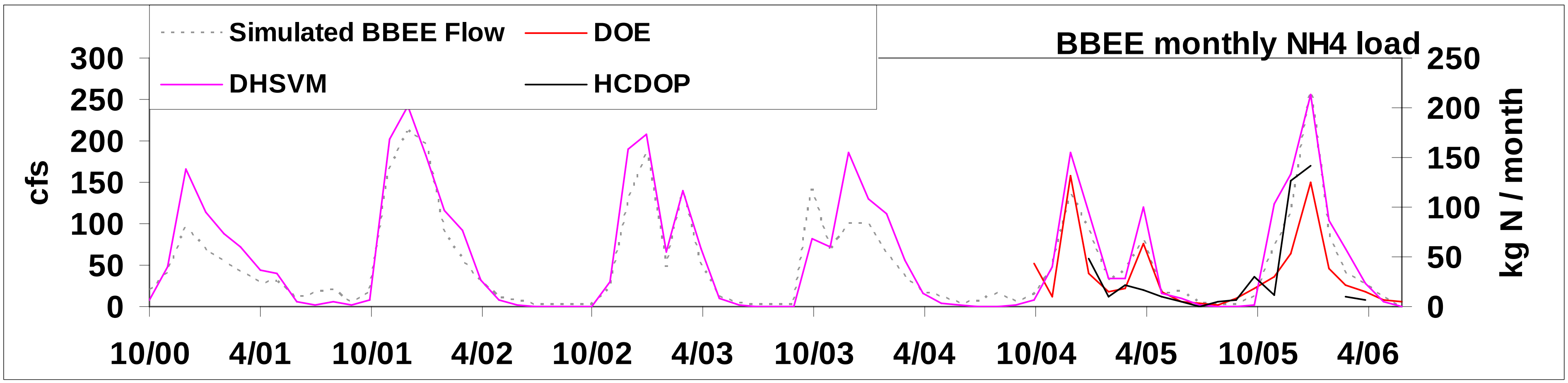

Figure 4.28. Comparison of Big Beef Creek monthly NH_4 loads from the simulation on average septic load scenario and field observation.

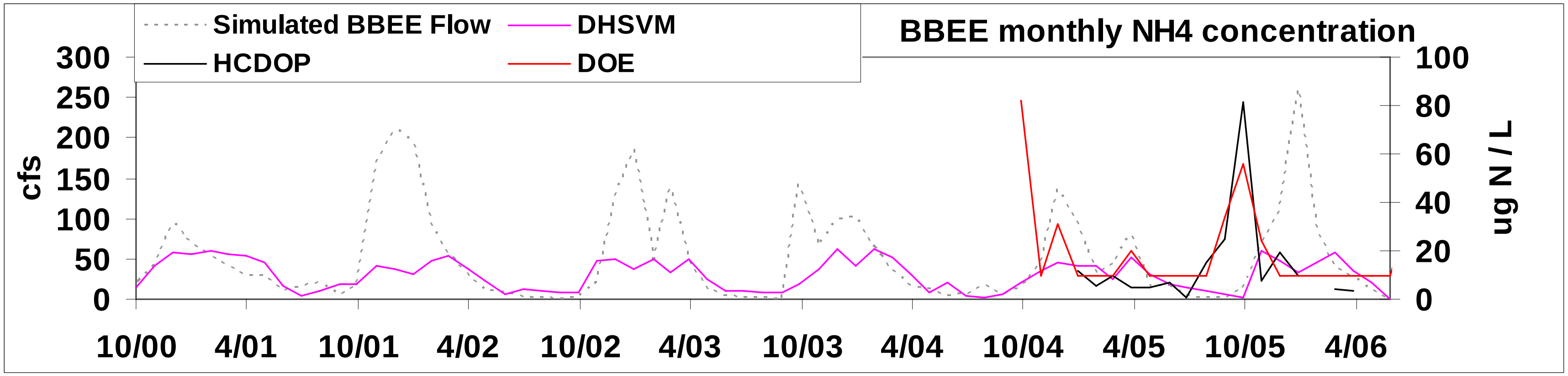

Figure 4.29. Comparison of Big Beef Creek monthly flow-weighted NH_4 concentration from the simulation on average septic load scenario and instantaneous observed NH_4 concentration.

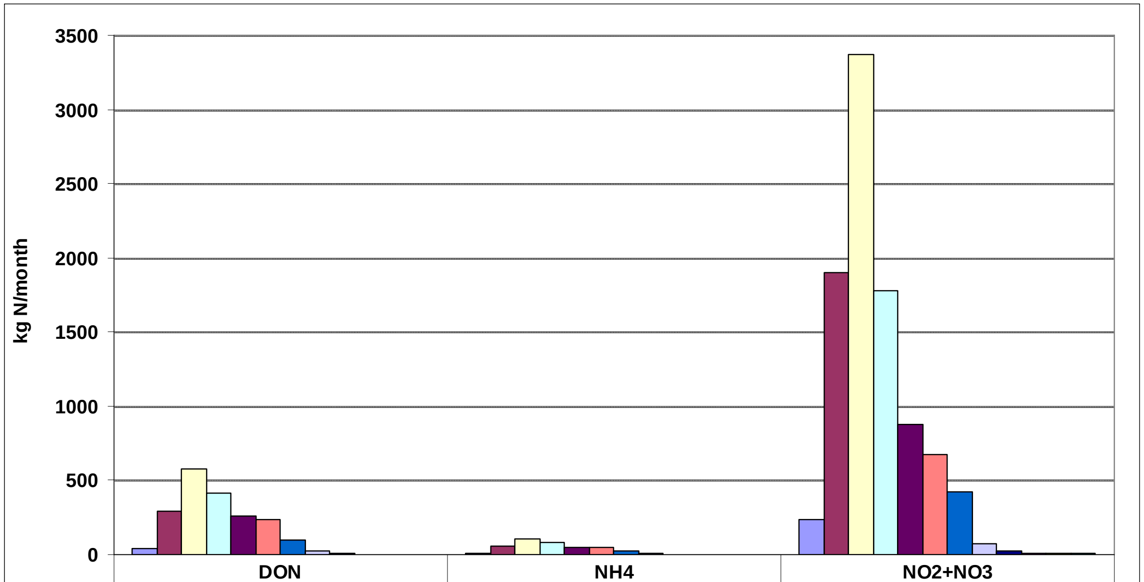

	DON	NH4	NO2+NO3
Oct	44.1	9.4	239
Nov	290.4	57.5	1897
Dec	576.7	103.1	3366
Jan	416.9	80.3	1775
Feb	262.9	52.0	878
Mar	232.4	49.1	677
Apr	101.2	24.1	423
May	20.5	6.5	75
Jun	6.1	2.3	25
Jul	1.8	0.7	10
Aug	2.0	0.8	9
Sep	1.1	0.4	7

Figure 4.30: Big Beef Creek average 1996-2005 monthly loads of each chemical species from October (left) to September (right).

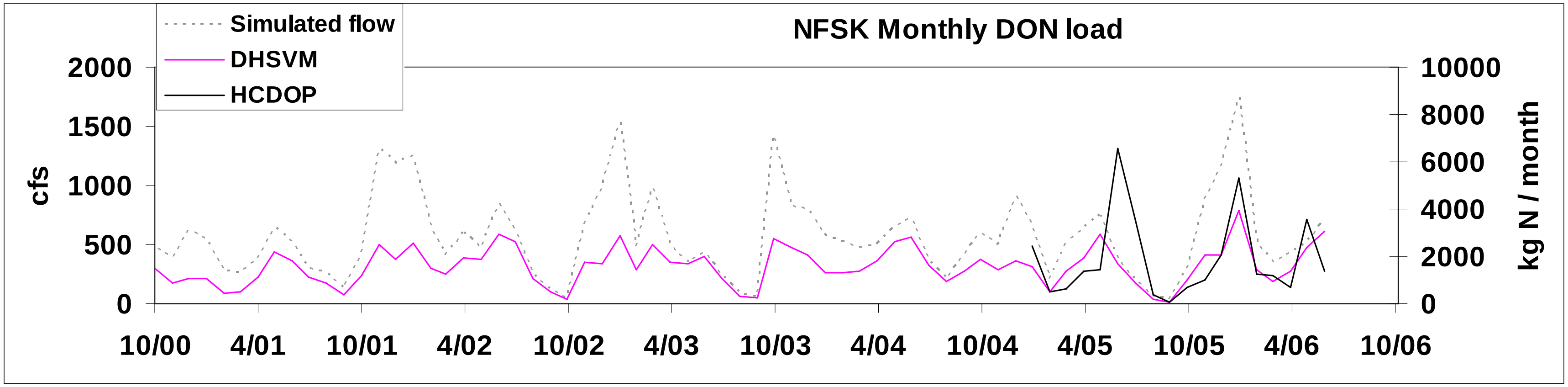

Figure 4.31. Comparison of North Fork Skokomish River monthly DON loads from the simulation and field observation.

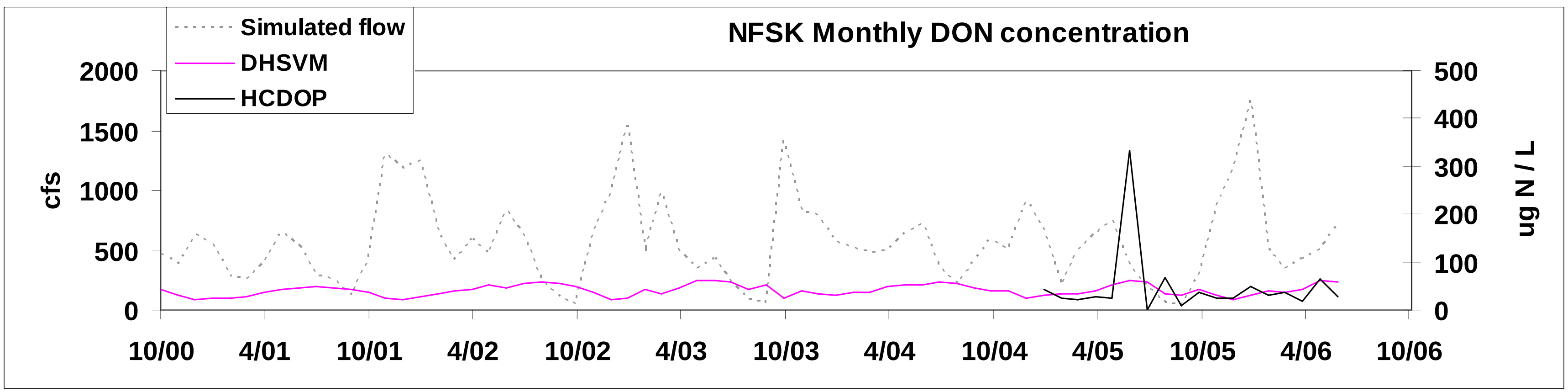

Figure 4.32. Comparison of North Fork Skokomish River monthly flow-weighted DON concentration from the simulation and instantaneous observed DON concentration.

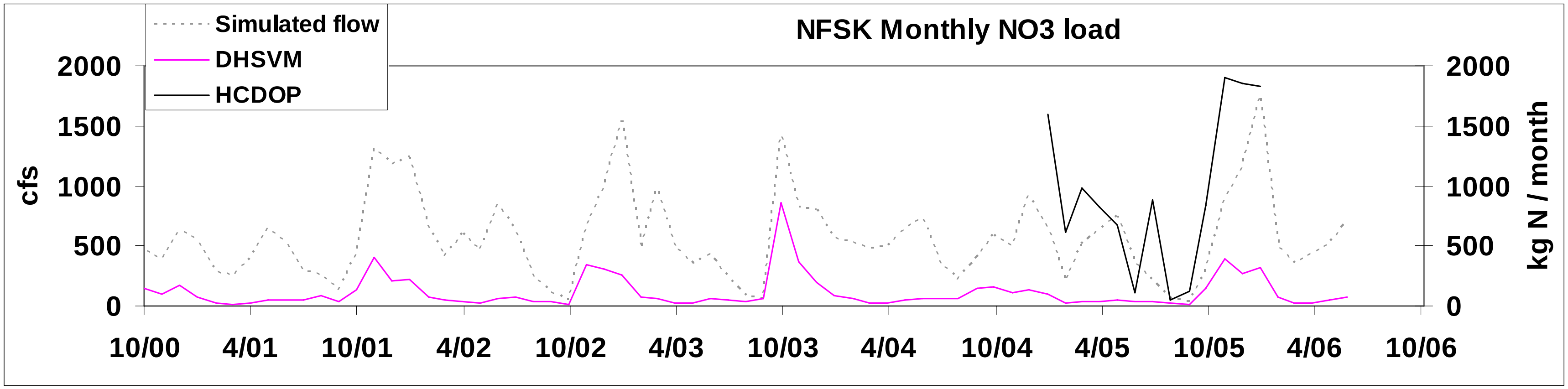

Figure 4.33. Comparison of North Fork Skokomish River monthly NO_3 loads from the simulation and field observation.

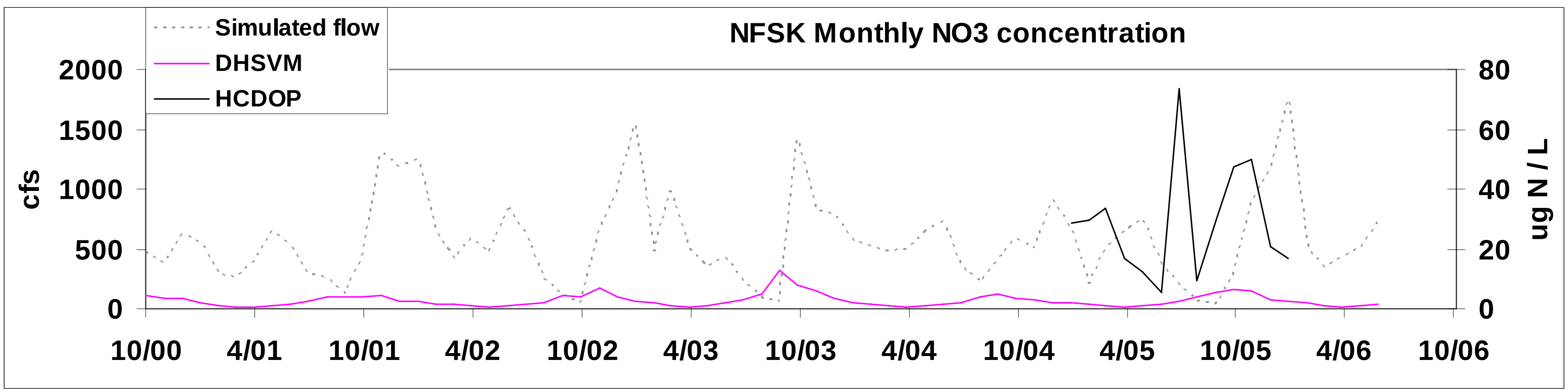

Figure 4.34. Comparison of North Fork Skokomish River monthly flow-weighted NO_3 concentration from the simulation and instantaneous observed NO_3 concentration.

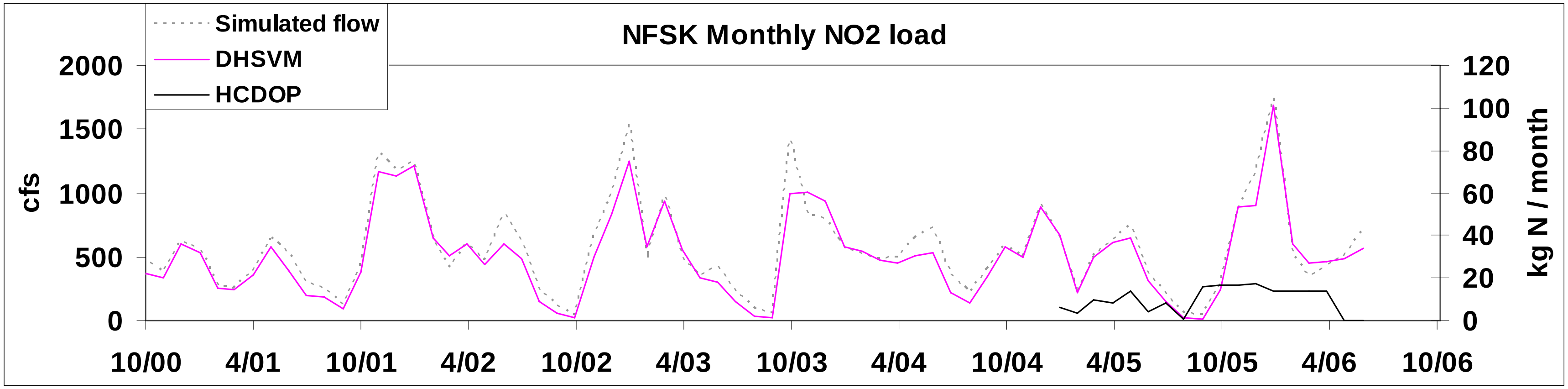

Figure 4.35. Comparison of North Fork Skokomish River monthly NO_2 loads from the simulation and field observation.

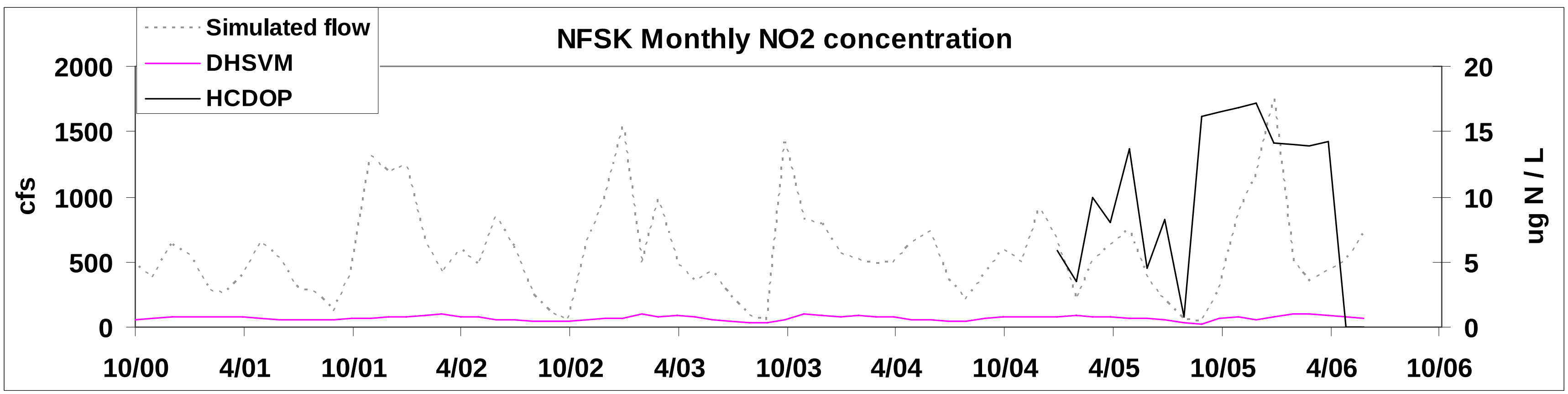

Figure 4.36. Comparison of North Fork Skokomish River monthly flow-weighted NO_2 concentration from the simulation and instantaneous observed NO_2 concentration.

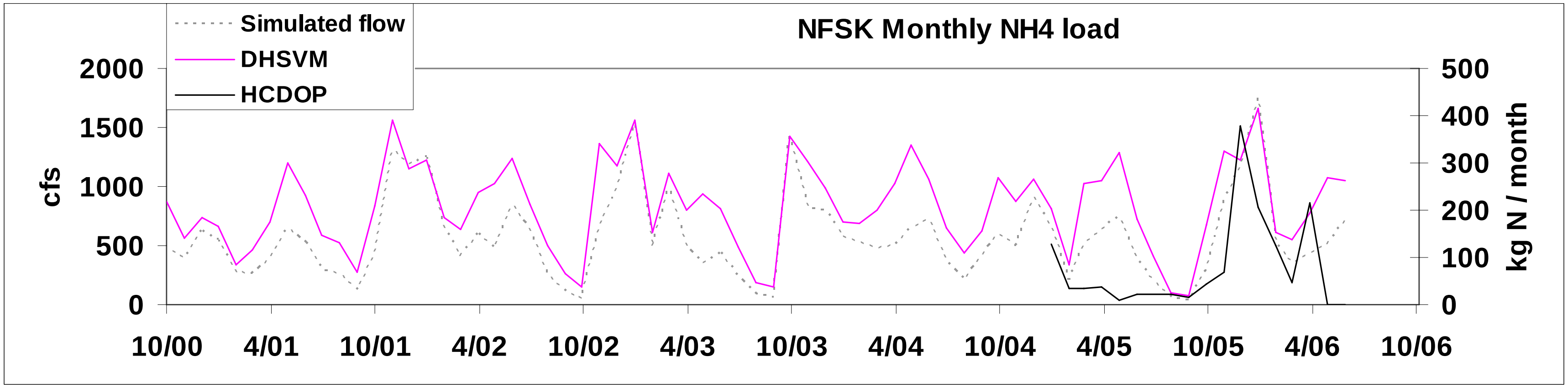

Figure 4.37. Comparison of North Fork Skokomish River monthly NH_4 loads from the simulation and field observations.

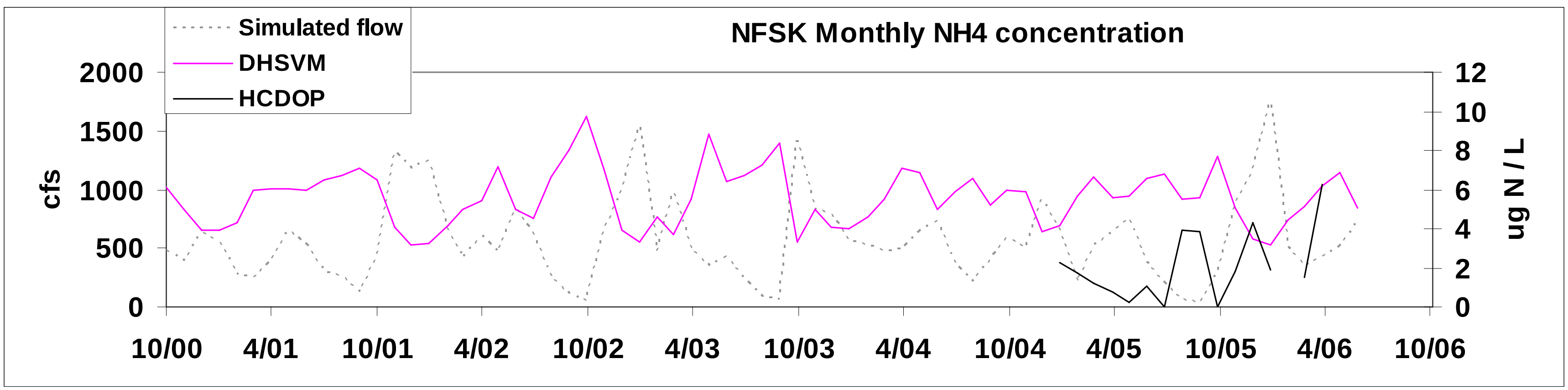

Figure 4.38. Comparison of North Fork Skokomish River monthly flow-weighted NH_4 concentration from the simulation and instantaneous observed NH_4 concentration

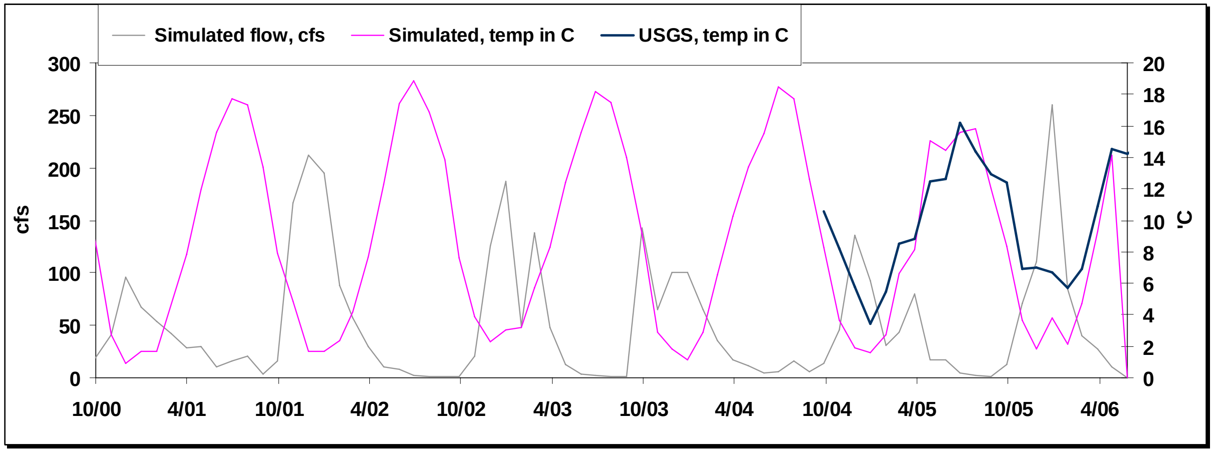

Figure 4.39. Comparison of Big Beef Creek simulated stream temperature and observed temperature from USGS samples.

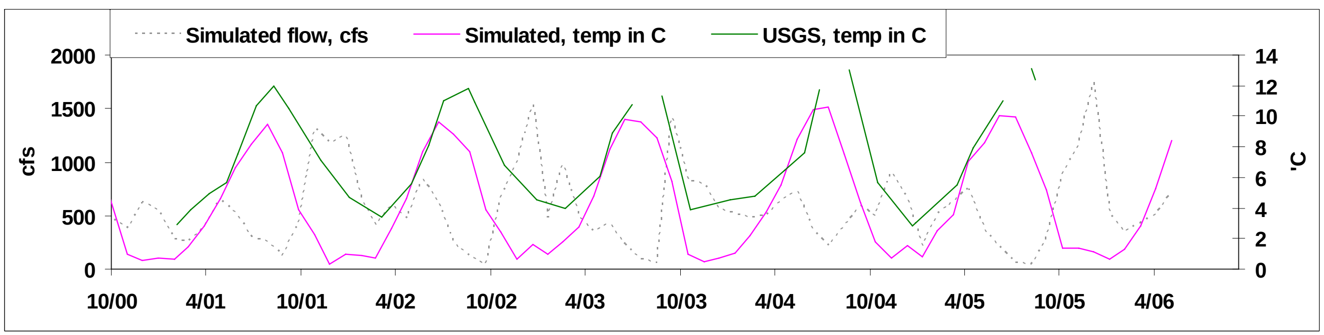

Figure 4.40. Comparison of North Fork Skokomish River simulated and observed (USGS) stream temperatures.

References

Akanda, A.S., Horowitz, J., James, A., Miller, S.F. (2006). *Nitrogen Loading from Septic Systems into Hood Canal, WA.* University of Washington, Seattle, WA.

Alford, D. (1992). Stream flow and sediment transport from mountain watersheds of the Chao Phraya Basin, northern Thailand: a reconnaissance study. *Mountain Research and Development* 12 (3), 257-268.

Barton, L., McLay, C.D.A., Schipper, L.A., Smith, C.T. (1999). Annual denitrification rates in agricultural and forest soils: a review. *Australian Journal of Soil Research* 37 (6), 1073-1093.

Batjes, N.H. (ed.) (1995). *A Homogenized Soil Data File for Global Environmental Research: A Subset of FAO, ISRIC and NRCS Profiles (Version 1.0).* Working paper and preprint 95/10b. International Soil Reference and Information Centre, Wageningen, The Netherlands.

Beckers, J., Alila, Y. (2004). A model of rapid preferential hillslope runoff contributions to peak flow generation in a temperate rain forest watershed. *Water Resources Research* 40 (3), Art. no. W03501.

Benfield, E.F. (1997). Comparison of litterfall input to streams. *Journal of the North American Benthological Society* 16 (1), 104-108.

Bicknell, B.R., Imhoff, J.C., Kittle, J.L., Donigian, A.S., Johanson, R.C. (1993). *Hydrological Simulation Program-Fortran (HSPF): User's manual for release 10.0*. EPA-600/3-84-066. Environmental Research Laboratory, USEPA. Athens, GA.

Binkley, D., Sollins, P., Bell, R., Sachs, D. (1992). Biochemistry of adjacent conifer and alder-conifer stands. *Ecology* 73 (6), 2022-2033.

Binkley, D., Cromack, K. Jr., Baker, D. (1994). Nitrogen fixation by Red Alder: biology, rates, and controls, in: Hibbs, D. (Ed.), *The Biology and Management of Red Alder*. Oregon State University Press, Corvallis. pp. 57-72.

Bowling, L.C., Storck, P., Lettenmaier, D.P. (2000). Hydrologic effects of logging in western Washington, United States. *Water Resources Research* 36 (11), 3223-3240.

Bowling, L.C., Lettenmaier, D.P. (2001). The effects of forest roads and harvest on catchment hydrology in a mountainous maritime environment, in: Wigmosta, M.S., Burges, S.J. (Eds.), *Land Use and Watersheds: Human Influence on Hydrology and Geomorphology in Urban and Forest Areas: Vol. 2. Water Science and Application.* American Geophysical Union, DC., pp. 145-164.

Boyer, E.W., Goodale, C.L., Jaworski, N.A., Howarth, R.W. (2002). Anthropogenic nitrogen sources and relationships to riverine nitrogen export in the northeastern U.S.A. *Biogeochemistry* 57/58, 137-169.

Brett, M.T., Arhonditsis, G.B., Mueller, S.E., Hartley, D.M., Frodge, J.D., Funke, D.E. (2005). Non-point-source impacts on stream nutrient concentrations along a forest to urban gradient. *Environmental Management* 35 (3), 330-342.

Bruijnzeel, L.A. (2004). Hydrological functions of tropical forests: not seeing the soil for the trees? *Agriculture Ecosystems and Environment* 104 (1), 185-228.

Cairns, M., Lajtha, K. (2005). Effects of succession on nitrogen export in the west-central cascades, Oregon. *Ecosystems* 8, 583-601.

Carter, A.J., Scholes, R.J. (1999). *Generating a Global Database of Soil Properties*. Environmentek CSIR, Pretoria, South Africa.

Compton, J.E., Church, M.R., Larned, S.T., Hogsett, W.E. (2003). Nitrogen export from forested watersheds in the Oregon Coast Range: the role of N2-fixing Red Alder. *Ecosystems* 6, 773-785.

Croke, B.F.W., Merritt, W.S., Jakeman, A.J. (2004). A dynamic model for predicting hydrologic response to landcover changes in gauged and ungauged catchments. *Journal of Hydrology* 291 (1-2), 115-131.

Cuo, L., Giambelluca, T.W., Ziegler, A.D., Nullet, M.A. (2006). Use of the distributed hydrology soil vegetation model to study road effects on hydrological processes in Pang Khum Experimental Watershed, northern Thailand. *Forest Ecology and Management* 224 (1-2), 81-94.

Currie, W.S., Aber, J.D. (1997). Modeling leaching as a decomposition process in humid montane forests. Ecology 78(6), 1844-1860.

Dairaku, K., Kuraji, K., Suzuki, M., Tangtham, N., Jirasuktaveekul, W., Punyatrong, K. (2000). The effect of rainfall duration and intensity on orographic rainfall enhancement in a mountainous area: a case study in the Mae Chaem watershed, Thailand. *Journal of the Japan Society of Hydrology and Water Resources* 13 (1), 57-68.

Dalva, M., Moore, T.R. (1991). Sources and sinks of dissolved organic carbon in a forested swamp catchment. *Biogeochemistry* 15, 1-19.

Edmonds, R.L., Blew, R.D., Marra, J.L., Blew, J., Barg, A.K., Murray, G., Thomas, T.B. (1998). *Vegetation Patterns, Hydrology, and Water Chemistry in Small Watersheds in the Hoh River Valley, Olympic National Park. Scientific Monograph*. NPSD/NRUSGS/NRSM-98/02. United States Department of the Interior, National Park Service, Washington, DC. 131 p.

Edmonds, R.L., Murray, G.L.D. (2002). Overstory litter inputs and nutrient returns in an old-growth temperate forest ecosystem, Olympic National Park, Washington. *Canadian Journal of Forest Research*, 32 (4), 742-750.

Edmonds, R.L. (1987). Decomposition rates and nutrient dynamics in small-diameter woody litter in 4 forest ecosystems in Washington, USA. *Canadian Journal of Forest Research* 17 (6): 499-509.

Edmonds, R.L. (1980). Litter decomposition and nutrient release on Douglas-fir, Red Alder, Western Hemlock, and Pacific Silver Fir ecosystems in western Washington. *Canadian Journal of Forest Research* 10 (3), 327-337.

Fenn, M.E., Haeuber, R., Tonnesen, G.S., Baron, J.S., Grossman-Clarke, S., Hope, D., Jaffe, D.A., Copeland, S., Geiser, L., Rueth, H.M., Sickman, J.O. (2003). Nitrogen emissions, deposition, and monitoring in the Western United States. *BioScience* 53 (4), 391-403.

Fenn, M.E., Poth, M.A., Terry, J.D., Blubaugh, T.J. (2005). Nitrogen mineralization and nitrification in a mixed-conifer forest in southern California: controlling factors, fluxes, and nitrogen fertilization response at a high and low nitrogen deposition site. *Canadian Journal of Forest Research* 35 (6), 1464-1486.

Food and Agriculture Organization of the United Nations (FAO) (1995). *Digital Soil Map of the World, Version 3.5*. FAO, Rome, Italy.

Gardner, S., Sidisunthorn, P., Anusarnsunthorn, V. (2000). *A Field Guide to Forest Trees of Northern Thailand.* Kobfai Publication Project. Chulalongkorn Book Center, Bangkok, Thailand.

Gessel, S.P., Turner, J. (1974). Litter production by Red Alder in Western Washington. *Forest Science* 20 (4), 325-329.

Godwin, D.C., Jones, C.A., Ritchie, J.T., Vlek, P.L.G., Youngdahl, L.G. (1984). The water and nitrogen components of the CERES models, in: *Proceedings of 1983 International Symposium on Minimum Data Sets for Agrotechnology Transfer.* International Crops Research Institute for the Semi-Arid Tropics, Patancheru, India, pp. 95-100.

Hangs, R.D., Knight, J.D., Van Rees, K.C.J. (2003). Nitrogen uptake characteristics for roots of conifer seedlings and common boreal forest competitor species. *Canadian Journal of Forest Research* 33, 156-163.

Hansen, P.K. (2001). *Environmental Variability and Agro-Ecological Stratification in a Watershed in Northern Thailand*. Capacity Building in Biodiversity Project. Technical paper no. 2.

Hénault, C., Germon, J.C. (2000). NEMIS, a predictive model of denitrification on the field scale. *European Journal of Soil Science* 51, 257-270.

Hull, T.E., Bryan, A. (2005). *Solving Hood Canal's Low Oxygen Problem: the Onsite System Factor*. Technical reports. Puget Sound Action Team. Retrieved October 22, 2006 from the Puget Sound Action Team website. http://www.psat.wa.gov/Programs/hoodcanal/hc_publications.htm

Inamdar, S.P., Sheridan, J.M., Williams, R.G., Bosch, D.D., Lowrance, R.R., Altier, L.S., Thomas, D.L. (1999-a). Riparian Ecosystem Management Model (Remm): I. Testing of the hydrologic component for a coastal plain riparian system. *Transactions of the ASAE*. 42(6), 1679-1689.

Inamdar, S.P., Lowrance, R.R., Altier, L.S., Williams, R.G., Hubbard, R.K. (1999). Riparian Ecosystem Management Model (REMM): II. testing of the water quality and nutrient cycling component for a coastal plain riparian system. *Transactions of the ASAE* 42 (6), 1691-1707.

Johnes, P. J. (1996). Evaluation and management of the impact of land use change on the nitrogen and phosphorus load delivered to surface waters: the export coefficient modeling approach. *Journal of Hydrology* 183 (3-4), 323-349.

Kalbitz, K., Solinger, S., Park, J.H., Michalzik, B., Matzner, E. (2000). Controls on the dynamics of dissolved organic matter in soils: a review. *Soil science* 165 (4), 277-304.

Koprivnjak, J.F., Moore, T.R. (1992). Sources, sinks and fluxes of dissolved organic carbon in subarctic fen catchments. *Arctic and Alpine Research* 24, 204-219.

Krause, P., Boyle, D.P., Bäse, F. (2005). Comparison of different efficiency criteria for hydrological model assessment. *Advances in Geosciences* 5, 89-97.

Kuraji, K., Punyatrong, K., Suzuki, M. (2001). Altitudinal increase in rainfall in the Mae Chaem watershed, Thailand. *Journal of the Meteorological Society of Japan* 79 (1B), 353-363.

Lavoie, M., Bradley, R.L. (2003). Short-term increases in relative nitrification rates due to trenching in forest floor and mineral soil horizons of different forest types. *Plant and Soil* 252 (2), 367-384.

Li, X., Ambrose, R.B., Araujo, R. (2004). Modeling mineral nitrogen export from a forest terrestrial ecosystem to streams. *Transactions of the ASAE* 47 (3), 727-739.

Liang, X., Lettenmaier, D.P., Wood, E.F., Burges, S.J. (1994). A simple hydrologically based model of land-surface water and energy fluxes for general-circulation models. *Journal of Geophysical Research-Atmospheres* 99 (D7), 14415-14428.

Liles, G. (2005). *Biogeochemistry of Managed Forest Headwater Streams in Low Elevation Western Washington.* Master's thesis. University of Washington, Seattle, WA.

Lipson D., Näsholm, T. (2001). The unexpected versatility of plants: organic and availability in terrestrial ecosystems. *Oecologia* 128, 305-316.

Matschonat, G., Matzner, E. (1995). Quantification of ammonium sorption in acid forest soils by sorption isotherms. *Plant and Soil* 168-169, 95-101.

Maurer, E.P., Wood, A.W., Adam, J.C., Lettenmaier, D.P., Nijssen, B. (2002). A long-term hydrologically based dataset of land surface fluxes and states for the conterminous United States. *Journal of Climate* 15 (22), 3237-3251.

McDowell, W.H., Likens, G.E. (1988). Origin, composition, and flux of dissolved organic carbon in the Hubbard Brook Valley, *Ecological Monographs* 58 (3), 177-195.

Mitchell, M.J., Driscoll, C.T., Kahl, J.S., Likens, G.E., Murdoch, P.S., Pardo, L.H. (1996). Climatic control of nitrate loss from forested watersheds in the northeast United States. *Environmental Science and Technology* 30, 2609-2612.

Mitsch, W. J., Day, J.W. Gilliam, J.W., Groffman, P.M., Hey, D.L., Randall, G.W., Wang, N. (2001). Reducing nitrogen loading to the Gulf of Mexico from the Mississippi River Basin: strategies to counter a persistent ecological problem. *BioScience* 51 (5), 373-388.

Murphy, D.V., Macdonald, A.J., Stockdale, E.A., Goulding, K.W.T., Fortune, S., Gaunt, J.L., Poulton, P.R., Wakefield, J.A., Webster, C.P., Wilmer, W.S. (2000). Soluble organic nitrogen in agricultural soils. *Biology and Fertility of Soils* 30 (5-6), 374-387.

Nadelhoffer, K.J., Aber, J.D., Melillo, J.M. (1984). Seasonal patterns of ammonium and nitrate uptake in nine temperate forest ecosystems. *Plant and Soil* 80 (3), 321-335.

Nash, J.E., Sutcliffe, J.V. (1970). River flow forecasting through conceptual models. Part I - a discussion of principles. *Journal of Hydrology* 10, 282-290.

Neff, J.C., Asner, G.P. (2001). Dissolved organic carbon in terrestrial ecosystems: synthesis and a model. *Ecosystems* 4, 29-48.

Neff, J.C., Chapin, F.S., Vitousek, P.M. (2003). Breaks in the cycle: dissolved organic nitrogen in terrestrial ecosystems. *Frontiers in Ecology and Environment* 1(4), 205-211.

Neitsch, S., Arnold, J., Kiniry, J., Williams, J. (2000). *Soil and Water Assessment Tool Theoretical Documentation 2000*. Grassland, Soil and Water Research Laboratory, Agricultural Research Service, Temple, TX. 506 pp.

Newbold, J.D., Sweeney, B.W., Jackson, J.K., Kaplan, L.A. (1995).Concentrations and export of solutes from 6 mountain streams in northwestern Costa-Rica. *Journal of the North American Benthological Society* 14 (1), 21-37.

Nodvin, S.C., Driscoll, C.T., Likens, G.E. (1986). Simple partitioning of anions and dissolved organic carbon in a forest soil. *Soil Science* 142 (1), 27-35.

Nordin, A., Högberg, P., Näsholm, T. (2001). Soil nitrogen form and plant nitrogen uptake along a boreal forest productivity gradient. *Oecologia* 129, 125-132.

Osborne, S. (2006). *Influence of Catchment Characteristics on Stream Nitrogen Transport and Hypoxic Conditions in South Hood Canal.* Master's thesis. University of Washington, Seattle, WA.

Parton, W. J., Stewart, J.W.B., Cole, C.V. (1988). Dynamics of C, N, P, and S in grassland soils: a model. *Biogeochemistry* 5(1), 109-131.

Parton, W.J., Mosier, A.R., Ojima, D.S., Valentine, D.W., Schimel, D.S., Weier, K., Kulmala, A.E. (1996). Generalized model for N-2 and N2O production from nitrification and denitrification. *Global Biogeochemical Cycles* 10 (3), 401-412.

Pastor, J., Binkley, D. (1998). Nitrogen fixation and the mass balances of carbon and nitrogen in ecosystems. *Biogeochemistry* 43, 63-78.

Paulson, A.J., Paulson, J., Konrad, C.P., Frans, L.M., Noble, M., Kendall, C., Josberger, E.G., Huffman, R.L., Olsen, T.D. (2006). *Freshwater and Saline Loads of Dissolved Inorganic Nitrogen to Hood Canal and Lynch Cove, Western Washington.* U.S. Geological Survey Scientific Investigations Report 2006-5106, Reston, VA. 92 p.

Peterson, B.J., Wollheim, W.M., Mulholland, P.J., Webster, J.R., Meyer, J.L., Tank J.L., Marti, E., Bowden, W.B., Valett, H.M., Hershey, A.E., McDowell, W.H., Dodds, W.K., Hamilton, S.K., Gregory, S., Morrall, D.D. (2001). Control of nitrogen export from watersheds by headwater streams. *Science* 292 (5514), 86-90.

Pinthong, J., Thomsen, A., Rasmussen, P., Iversen, B.V. (2000). *Studies of Soil and Water Dynamics. Approach and Methodology*. Working paper no. 2. Research Center on Forest and People in Thailand, Tjele, Denmark.

Praneetvatakul, S., Janekarnkij, P., Potchanasin, C., Prayoonwong, K. (2001). Assessing the sustainability of agriculture a case of Mae Chaem catchment, northern Thailand. *Environment International* 27 (2-3), 103-109.

Putivoranart, S. (1973). *Soil Survey Report No. 167 for Wang-Pa, Mae Chaem District, Chiang Mai* (translated from Thai title). The Land Development Department of Thailand, Thailand.

Quinn, T.P., Peterson, N.P. (1996). The influence of habitat complexity and fish size on over-winter survival and growth of individually marked juvenile coho salmon (Oncorhynchus kisutch) in Big Beef Creek, Washington. *Canadian Journal of Fisheries and Aquatic Science* 53, 1555-1564.

Reddy, K.R., Khaleel, R., Overcash, M.R., Westerman, P.W. (1979). Nonpoint source model for land areas receiving animal wastes.1. Mineralization of organic nitrogen. *Transactions of yhe ASAE* 22 (4), 863-872.

Richardson, J.S., Shaughnessy, C.R., Harrison, P.G. (2004). Litter breakdown and invertebrate association with three types of leaves in a temperate rainforest stream. *Archiv Fur Hydrobiologie* 159 (3), 309-325.

Roberts, M. 2006. Sources, Transport, and Fate of Terrestrial Organic Matter inputs to Small Puget Sound Lowland Streams: Effects of Urbanization, Floods, and Salmon. Dissertation. University of Washington, Seattle, WA.

Saxton, K.E., Rawls, W.J., Romberger, J.S., Papendick, R.I. (1986). Estimating generalized soil-water characteristics from texture. *Soil Science Society of America Journal* 50 (4), 1031-1036.

Schnorbus, M., Alila, Y. (2004). Forest harvesting impacts on the peak flow regime in the Columbia Mountains of southeastern British Columbia: an investigation using long-term numerical modeling. *Water Resources Research* 40 (5), Art. no. W05205.

Schreider, S.Y., Jakeman, A.J., Gallant, J., Merritt, W.S. (2002). Prediction of monthly discharge in ungauged catchments under agricultural land use in the Upper Ping basin, northern Thailand. *Mathematics and Computers in Simulation* 59 (1-3), 19-33.

Seiders, P., Hoyle-Dodson, G., Pickett, P., 2001. *Skokomish River Basin Fecal Coliform Bacteria Total Maximum Daily Load Study*. Washington State Department of Ecology Publication # 01-03-014. Environmental Assessment Program, Watershed Ecology Section, Olympia, WA.

Sharma, G., Sharma, R., Sharma, E., Singh, K.K. (2002). Performance of an age series of Alnus-cardamom plantations in the Sikkim Himalaya: nutrient dynamics. *Annals of Botany* 89 (3), 273-282.

Solinger, S., Kalbitz, K. Matzner, E. (2001). Controls on the dynamics of dissolved organic carbon and nitrogen in a Central European deciduous forest. *Biogeochemistry* 55, 327-349.

Storck, P. (2000). *Trees, Snow, and Flooding: An Investigation of Forest Canopy Effects on Snow Accumulation and Melt at the Plot and Watershed Scales in the Pacific Northwes*t. Water Resources Series Technical Report no. 161. University of Washington, Seattle, WA.

Stover, S.C., Montgomery, D.R. (2001). Channel change and flooding, Skokomish River, Washington. *Journal of Hydrology* 243, 272-286.

Strahm, B.D., Harrison, R.B. (2006). Nitrate sorption in a variable-charge forest soil of the Pacific Northwest. *Soil Science* 171 (4), 313-321.

Sullivan, D.M., Hart, J.M., Christensen, N.W. (1999). *Nitrogen Uptake and Utilization by Pacific Northwest Crops*. PNW 513. Washington State University Coorporative Extension, WA.

Swank, W.T., Vose, J.M. (1997). Long-term nitrogen dynamics of Coweeta forested watersheds in the southeastern United States of America. *Global Biogeochemical Cycles* 11, 657-671.

Tanaka, K., Takizawa, H., Tanaka, N., Kosaka, I., Yoshifuji, N., Tantasirin, C., Piman, S., Suzuki, M., Tangtham, N. (2003). Transpiration peak over a hill evergreen forest in northern Thailand in the late dry season: assessing the seasonal changes in evapotranspiration using a multilayer model. *Journal of Geophysical Research-Atmospheres* 108 (D17), Art. no. 4533.

Tangtham, N. (1999). Hydrological roles of highland watersheds in Thailand, in: Thaiutsa, B., Traynor, C., Thammincha, S. (Eds.), *Highland Ecosystem Management: Proceedings of the International Symposium on Highland Ecosystem Management*, 26-31 May 1998. Royal Angkhang Agricultural Station, Royal Project Foundation, Chiang Mai, Thailand.

Thomas, D., Preechapanya, P., Saipothong, P. (2002). Landscape agroforestry in upper tributary watersheds of northern Thailand. *Journal of Agriculture* (Thailand) 18 (supplement 1), S255-S302.

Tufford, D.L., McKellar, H.N., Hussey, J.R. (1998). Instream nonpoint source nutrient prediction with land-use proximity and seasonality. *Journal of Environmental Quality* 27, 100-111.

Turner, D.P., Sollins, P., Leuking, M., Rudd, N. (1993). Availability and uptake of inorganic nitrogen in a mixed old-growth coniferous forest. *Plant and Soil* 148 (2), 163-174.

Vanderbilt, K.L, Lajtha, K., Swanson, F.J. (2003). Biogeochemistry of unpolluted forested watersheds in the Oregon Cascades: temporal patterns of precipitation and stream nitrogen fluxes. *Biogeochemistry* 62, 87-117.

VanShaar, J.R., Haddeland, I., Lettenmaier, D.P. (2002). Effects of land-cover changes on the hydrological response of interior Columbia River basin forested catchments. *Hydrological Processes* 16 (13), 2499-2520.

Volk, C.J. (2004). *Nutrient and Biological Responses to Red Alder (Alnus rubra) Presence along Headwater Streams: Olympic Peninsula, Washington*. Master’s thesis. University of Washington, Seattle, WA.

Waichler, S.R., Wigmosta, M.S. (2003). Development of hourly meteorological values from daily data and significance to hydrological modeling at H.J. Andrews Experimental Forest. *Journal of Hydrometeorology* 4 (2), 251-263.

Walker, A. (2002). *Forests and Water in Northern Thailand.* Resource Management in Asia-Pacific Working Paper no. 37. Resource Management in Asia-Pacific Program. The Australian National University, Canberra, Australia.

Walker, A. (2003). Agricultural transformation and the politics of hydrology in northern Thailand. *Development and Change* 34 (5), 941-964.

Whitaker, A., Alila, Y., Beckers, J., Toews, D. (2003). Application of the Distributed Hydrology Soil Vegetation Model to Redfish Creek, British Columbia: model evaluation using internal catchment data. *Hydrological Processes* 17 (2), 199-224.

Wigmosta, M.S., Vail, L.W., Lettenmaier, D.P. (1994). A distributed hydrology-vegetation model for complex terrain. *Water Resources Research* 30 (6), 1665-1679.

Wiley, M. (2006). *Implementation and Validation of a Distributed Hydrologic Model as a Component of the Integrated Assessment of Water Quality in Hood Canal*, Washington. University of Washington, Seattle, WA.

Young, R. A., Onstad, C.A., Bosch, D.D. (1995). AGNPS: An agricultural nonpoint source model, in: Singh, V.P. (Ed.) *Computer Models of Watershed Hydrology.* Water Resource Publications, Highlands Ranch, Colo.

Ziegler, A.D., Giambelluca, T.W., Tran, L.T., Vana, T.T., Nullet, M.A., Fox, J., Vien, T.D., Pinthong, J., Maxwell, J.F., Evett, S. (2004). Hydrological consequences of landscape fragmentation in mountainous northern Vietnam: evidence of accelerated overland flow generation. *Journal of Hydrology* 287 (1-4), 124-146.

No author, no date. The physical environment, flora and fauna of Big Beef Creek. Retrieved October 22, 2006, from http://www.cofs.washington.edu/bbc/florafauna.html). Descriptions from the Field Report by Charles A. Durin, of the US Fish & Wildlife Service. 1981.

Appendix 1: Individual biogeochemical process representations (based on 3-hour timestep)

The following equations in this appendix represent the processes as implemented in D-SEM version 0.9.58 (the current version as of December 16, 2006). As D-SEM evolves, the implementation will inevitably also change. If you have questions, please email Porranee Thanapakpawin at PorraneeT@CWITE.Org

All equations are written in terms of mass as carbon and mass as nitrogen. In the actual mass balance computation, which is performed on the basis of mass of species, the process rates were converted to the unit of mass of species.

A1.1: Rate of metabolic detrital organic carbon input from overstory and understory litterfall

$$MetDetrCLitterInput = \sum_{v=1}^{m} MetDetrCLitterInput_v$$

$$MetDetrCLitterInput_v = A_{cell} \cdot MetLitterFlux_{\Delta t,v} \cdot f_{C\_Met,v}$$

$$MetLitterFlux_{\Delta t,v} = LitterFlux_{\Delta t,v} \cdot f_{Met,v}$$

$$LitterFlux_{\Delta t,v} = \frac{Lv \cdot MonthLitterFr_v}{nt_{Litterfall}}$$

$$f_{Met,v} = 0.85 - 0.018 \cdot r_{LigninN}$$

$MetDetrCLitterInput$ = Total metabolic detrital organic carbon input rate in each time step, $\frac{kgC}{3h}$

$MetDetrCLitterInput_v$ = Metabolic detrital organic carbon input rate from vegetation layer v in each time step, $\frac{kgC}{3h}$

m = Number of vegetation layers in the current vegetation type

A_{cell} = Area of pixel, m^2

$MetLitterFlux_{\Delta t,v}$ = Flux of litterfall of vegetation layer v that is metabolic in each time step, $\frac{kgC}{m^2 - 3h}$

$LitterFlux_{\Delta t,v}$ = Flux of litter fall of vegetation layer v in each time step, $\frac{kgC}{m^2-3h}$

$MonthLitterFr_v$ = Fraction of annual flux of litterfall of vegetation layer v for each month (January – December)

$f_{Met,v}$ = Fraction of fresh detrital organic matter or residue of vegetation layer v that is metabolic

Lv = Annual litterfall mass flux of vegetation layer v, $\frac{kg}{m^2-yr}$

$f_{C\_Met,v}$ = Mass fraction of carbon in the metabolic litterfall of vegetation layer v

$nt_{Litterfall}$ = Number of time steps of simulation in the current month

$r_{LigninN,v}$ = Lignin to nitrogen mass ratio for each layer, $\frac{mgLignin}{mgN}$

A1.2: Rate of metabolic detrital organic carbon decomposition

This function is a first order kinetics reaction and is a function of soil moisture, soil temperature, and nitrogen availability of the top soil layer, in order to decompose the litter on the ground surface. The equation was derived from the litter decomposition scheme in REMM and residue decomposition scheme in SWAT.

$$MetDetrCDecomp = Keff_{MetDecomp} \cdot \left[MetDetrC \right]_G$$

$$Keff_{MetDecomp} = K_{MetDecomp} \cdot \phi_{T,Decomp} \cdot \phi_{N,Decomp} \cdot \phi_{\theta,Decomp}$$

$$\phi_{T,Decomp} = \begin{cases} 0 & T_{top} < 0 \\ 2^{\left(\frac{T_{top} - T_{opt,litterDecomp}}{10}\right)} & T_{top} < T_{opt,litterDecomp} \\ 1 & T_{top} >= T_{opt,litterDecomp} \end{cases}$$

$$\phi_{N,Decomp} = \min\left(\exp\left[-0.693 \cdot \frac{\left(EffMetDetrCtoN - 25 \right)}{25} \right], 1 \right)$$

$$\phi_{\theta,Decomp} = \begin{cases} 0.0075 \cdot P_{sat,top} & P_{sat,top} \le 20 \\ -0.253 + 0.0203 \cdot P_{sat,top} & 20 < P_{sat,top} < 60 \\ 3.617 \cdot \exp\left(-0.02274 \cdot P_{sat,top}\right) & 60 \le P_{sat,top} \end{cases}$$

$$EffMetDetrCtoN = \frac{\left[MetDetrC\right]_G}{TotResidueN}$$

$$TotResidueN = \left[MetDetrN\right]_G + \left[NO_3\right]_L$$

$MetDetrCDecomp$ = Rate of metabolic detrital organic carbon decomposition in each time step, $\frac{kgC}{3h}$

$Keff_{MetDecomp}$ = Effective rate constant for metabolic detrital organic carbon decomposition, $\frac{1}{3h}$

$K_{MetDecomp}$ = Metabolic detrital organic carbon decomposition rate, $\frac{1}{3h}$

$\phi_{T,Decomp}$ = Temperature factor for the decomposition of detrital organic carbon, dimensionless

$\phi_{N,Decomp}$ = Nutrient factor for the decomposition of detrital organic carbon, dimensionless

$\phi_{\theta,Decomp}$ = Moisture factor for the decomposition of detrital organic carbon, dimensionless

$T_{opt,litterDecomp}$ = Optimum temperature for litter decomposition process, ^{o}C

T_{top} = Temperature of the top soil layer, ^{o}C

$EffMetDetCtoN$ = Effective carbon to nitrogen ratio

$TotResidueN$ = Total residue nitrogen available for microbe use in the decomposition, kg N

$$P_{sat,top} = 100 \cdot \frac{\theta_{top}}{\theta_{P,top}}$$

$P_{sat,top}$ = Percent of soil saturation extent of the top soil layer

θ_{top} = volumetric soil moisture content, $\frac{m^3}{m^3}$

$\theta_{P,top}$ = Soil porosity of the top soil layer, $\frac{m^3}{m^3}$

A1.3: Rate of structural detrital organic carbon input from overstory and understory litterfall

$$StrucDetrCLitterInput \quad = \quad A_{cell} \cdot \sum_{v=1}^{m} \left(SturcLitterFlux_{\Delta t,v} \cdot f_{C\_Struc,v} \right)$$

$$SturcLitterFlux_{\Delta t,v} \quad = \quad LitterFlux_{\Delta t,v} \cdot \left(1 - f_{Met,v}\right)$$

$StrucDetrCLitterInput$ = Total structural detrital organic carbon input rate in each time step, $\frac{kgC}{3h}$

$StrucLitterFlux_{\Delta t,v}$ = Flux of litterfall of vegetation layer v that is structural in each time step, $\frac{kgC}{m^2-3h}$

$f_{C\_Struc,v}$ = Mass fraction of carbon in the structural litterfall of vegetation layer v

A1.4: Rate of structural detrital organic carbon decomposition

$$StrucDetrCDecomp = Keff_{StrucDecomp} \cdot [StrucDetrC]_G$$

$$Keff_{StrucDecomp} = K_{strucDecomp} \cdot \phi_{T,Decomp}$$

$StrucDetrCDecomp$ = Rate of structural detrital organic carbon decomposition, $\frac{kgC}{3h}$

$Keff_{StrucDecomp}$ = Effective structural detrital organic carbon decomposition rate, $\frac{1}{3h}$

$K_{strucDecomp}$ = Structural detrital organic carbon decomposition rate, $\frac{1}{3h}$

A1.5: Rate of metabolic detrital organic nitrogen input from overstory and understory litterfall

$$MetDetrNLitterInput = \sum_{v=1}^{m} MetDetrNLitterInput_v$$

$$MetDetrNLitterInput_v = \frac{MetDetrCLitterInput_v}{r_{cn\_Met,v}}$$

$MetDetrNLitterInput$ = Total metabolic detrital organic nitrogen input rate in each time step, $\frac{kgN}{3h}$

$MetDetrCLitterInput_v$ = Metabolic detrital organic nitrogen input rate from vegetation layer v in each time step, $\frac{kgN}{3h}$

$r_{cn\_Met,v}$ = Carbon to nitrogen mass ratio for metabolic litter pool of each vegetation layer

A1.6: Rate of metabolic detrital organic nitrogen decomposition

$$MetDetrNDecomp \quad = \quad \min(PotTotalNForDecomp, \left[MetDetrN\right]_G)$$

$$PotTotalNForDecomp \quad = \quad \frac{MetDetrCDecomp}{EffMetDetrCtoN}$$

$MetDetrNDecomp$ = Rate of metabolic detrital organic nitrogen decomposition, $\frac{kgN}{3h}$

$PotTotalNForDecomp$ = Potential total nitrogen available for decomposition of metabolic detrital organic matter, $\frac{kgN}{3h}$

If $MetDetrNDecomp$ is less than $PotTotalNForDecomp$, then $MetDetrCDecomp$ calculated from A1.2 was readjusted in order to meet the stoichiometric requirement.

A1.7: Rate of structural detrital organic nitrogen input from overstory and understory litterfall

$$StrucDetrNLitterInput \quad = \quad \sum_{v=1}^{m} StrucDetrNLitterInput_v$$

$$StrucDetrNLitterInput_v \quad = \quad \frac{StrucDetrCLitterInput_v}{r_{cn\_Struc,v}}$$

$StrucDetrNLitterInput$ = Total structural detrital organic nitrogen input rate in each time step, $\frac{kgN}{3h}$

$StrucDetrNLitterInput_v$ = Structural detrital organic nitrogen input rate from vegetation layer v in each time step, $\frac{kgN}{3h}$

$r_{cn\_Struc,v}$ = Carbon to nitrogen ratio of structural litter pool of each vegetation layer

A1.8: Rate of structural detrital organic nitrogen decomposition

$$StrucDetrNDecomp \quad = \quad \min(PotStrucDetrNDecomp, \left[StrucDetrN\right]_G)$$

$$PotStrucDetrNDecomp = \frac{StrucDetrCDecomp}{EffStrucDetrCtoN}$$

$StrucDetrNDecomp$ = Rate of structural detrital organic nitrogen decomposition, $\frac{kgN}{3h}$

$PotStrucDetrNDecomp$ = Potential decomposed structural detrital organic nitrogen, $\frac{kgN}{3h}$

$EffStrucDetrCtoN$ = Effective carbon to nitrogen ratio of the structural litter pool, and is a weighted-average value of carbon to nitrogen ratio of all vegetation layers

If $StrucDetrNDecomp$ is less than $PotStrucDetrNDecomp$, then $StrucDetrCDecomp$ calculated from A1.4 was readjusted in order to meet the stoichiometric requirement.

A1.9: Rate of DOC inputs into soil column from the vegetation decomposition

The products from litter C decomposition were mineralized C and leachate of DOC, and the partitioning between the two products depend on the fraction of leachate.

$$LitterLeachedDOC = MetDetrCDecomp \cdot f_{MetLeachDOC} + StrucDetrCDecomp \cdot f_{StrucLeachDOC}$$

$$f_{MetLeachDOC} = \frac{\sum_{v=1}^{m} \left(f_{MetLeachDOC,v} \cdot L_v \right)}{\sum_{v=1}^{m} L_v}$$

$$f_{StrucLeachDOC} = \frac{\sum_{v=1}^{m} \left(f_{StrucLeachDOC,v} \cdot L_v \right)}{\sum_{v=1}^{m} L_v}$$

$LitterLeachedDOC$ = Rate of DOC inputs from the decomposition of litterfall, $\frac{kgC}{3h}$

$f_{MetLeachDOC}$ = Average value of fraction of decomposed metabolic detrital organic carbon that is available for leaching

$f_{MetLeachDOC,v}$ = Fraction of decomposed metabolic detrital organic carbon that is available for leaching from vegetation layer *v*

$f_{StrucLeachDOC}$ = Average value of fraction of decomposed structural detrital organic carbon that is available for leaching

$f_{StrucLeachDOC,v}$ = Fraction of decomposed structural detrital organic carbon that is available for leaching from vegetation layer *v*

A1.10: Rate of soil DOC respired by microbes

$$soilDOCresp = Keff_{Soilresp} \cdot [DOC]_L$$

$$Keff_{Soilresp} = K_{Soilresp} \cdot \phi_{m\_resp} \cdot \phi_{T\_resp}$$

$$\phi_{m\_resp} = \begin{cases} 0.0075 \cdot P_{sat} & P_{sat} < 20\% \\ -0.253 + 0.0203 \cdot P_{sat} & 20 \leq P_{sat} < 60\% \\ 3.617 \cdot \exp[-0.02274 \cdot P_{sat}] & P_{sat} \geq 60\% \end{cases}$$

$$P_{sat} = 100 \cdot \frac{\theta}{\theta_P}$$

$$\phi_{T\_resp} = \begin{cases} 0 & T \le 0^{o}C \\ 2^{\left(\frac{T-T_{opt}}{10}\right)} & 0 < T < T_{opt} \\ 1 & T \ge T_{opt} \end{cases}$$

$soilDOCresp$ = Rate of soil DOC respiration, $\frac{kgC}{3h}$

$Keff_{Soilresp}$ = Effective rate constant for soil DOC respiration, $\frac{1}{3h}$

$K_{Soilresp}$ = Base value rate constant for soil DOC respiration, $\frac{1}{3h}$

ϕ_{m_resp} = Moisture factor for soil respiration, dimensionless

P_{sat} = Percent of soil saturation extent, defined in Equation 2.

ϕ_{T_resp} = Temperature factor for soil respiration, dimensionless

T_{opt} = Optimum temperature for the microbe respiration of DOC, ^{o}C

T = Average temperature of all soil layers, excluding the deep soil below the root zone (average temperature of the nutrient reservoir)

θ = Average volumetric soil moisture content of all soil layers, excluding the deep soil below the root zone

A1.11: Rate of DON inputs into soil column from the vegetation decomposition

$$LitterLeachedDON = MetDetrNDecomp \cdot f_{MetLeachDON} + StrucDetrNDecomp \cdot f_{StrucLeachDON}$$

$$f_{MetLeachDON} = \frac{\sum_{v=1}^{m}\left(f_{MetLeachDON,v} \cdot L_v \right)}{\sum_{v=1}^{m} L_v}$$

$$f_{StrucLeachDON} = \frac{\sum_{v=1}^{m}\left(f_{StrucLeachDON,v} \cdot L_v\right)}{\sum_{v=1}^{m} L_v}$$

$LitterLeachedDON$ = Rate of DON inputs from decomposed litter, $\frac{kgN}{3h}$

$f_{MetLeachDON}$ = Average value of fraction of decomposed metabolic detrital organic nitrogen that is available for leaching

$f_{MetLeachDON,v}$ = Fraction of decomposed metabolic detrital organic nitrogen that is available for leaching from vegetation layer v

$f_{StrucLeachDON}$ = Average value of fraction of decomposed structural detrital organic nitrogen that is available for leaching

$f_{StrucLeachDON,v}$ = Fraction of decomposed structural detrital organic nitrogen that is available for leaching from vegetation layer v

A1.12: Rate of soil DON mineralized to NH_4 by microbes

$$soilDONmineraliz = \frac{soilDOCresp}{r_{cn\_mineraliz}}$$

$soilDONmineraliz$ = Rate of soil DON mineralization, $\frac{kgN}{3h}$

$r_{cn\_mineraliz}$ = Carbon to nitrogen mass ratio of dissolved organic matter being decomposed

A1.13: Rate of biological nitrogen fixation by Red Alder (*Alnus rubra*)

Nitrogen-fixing by Red Alder (*Alnus rubra*)

$$N_2 + 8H^+ + 8e^- \longrightarrow 2NH_3 + H_2$$

$$N_2\,fixation = N_{fixRate} \cdot \phi_{age} \cdot f_{alder} \cdot \phi_{T,Nfix}$$

$$\phi_{age} = \begin{cases} \dfrac{A_g}{15} & A_g \le 15 \quad years \\ 1 & 15 < A_g < 49 \quad years \\ \dfrac{A_g - 49}{49} & A_g \ge 49 \quad years \end{cases}$$

$$\phi_{age} = \begin{cases} \dfrac{A_g}{15} & A_g \le 15 \quad years \\ 1 & 15 < A_g < 49 \quad years \\ \dfrac{A_g - 49}{49} & A_g \ge 49 \quad years \end{cases}$$

$$N_{fixRate} \quad \phi_{T,Nfix} = \begin{cases} 0 & T \le 0 \\ 2^{\left(\frac{T - T_{opt,Alder}}{10}\right)} & 0 < T < T_{opt,Alder} \\ 1 & T \ge T_{opt,Alder} \end{cases}$$

$N_2\,fixation$ = Rate of nitrogen fixation in the soil, $\dfrac{kgN}{3h}$

f_{alder} = Fraction of stand that is Red Alder, dimensionless

$N_{fixRate}$ = Reference flux for nitrogen fixation in pure stand of Red Alder, $\frac{kgN}{m^2 - 3h}$ (need to convert user inputs $\frac{kgN}{ha - yr}$ to time step flux)

ϕ_{age} = Red Alder age factor, dimensionless

$\phi_{T,Nfix}$ = Temperature factor for N fixation

f_{alder} = Fraction of stand that is Red Alder

$T_{opt,Alder}$ = Optimum temperature for N fixation, ^{o}C

A_g = Average stand age, years

A1.14: Rate of ammonium inputs from decomposed metabolic detrital organic nitrogen that was mineralized

$$MineralizMetDetrN \quad = \quad MetDetrNDecomp \cdot \left(1 - f_{MetLeachDON}\right)$$

$MineralizMetDetrN$ = Rate of ammonium inputs from decomposed metabolic detrital organic nitrogen, $\frac{kgN}{3h}$

A1.15: Rate of ammonium inputs from decomposed structural detrital organic nitrogen that was mineralized

$$MineralizStrucDetrN \quad = \quad StrucDetrNDecomp \cdot \left(1 - f_{StrucLeachDON}\right)$$

$MineralizStrucDetrN$ = Rate of ammonium inputs from decomposed structural detrital organic nitrogen, $\frac{kgN}{3h}$

A1.16: Combined rate of nitrification and volatilization of NH_4

Nitrification

$$2NH_4^+ + 3O_2 \longrightarrow 2NO_2^- + 2H_2O + 4H^+$$
$$2NO_2^- + O_2 \longrightarrow 2NO_3^-$$

Ammonia volatilization

$$NH_4^+ + OH^- \longrightarrow H_2O + NH_3$$

This equation is based on the scheme in SWAT. The original equation in SWAT was formulated for a daily timestep. Therefore, 1/8 was a conversion to convert from daily to 3-h time step.

$$NitriAndVolatilz = \left(1 - \exp\left[-\phi_{Nitri} - \phi_{Volatiliz}\right]\right) \cdot \left[NH_4\right]_L \cdot \frac{1}{8}$$

$$\phi_{Nitri} = \phi_{T,nitri} \cdot \phi_{m,nitri}$$

$$\phi_{Volatiliz} = \phi_{depth} \cdot \phi_{T,nitri}$$

$$\phi_{T,Nitri} = \begin{cases} 0 & T \le 4 \\ 2^{\left(\frac{T - T_{opt,nitrification}}{10}\right)} & 4 < T < T_{opt,nitrification} \\ 1 & T \ge T_{opt,nitrification} \end{cases}$$

$$\phi_{m,Nitri} = \begin{cases} \dfrac{\theta - \theta_{wp}}{0.25 \cdot \left(\theta_F - \theta_{wp}\right)} & \left(\theta - \theta_{wp}\right) < 0.25 \cdot \left(\theta_F - \theta_{wp}\right) \\ 1 & \left(\theta - \theta_{wp}\right) \ge 0.25 \cdot \left(\theta_F - \theta_{wp}\right) \end{cases}$$

$$\phi_{depth} = \frac{1 - 1000 \cdot Z_{mid}}{1000 \cdot Z_{mid} + \exp\left[4.706 - 0.305 \cdot 1000 \cdot Z_{mid}\right]}$$

$$Z_{mid} = \frac{SoilLayerDepth}{2}$$

$NitriAndVolatilz$ = Total rate of nitrification and volatilization, $\frac{kgN}{3h}$

ϕ_{Nitri} = Nitrification regulator, dimensionless

$\phi_{Volatiliz}$ = Volatilization regulator, dimensionless

ϕ_{depth} = Volatilization depth factor, dimensionless

$\phi_{T,nitri}$ = Temperature factor for nitrification, dimensionless

$\phi_{m,Nitri}$ = Moisture factor for nitrification, dimensionless

Z_{mid} = Depth from the soil surface to the middle of the layer, m

$SoilLayerDepth$ = The depth of the soil layer, m

θ_{wp} = Soil wilting point, $\frac{m^3}{m^3}$

θ_F = Soil field capacity, $\frac{m^3}{m^3}$

$T_{opt,nitrification}$ = Optimum temperature for nitrification and mineralization, ^{o}C

A1.17: Rate of NH_4 uptake by vegetation

$$NH_4PlantUptake = \frac{V_{\max,NH_4} \cdot \left[NH_4\right]_{sol}}{K_{NH_4uptake} + \left[NH_4\right]_{sol}} \cdot A_{cell}$$

$NH_4PlantUptake$ = Rate of NH_4 uptake by vegetation, $\frac{kgN}{3hr}$

$V_{\max,NH_4}$ = Maximum ammonium intake flux, $\frac{kgN}{m^2-3hr}$

$K_{NH_4uptake}$ = Half-rate ammonium uptake constant, $\frac{kgN}{m^3}$

$\left[NH_4\right]_{sol}$ = Ammonium concentration in soil water, $\frac{kgN}{m^3}$

A1.18: Rate of nitrification

$$Nitri = \frac{f_{nitri}}{f_{nitri} + f_{volatiliz}} \cdot NitriAndVolatilz$$

$$f_{nitri} = 1 - \exp\left[-\phi_{Nitri}\right]$$

$$fvolatiliz = 1 - \exp\left[-\phi_{Volatiliz}\right]$$

$Nitri$ = Rate of nitrification, $\frac{kgN}{3h}$

f_{nitri} = Fraction of ammonium removed by nitrification process, dimensionless

$f_{volatiliz}$ = Fraction of ammonium removed by volatilization process, dimensionless

A1.19: Rate of NO_3 lost from the soil pool due to the decomposition of detrital organic matter

$$NO_3lsDetrDecomp = \begin{cases} 0 & PotTotalNForDecomp \le MetDetrNDecomp \\ PotTotalNForDecomp - MetDetrNDecomp & PotTotalNForDecomp > MetDetrNDecomp \end{cases}$$

$NO_3lsDetrDecomp$ = Rate of NO_3 lost from the soil pool due to the decomposition of detrital organic matter, $\frac{kgN}{3h}$

A1.20: Rate of NO_3 uptake by vegetation

$$NO_3PlantUptake = \begin{cases} 0 & T < 4 \; or \; \theta < \theta_{wp} \; or \; t_{cur} < t_{startNuptake} \\ \dfrac{\exp\left[-\dfrac{\left(\left(t_{cur} - t_{startNuptake}\right) - t_{\max Nuptake}\right)^2}{\left(2 \cdot \left(\dfrac{t_{PhaseII}}{3}\right)^2\right)}\right]}{\left(\left(\dfrac{t_{PhaseII}}{3}\right) \cdot \sqrt{(2 \cdot \pi)}\right)} \cdot 1.1 \cdot N_{\max Accum} & t_{cur} > t_{startNuptake} \end{cases}$$

$NO_3PlantUptake$ = Rate of NO_3 uptake by vegetation, $\frac{kgN}{3h}$

t_{cur} = Current day in the Julian year (January 1 is day 1)

$t_{startNuptake}$ = Growing season start day in Julian year

$t_{\max Nuptake}$ = Maximum nitrogen uptake delays, days

$t_{PhaseII}$ = Growing season length, days

$N_{\max Accum}$ = Maximum nitrogen accumulation of crop or maximum annual nitrogen uptake flux for forests, $\frac{kgN}{m^2}$

A1.21: Rate of denitrification of NO_3

$$Denitrif = Denitrif_{potential} \cdot \phi_{T,denitrif} \cdot \phi_{NO_3} \cdot \phi_{m,denitrif}$$

$$\phi_{T,denitrif} = \begin{cases} \exp\left[\dfrac{(T-11)\cdot\ln(89)-5\cdot\ln(2.1)}{10}\right] & T < 11^{o}C \\ \exp\left[\dfrac{(T-20)\cdot\ln(2.1)}{10}\right] & T \geq 11^{o}C \end{cases}$$

$$\phi_{NO_3} = \frac{SoilNO3perSoilMass}{\left(K_{m,denitrif} + SoilNO3perSoilMass\right)}$$

$$\phi_{m,denitrif} = \begin{cases} 0 & f_{sat} < \theta_{c,denit} \\ \left(\dfrac{f_{sat}-0.62}{0.38}\right)^{1.74} & f_{sat} \geq \theta_{c,denit} \end{cases}$$

$Denitrif$ = Rate of denitrification , $\dfrac{kgN}{3h}$

$Denitrif_{potential}$ = Potential denitrification flux, $\dfrac{kgN}{m^2-3h}$

$\phi_{T,denitrif}$ = Temperature factor for denitrification, dimensionless

ϕ_{NO_3} = Nutrient factor for denitrification, dimensionless

$\theta_{c,denit}$ = Denitrification saturation threshold, dimensionless

f_{sat} = Soil moisture saturation extent, dimensionless

$SoilNO3perSoilMass$ = Soil NO_3 mass concentration, $\frac{kgN}{kgSoil}$

$K_{m,denitrif}$ = Nitrate reduction half saturation constant, $\frac{kgN}{kgSoil}$

A1.22: Rate of in-stream DOC respiration

$$StreamDOCresp = \mu_{DOCresp,Tw} \cdot \left[DOC\right]_S$$

$$\mu_{DOCresp,Tw} = \mu_{DOCresp,20} \cdot 1.047^{(Tw-20)}$$

$StreamDOCresp$ = Rate of in-stream DOC respiration to carbon dioxide, $\frac{kgC}{3h}$

$\mu_{DOCresp,Tw}$ = Rate constant for in-stream DOC respiration at temperature Tw, $\frac{1}{3h}$

$\mu_{DOCresp,20}$ = Rate constant for in-stream DOC respiration at 20 ^{o}C, $\frac{1}{3h}$

A1.23: Rate of in-stream DON mineralization or hydrolysis to NH_4

$$StreamDONhydr = \mu_{Nhydr,Tw} \cdot [DON]_S$$

$$\mu_{Nhydr,Tw} = \mu_{Nhydr,20} \cdot 1.047^{(Tw-20)}$$

$StreamDONhydr$ = Rate of in-stream DON mineralization toNH_4, $\frac{kgN}{3h}$

$\mu_{Nhydr,Tw}$ = Rate constant for in-stream DON mineralization at water temperature Tw, $\frac{1}{3h}$

$\mu_{Nhydr,20}$ = Rate constant for in-stream DON mineralization at 20 °C, $\frac{1}{3hr}$

A1.24: Rate of in-stream nitrification from NH_4 to NO_2

$$StreamNitri1 \quad = \quad \mu_{nitri1,Tw} \cdot \left[NH_4\right]_S$$

$$\mu_{nitri1,Tw} \quad = \quad \mu_{nitri1,20} \cdot 1.07^{(Tw-20)}$$

$StreamNitri1$ = Rate of in-stream nitrification from NH_4 to NO_2, $\frac{kgN}{3h}$

$\mu_{nitri1,Tw}$ = Rate constant for in-stream nitrification rate from NH_4 to NO_2 at temperature Tw, $\frac{1}{3h}$

$\mu_{nitri1,20}$ = Rate constant for in-stream nitrification rate from NH_4 to NO_2 at 20 °C, $\frac{1}{3h}$

A1.23: Nitrification from NO_2 to NO_3

$$streamNitri2 \quad = \quad \mu_{nitri2,Tw} \cdot [NO_2]_S$$

$$\mu_{nitri2,Tw} \quad = \quad \mu_{nitri2,20} \cdot 1.07^{(Tw-20)}$$

$streamNitri2$ = Rate of in-stream nitrification from NO_2 to NO_3 , $\frac{kgN}{3h}$

$\mu_{nitri2,Tw}$ = Rate constant for the nitrification step converting NO_2 to NO_3, at temperature Tw, $\frac{1}{3h}$

$\mu_{nitri2,20}$ = Rate constant for the nitrification step converting NO_2 to NO_3, at 20 °C, $\frac{1}{3h}$

A1.24: Calculation of the soluble fraction of soil nutrient for use in the calculation of soil water concentration.

$$f_{sol} = \begin{cases} 0 & \theta < \theta_{wilt} \cdot 1.005 \\ f_{soil\max} \cdot 2^{\left(\frac{\theta - \theta_P}{\frac{\theta_P}{5}}\right)} & \theta_{wilt} \cdot 1.005 \leq \theta < 0.65 \\ f_{soil\max} \cdot 2^{\left(\frac{\theta - \theta_P}{\frac{\theta_P}{2.5}}\right)} & \theta \geq 0.65 \end{cases}$$

f_{sol} = Actual soluble fraction of nutrient mass in the soil

$f_{sol\max}$ = Maximum soluble fraction of nutrient mass in the soil

θ = Average volumetric moisture content of all soil layers, excluding the deep soil below root zones, $\frac{m^3}{m^3}$

θ_{wilt} = Average soil wilting point of all soil layers, excluding the deep soil below root zones, $\frac{m^3}{m^3}$

Appendix 2: DHSVM function calls

Start **DHSVM.EXE:MainDHSVM()** Initialization, then loops through time, performing water and chemistry routing/calulations.

- InitSoilChemistry()
- **InitChemTable()** – Establishes hardcoded properties of chemical species. This is where molecular weights are set.
- **RestoreChemState()** – Reads state of all species for surface, soil and groundwater
- **InitPointSource()** – Establishes location and opens file for point source inputs
- **InitStreamChemDump() –** Opens Stream.Chem output file
- Iterate though time steps (start date to end date)
  - **GetPointSources()** – Read current time step input for point sources
  - **GetDistributed Sources()** – Read maps and inputs of distributed inputs such as septic loads.
  - **ApplySources()** – Apply point and distributed source inputs to correct locations
  - Iterate through grid cells (*x* and *y* location) calling **MassEnergyBalance()** which calls the following functions:
  - **SurfaceChemistry()** routes water and chemical sepcies infiltration from surface
  - **LitterFall() –** Calculates DOC and DON deposited in cell from veg layers
  - **AtmosphericDeposition()** – Calculates chemical species mass deposited on cell with rainfall. SurfaceChemisty then does the routing of dissolved chemical species infiltrating to soil layer. Surface Mineralization of DOC and DON was calculated
  - **Respiration()** – Calculates rates of respiration fluxes
  - DOC removed and converted to CO_2 (a lost from system)
  - DON removed and converted to NH_4
  - **Nitrificaction() –** includes nitrification and volatilization of NH_4
  - **Denitrification()** – includes denitrification and loss of NO_3 used in litter decomposition
  - **VegNFixation()** – adds NH_4 to soil based on vegetation type. This is input due to the "Red Alder" effect.
  - **PlantUptake()** – removes NH_4 and NO_3 from soil
  - **UpdateChemTables()** – Update the Chemistry concentration tables
  - **RouteSubSurface() -**Contains routing routines for dissolved chemical species along with subsurface flow
  - **RouteSurface() -**Contains routing routines to move dissolved chemical species along with surface flow
  - **RouteChannel() -**Contains routing routines to move dissolved chemical species in stream channel downstream, including Mineralization, Hydrolysis, and Nitrification.
  - **ExecDump()** – code to dump output for the current timestep to Stream.Chem (for post processing).

Vita

PORRANEE THANAPAKPAWIN

Porranee was born in Bangkok, Thailand and came to Seattle in 1998 after receiving Bachelor of Engineering from the Department of Chemical Engineering at Chulalongkorn University in Bangkok. She acquired her Master of Science in Chemical Engineering at the University of Washington in 2000. Her thesis topic was "Effects of oligosaccharides on the properties of paper". That same year, she also obtained a Graduate Certificate in Environmental Management from the Program on Environment at the University of Washington. With her interest in interdisciplinary study in water resource and management, she began her Ph.D. study in Chemical Engineering at the University of Washington, from which received her Ph.D. in 2007.

PUBLICATIONS

Thanapakpawin, P., Richey, J., Thomas, D., Rodda, S., Campbell, B., Logsdon, M. Effects of landuse change on the hydrologic regime of the Mae Chaem river basin, NW Thailand. *Journal of Hydrology* 2006, doi:10.1016/j.jhydrol.2006.10.012.

G.G. Allan, **P. Thanapakpawin**, M. Harsono, J. Ohsie, M.St. Lawrence. Oligosaccharifications; a new approach to recycling paper-plastic combinations. *Cellulose Chemistry and Technology* 40 (1-2): 63-70, 2006.

G.G. Allan, **P. Tanapakpawin**, T. Rattanaviwatpong, D. Sasaki. The movement of fluids through complex nonwoven structures. *Nonwovens Industry*. December issue, 2005.

G.G. Allan, **P. Rattanaviwatpong**, E.B. Guyette, T.C.S. Ho, J.C. Mallari, A. Pfeif. Sugar-cellulose composites VII. A comparative assessment of corn syrup as a fiber substitute in paper. *Bioresource Technology* 96: 1645-1649, 2005.

ORAL PRESENTATIONS

Influence of landscape disturbance on carbon and nitrogen export from headwater streams in the Pacific Northwest. November 1, 2004.
American Water Resources Association National Conference, Orlando, FL

Following the falling leaves: Modeling nutrient escapes. May 18, 2004.
Tuesday Morning Seminar, Center for Water and Watershed Studies, UW, Seattle, WA

Impacts of land-use change on hydrology of a mountainous watershed: Water resource tension in northern Thailand. February 06, 2004.
Annual Review of Research, Center for Water and Watershed Studies, UW, Seattle, WA

Distributed regional-scale stressor-response model for watersheds in King County: Preliminary design. May 21, 2002.
Tuesday Morning Seminar, Center for Water and Watershed Studies, UW, Seattle, WA

Sugar…Alternative fiber substitute for cost saving. March 19, 2002.
TAPPI Pacific Section 64th Shibley Award Competition, North Pacific Paper Corp., Longview, WA